# Bounds on Performance in Continuous and Discrete Thermal Machines: Insights from Quantum and Thermal Fluctuations

विद्या वाचस्पति की
उपाधि की अपेक्षाओं की आंशिक पूर्ति में प्रस्तुत शोध प्रबंध

A thesis submitted in partial fulfillment of the requirements of the degree of Doctor of Philosophy


द्वारा / By
संदीपन महंता / Sandipan Mohanta

पंजीकरण सं. / Registration No.: 20193702

शोध प्रबंध पर्यवेक्षक / Thesis Supervisor:
डॉ. विजय कुमार अग्रवाला / Dr. Bijay Kumar Agarwalla

भारतीय विज्ञान शिक्षा एवं अनुसंधान संस्थान पुणे

INDIAN INSTITUTE OF SCIENCE EDUCATION AND RESEARCH PUNE


2024

*Dedicated to My beloved Parents*

# Declaration

Name of Student: Sandipan Mohanta
Reg. No.: 20193702
Thesis Supervisor: Dr. Bijay Kumar Agarwalla
Department: Physics
Date of joining program: August 1, 2019
Date of Pre-Synopsis Seminar: June 18, 2024
Title of Thesis: Bounds on Performance in Continuous and Discrete Thermal Machines: Insights from Quantum and Thermal Fluctuations

I declare that this written submission represents my ideas in my own words and where others' ideas have been included, I have adequately cited and referenced the original sources. I declare that I have acknowledged collaborative work and discussions wherever such work has been included. I also declare that I have adhered to all principles of academic honesty and integrity and have not misrepresented or fabricated or falsified any idea/data/fact/source in my submission. I understand that violation of the above will be cause for disciplinary action by the Institute and can also evoke penal action from the sources which have thus not been properly cited or from whom proper permission has not been taken when needed.

The work reported in this thesis is the original work done by me under the guidance of Dr. Bijay Kumar Agarwalla.

Sandipan Mohanta

*Date: October 28, 2024*

*Sandipan Mohanta*
*Reg. No. 20193702*

# Certificate

---

Certified that the work incorporated in the thesis entitled "*Bounds on Performance in Continuous and Discrete Thermal Machines: Insights from Quantum and Thermal Fluctuations*", submitted by *Sandipan Mohanta* was carried out by the candidate, under my supervision. The work presented here or any part of it has not been included in any other thesis submitted previously for the award of any degree or diploma from any other university or institution.

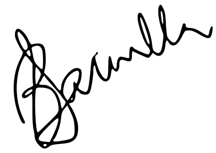

*Date: October 28, 2024*

*Dr. Bijay Kumar Agarwalla*
*Thesis Supervisor*

# Acknowledgements

First and foremost, I would like to express my deepest gratitude to my supervisor, Dr. Bijay Kumar Agarwalla, for his exceptional mentorship, expertise, and the countless insightful discussions we had during my Ph.D. journey. His unwavering patience and guidance, even when my research seemed to meander endlessly, have been invaluable, and for this, I am forever indebted. I also extend my sincere thanks to my collaborators, especially to Dr. B. Prasanna Venkatesh from IITGN, as well as to the members of my Research Advisory Committee (RAC): Prof. Ramandeep S. Johal from IISER Mohali, and Prof. T. S. Mahesh and Dr. Rejish Nath from IISER Pune. I also wholeheartedly appreciate the administrative staff of the Physics Department and the administrative team at IISER Pune, whose support made my ('non'-academic) work life smoother.

Second, I owe my deepest appreciation to my family, especially my parents, whose constant support and encouragement (and 'occasional' 'well-placed' doubts) fueled my Ph.D. journey. To my sister, my confidante, thank you for always being cooler than I am and for being there whenever I needed to vent. A special thanks to Anuja, my partner in every sense of the word, who managed to 'graciously' tolerate my absence and neglect during this journey and endured my promises of "just one more chapter" and "I'll be done soon." Love you!

Third, I am also profoundly grateful to my friends and colleagues at IISER Pune, who understood that Ph.D. life is not just about research but also about survival—and who shared that struggle with me, occasionally making it enjoyable and a little more bearable.

Lastly, I acknowledge the financial support provided by CSIR, India (File number: 09/936(0273)/2019-EMR-I).

*Sandipan Mohanta*

# Contents

# Abstract


Fluctuations play a crucial role in the operation of small-scale devices, where thermal and quantum effects significantly influence the efficiency, power output, and stability of machines. This thesis investigates performance constraints of small-scale thermodynamic machines, focusing on the impact of fluctuations in both autonomous and non-autonomous setups, as well as in continuous and discrete cycles.

For autonomous absorption refrigerators operating in the linear response regime, we uncover a hierarchy among the relative fluctuations in the currents associated with the cold, hot, and work terminals. This hierarchy, established using Onsager reciprocity and refrigeration conditions, reveals that the tightest bound on cooling power is governed by the fluctuation of the work current. These universal bounds can be stricter than those predicted by standard thermodynamic uncertainty relations (TURs) and converge in the tight-coupling limit. The results are demonstrated using two models: a four-level system in the weak coupling regime and a two-level system with strong system-bath interactions.

We then extend our analysis to non-autonomous continuous machines, where time-reversal symmetry is broken. By symmetrizing the operational regime, we derive a universal relationship between the relative fluctuations of input and output currents, even in the absence of Onsager reciprocity. These results are illustrated with a periodically driven classical Brownian heat engine.

For discrete machines, specifically the quantum Otto cycle, we examine work and heat fluctuations for asymmetrically driven engines. First, we analyze Otto cycles with specific working fluids, such as a single qubit and a harmonic oscillator, noting that unlike continuous machines, these cycles lack a well-established linear response formalism. We establish bounds on non-equilibrium fluctuations for both engine and refrigerator regimes, revealing distinct relationships between the fluctuations of work and heat in different reservoirs compared to continuous machines. Additionally, we

derive generalized thermodynamic uncertainty relations (GTURs) for the qubit-Otto cycle, which remain valid even under far-from-equilibrium driving.

Finally, we develop a rigorous linear response framework for generic Otto cycles using the Schwinger-Keldysh nonequilibrium Green's function (NEGF) technique. This approach uncovers that the fluctuation-dissipation relation (FDR) for the work current breaks down in the quantum domain due to external driving, while it remains valid for heat. This leads to important consequences for fluctuation bounds and thermodynamic performance in different operational regimes (engine and refrigerator). The violation of the work-FDR in the Otto cycle explains the observed differences in fluctuation bounds between discrete and continuous machines.

# List of Publications

(i) Sandipan Mohanta and Bijay Kumar Agarwalla, *Full statistics of nonequilibrium heat and work for many-body quantum Otto engines and universal bounds: A nonequilibrium Green's function approach*, Phys. Rev. E **108**, 064127 (2023).

(ii) Sandipan Mohanta, Madhumita Saha, B. Prasanna Venkatesh, and Bijay Kumar Agarwalla, *Bounds on nonequilibrium fluctuations for asymmetrically driven quantum Otto engines*, Phys. Rev. E **108**, 014118 (2023).

(iii) Sandipan Mohanta, Sushant Saryal, and Bijay Kumar Agarwalla, *Universal bounds on cooling power and cooling efficiency for autonomous absorption refrigerators*, Phys. Rev. E **105**, 034127 (2022).

(iv) Sushant Saryal, Sandipan Mohanta, and Bijay Kumar Agarwalla, *Bounds on fluctuations for machines with broken time-reversal symmetry: A linear response study*, Phys. Rev. E **105**, 024129 (2022).

**Not included in this thesis**

(i) Bishal Ghosh, Sandipan Mohanta, Manas Kulkarni, and Bijay Kumar Agarwalla, *Impact of dephasing probes on incommensurate lattices*, J. Stat. Mech. **2024**, 063101 (2024).

# 1

# Introduction

Thermodynamic machines have profoundly shaped modern society—from the steam engines of the Industrial Revolution in 1760 to the internal combustion engines that power modern automobiles, and the advanced refrigeration systems and everyday devices we often take for granted. Converting energy from one form to another, these machines power the very infrastructure of contemporary civilization.

Traditionally, thermodynamics provides a framework for understanding energy conversion in terms of bulk or macroscopic properties of systems by focusing primarily on averages or mean values of thermodynamic quantities [1–4]. However, in recent decades, technological advancements have opened new frontiers, where the principles of thermodynamics are no longer confined to large-scale systems. Today, we possess the capability to fabricate thermodynamic machines at the mesoscopic scale, where quantum effects and stochastic fluctuations become crucial. These small-scale thermal machines–realized in experimental platforms such as quantum dots, molecular junctions, optomechanical systems, cold atoms, NV centers, and NMR setups–demand a reassessment of traditional assumptions of thermodynamics [5–27]. The inherent randomness dominates at this scale because the system is open—interacting with an environment (e.g., a heat bath) whose microscopic details are unresolved, leading to unpredictable energy exchanges. Quantum mechanics introduces additional uncertainty; for instance, conjugate variables cannot be measured precisely simultaneously. Thus, fluctuations—not just averages—govern behavior.

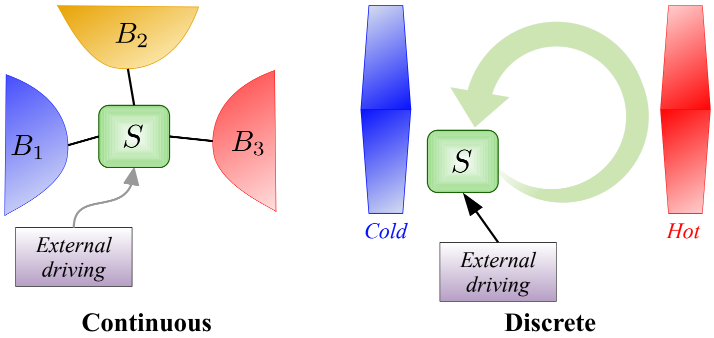


Figure 1.1: Schematic for (Left) Continuous machine: A working medium (S) couples simultaneously to multiple baths ($B_1$, $B_2$, $B_3$), with an optional external drive (faded arrow) for non-autonomous operation, and (Right) Discrete machine: The working medium alternates between hot and cold reservoirs through driven expansion/compression strokes, requiring mandatory external control (solid arrow).

Over recent decades, new disciplines such as stochastic thermodynamics and quantum thermodynamics have emerged [28–44], which incorporate fluctuations into their theoretical frameworks. One of the central themes of these disciplines is to understand and quantify how random variations in energy and particle flows influence the performance of nanoscale thermal devices [33, 42, 45–63]. Moreover, thermal and quantum fluctuations can either enhance or hinder performance, so understanding them is essential for developing a comprehensive theory of nanoscale thermodynamics and for designing devices that operate reliably in fluctuating environments [10, 17, 26, 64–71].

This thesis focuses on deriving bounds on the performance of a wide class of small-scale thermal machines, with fluctuations serving as a central theme of our analysis. A generic thermal machine typically consists of a working medium, heat and/or particle reservoirs, and a work source that drives energy consumption or extraction. In general, regardless of the underlying dynamics, thermal machines can be broadly classified into two categories [72, 73] (see Fig. 1.1):

(i) **Continuous thermal machines**–where all components are coupled to the working medium simultaneously, allowing the machine to operate in a nonequilibrium steady state (NESS). Examples include thermoelectric setups, work-to-work converters, and absorption refrigerators.

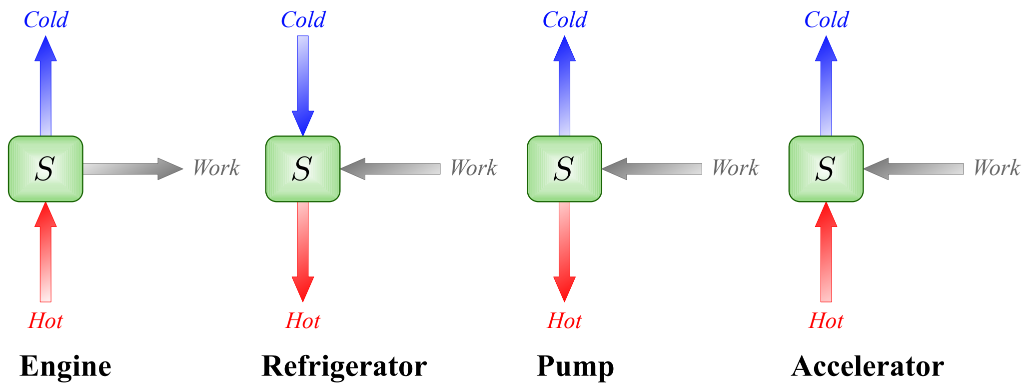


Figure 1.2: Schematic for different operational regimes of a generic thermal machine.

(ii) **Discrete thermal machines**–where not all components are coupled to the working medium simultaneously. Instead, the machine operates in a limit-cycle, as exemplified by different thermodynamic cycles such as Carnot, Otto, Stirling, Brayton, and Diesel cycles.

A thermal machine, whether continuous or discrete, operating between two heat reservoirs (hot and cold) and a work source (which could be an external drive or another heat bath), can operate in four distinct regimes, dictated by the first and second laws of thermodynamics. We follow a sign convention where energy entering the working medium is positive, and define the average heat and work fluxes as $\langle j_h \rangle$, $\langle j_c \rangle$ and $\langle j_w \rangle$, which correspond to the hot reservoir, cold reservoir, and work source, respectively. Each of these fluxes can, in principle, take positive or negative values, giving $2^3 = 8$ possible sign combinations. However, the first and second law of thermodynamics allow four permissible operational regimes [74, 75] (see Fig. 1.2):

Table 1.1: Operational Regimes of a Thermal Machine

| **Operational Regime** | **Sign Convention for Fluxes** |
|---|---|
| Engine | $\langle j_h \rangle > 0,\ \langle j_c \rangle < 0,\ \langle j_w \rangle < 0$ |
| Refrigerator | $\langle j_h \rangle < 0,\ \langle j_c \rangle > 0,\ \langle j_w \rangle > 0$ |
| Pump | $\langle j_h \rangle < 0,\ \langle j_c \rangle < 0,\ \langle j_w \rangle > 0$ |
| Accelerator | $\langle j_h \rangle > 0,\ \langle j_c \rangle < 0,\ \langle j_w \rangle > 0$ |

These regimes describe the various ways energy can be transferred between the reservoirs and the work source. The most widely studied types of machines are engines and refrigerators, and in this thesis, we focus our discussions primarily on these two operational modes.

## 1.1 Background

Thermodynamic machines operate in nonequilibrium conditions. Although equilibrium thermodynamics has a well-established and elegant structure, much less is known about universal laws governing nonequilibrium systems or processes, which are ubiquitous in nature. In fact, over the last two decades, the development of stochastic thermodynamics has substantially enriched our understanding of the thermodynamic structure of nonequilibrium mesoscopic systems. Below we describe some of the key discoveries made by stochastic thermodynamics.

### 1.1.1 Fluctuation-Dissipation theorem

Small systems are susceptible to fluctuations. The universal fluctuation-dissipation relation (FDR) states that the response of a mesoscopic system, initially prepared in thermal equilibrium, to external perturbations near equilibrium is directly related to its intrinsic equilibrium fluctuations in the absence of perturbation [76–91]. The first antecedent of this fundamental theorem was provided independently by Sutherland [92, 93], Einstein [94] and Smoluchowski [95] over a century ago, demonstrating that (the Einstein version), in the presence of an external force, the mobility $\mu$ of a Brownian particle (dissipation) is related to its diffusion constant $D$ (fluctuation), $D = \mu k_B T$. Another significant finding in line with the FDR emerged in 1928 from Johnson and Nyquist, who showed that the resistance (dissipation) of a circuit is related to the current fluctuations in the absence of a voltage bias [96, 97]. However, a formal proof of the FD theorem came in the 1950s through the work of Callen and Welton [76], and was further expanded by Green and Kubo [77–80].

### 1.1.2 Linear Response theory

In the 1930s, Lars Onsager developed his theory of linear response, showing that under small nonequilibrium constraints $\mathcal{A}_\alpha$—also known as thermodynamic affinities or biases—the thermodynamic fluxes $\langle j_\alpha \rangle$ can be expressed as linear expansions of these biases, allowing the formulation of the linear equation [98, 99]

$$\langle j_\alpha \rangle = \sum_\gamma L_{\alpha\gamma} \mathcal{A}_\gamma. \tag{1.1.1}$$

The matrix $L$, known as the Onsager matrix, contains the transport or response coefficients, $L_{\alpha\gamma} = \partial_{\mathcal{A}_\gamma} \langle j_\alpha \rangle \big|_{\{\mathcal{A}\}=0}$. In his seminal work, Onsager established that when time reversal symmetry is preserved, the Onsager matrix is symmetric, leading to the famous Onsager reciprocity relation, $L_{\alpha\gamma} = L_{\gamma\alpha}$. Moreover, positivity of entropy production, $\langle \sigma \rangle = \sum_{\alpha,\gamma} L_{\alpha\gamma} \mathcal{A}_\gamma \mathcal{A}_\alpha \geq 0$, asserts that $L$ is positive semi-definite,

$$L_{\alpha\alpha} \geq 0, \qquad \text{and} \qquad \det(L) \geq 0. \tag{1.1.2}$$

The FD theorem, furthermore, connects these response coefficients to equilibrium fluctuations [88–91, 100–103] (a detailed proof is given in the formalism section 1.2.3),

$$2L_{\alpha\gamma} = \langle\!\langle j_\alpha j_\gamma \rangle\!\rangle. \tag{1.1.3}$$

### 1.1.3 Fluctuation theorems

One of the most significant achievements of stochastic thermodynamics is the discovery of the fluctuation theorems (FTs), which have substantially extended our understanding of non-equilibrium fluctuations beyond the linear response regime [104–123].

Within the framework of stochastic thermodynamics, a system evolves along random trajectories through its phase space (in classical systems) or state space (in systems with discrete states) [44, 115]. These trajectories represent the microscopic evolution of the system under the influence of both deterministic forces (arising from potentials or external fields) and stochastic forces (such as thermal noise). To each trajectory, one can consistently assign thermodynamic quantities such as energy, entropy, work and heat [115, 117]. For every forward trajectory $\Upsilon$, there is a corresponding time-reversed trajectory $\widetilde{\Upsilon}$, where the system evolves backward in time with time-reversed forces and initial conditions. The universal FTs compare the probability of a trajectory producing heat, work, or entropy to that of its time-reversed counterpart absorbing the same quantities. One such example is

$$\frac{P_{\Upsilon}(\Delta s_{\text{tot}})}{P_{\tilde{\Upsilon}}(-\Delta s_{\text{tot}})} = e^{\Delta s_{\text{tot}}}, \tag{1.1.4}$$

where $P_{\Upsilon}(\Delta s_{\text{tot}})$ represents the probability of total entropy production $\Delta s_{\text{tot}}$ along the forward-trajectory $\Upsilon$. In general, FTs take the form [36, 124]:

$$\frac{P_f(\mathbf{x})}{P_r(-\mathbf{x})} = e^{\alpha \mathbf{x}} \tag{1.1.5}$$

where $\alpha$ is a real constant related either to the equilibrium properties of the system's initial state or to nonequilibrium constraints determining a NESS. $P_f(\mathbf{x})$ and $P_r(\mathbf{x})$ denote the probabilities of observing a given quantity $\mathbf{x}$ along the forward and the backward/reverse processes, respectively. These relations are known as detailed FTs [35, 119].

By utilizing the normalization the reverse process probability, $\int d\mathbf{x} P_r(\mathbf{x}) = 1$, we arrive at integral fluctuation theorems [35, 119], which can be written as

$$\langle e^{-\alpha \mathbf{x}} \rangle = 1. \tag{1.1.6}$$

Applying Jensen's inequality, $\langle e^X \rangle \geq e^{\langle X \rangle}$, leads to a second law-type inequality: $\langle \alpha \mathbf{x} \rangle \geq 0$. The integral FTs are considered a major breakthrough in modern thermodynamics, as they refine traditional second law inequalities into equalities.

In addition to the general form of the fluctuation theorems presented, several specific FTs have been pivotal in shaping our understanding of nonequilibrium thermodynamics. For instance, the **Jarzynski equality** [104, 105] links nonequilibrium work to equilibrium free energy changes, while **Crooks FT** [106, 107] provides a detailed relationship between forward and reverse work distributions. The **Evans–Searles FT** [108] highlights the probabilistic nature of entropy production during transient processes, and the **Gallavotti-Cohen FT** [112] extends this to systems in NESS, establishing a relationship between entropy production and its fluctuations. The **Hatano-Sasa FT** [110] refines the second law for systems driven between nonequilibrium steady states, quantifying the excess entropy produced during these transitions. These theorems provide a robust framework for understanding fluctuations across a wide range of nonequilibrium processes.

However, the problems discussed in this thesis are primarily quantum in nature. Extending the trajectory-based derivations of FTs to the quantum regime is not straightforward for several reasons: (i) the lack of a clear trajectory picture in quantum systems, and (ii) the difficulty in defining quantities like work and heat, due to the noncommutative nature of quantum operators at different times. Despite these challenges, the two-time projective measurement (TPM) scheme has proven useful in obtaining probability distributions for fluctuating quantities in quantum systems, leading to various quantum FTs [35, 125–128]. We will explore this issue in more detail in the formalism section 1.2.2.

### 1.1.4 Thermodynamic Uncertainty Relations

Another crucial discovery of Stochastic thermodynamics is the Thermodynamic Uncertainty Relations (TURs), introduced relatively recently [129–131]. The TURs establish a fundamental trade-off between the precision of a thermodynamic current and the associated dissipation [42, 43, 129–144]. Precision is quantified by the relative fluctuation of a current, defined as the ratio $\langle\langle j_\alpha^2\rangle\rangle/\langle j_\alpha\rangle^2$, where $\langle j_\alpha\rangle$ is the mean current and $\langle\langle j_\alpha^2\rangle\rangle$ represents the variance, or fluctuation around this mean value. Dissipation, on the other hand, is given by the average total entropy production rate $\langle\sigma\rangle$. The TUR, proposed by Barato and Seifert [129], is stated as

$$\langle\sigma\rangle \frac{\langle\langle j_\alpha^2\rangle\rangle}{\langle j_\alpha\rangle^2} \geq 2k_B \quad \forall\alpha. \tag{1.1.7}$$

Here, we explicitly show the Boltzmann constant $k_B$ for dimensional clarity. Throughout this work, we set $k_B = 1$, unless otherwise noted. This inequality was first derived in the context of biochemical networks [129], and later rigorously proved using large deviation theory [130, 145]. However, this traditional form of the TUR has limited applicability, as it assumes the system follows continuous-time Markovian dynamics and operates in or near a NESS [145, 146]. Importantly, in the linear response regime–when time reversal symmetry is preserved–the original TUR inequality (1.1.7) holds [132].

In recent years, substantial efforts have been made to generalize the TURs to various contexts, such as discrete-time Markov chains [147, 148], Bayesian networks [149], deterministic chemical reaction networks [150], first-passage times [151, 152], finite-time statistics [145, 146, 153, 154], periodically driven systems [155, 156], measurement and feedback control [157–159], broken time-reversal symmetric systems [160], active matter systems [161, 162], and quantum Markovian dynamics [143, 163]. Particularly, the fluctuation theorems have been shown to impose bounds on precision by involving exponentiated entropy production [133–136],

$$\frac{\langle\langle j_\alpha^2\rangle\rangle}{\langle j_\alpha\rangle^2} \geq \frac{2}{e^{\langle\sigma\rangle}-1}. \tag{1.1.8}$$

## 1.2 Formalism

### 1.2.1 Two-time projective measurements and Full Counting Statistics

We consider a isolated system, possibly driven, initialized at $\rho(0)$. Its dynamics is governed by von Neumann equation:

$$\frac{d}{dt}\rho(t) = -i[H(t),\rho(t)]. \tag{1.2.1}$$

The formal solution is given by

$$\rho(t) = U(t,0)\rho(0)U^\dagger(t,0), \tag{1.2.2}$$

where the unitary propagator is

$$U(t,0) = \mathcal{T}_+ \exp\Big[-\frac{i}{\hbar}\int_0^t H(t')\,dt'\Big]. \tag{1.2.3}$$

Here, $\mathcal{T}_+$ is the time-ordering operator that arranges the operators from left to right with decreasing time.

Let $O(t)$ be an observable of interest in the Schrödinger picture. The explicit time dependence in $O(t)$ solely originates from an external driving. The operator

$O(t)$ in its eigenbasis can be written as

$$O(t) = \sum_{o_t} o_t |o_t\rangle\langle o_t| = \sum_{o_t} o_t \Pi_{o_t}, \tag{1.2.4}$$

where $o_t$ are the instantaneous eigenvalues and $\Pi_{o_t} = |o_t\rangle\langle o_t|$ are the projection operators.

(I) The first projective measurement of $O(t)$ occurs at $t = 0$. According to the measurement postulate of quantum mechanics, the possible outcomes of this measurement come from the set of eigenvalues $\{o_0\}$ of the operator $O(0)$. The probability of obtaining an outcome $o_0$ is given by

$$P(o_0) = \mathrm{Tr}[\Pi_{o_0}\rho(0)\Pi_{o_0}]. \tag{1.2.5}$$

The post-measurement state will be an eigenstate of $O(0)$

$$\rho'(0) = \frac{\Pi_{o_0}\rho(0)\Pi_{o_0}}{\mathrm{Tr}[\Pi_{o_0}\rho(0)\Pi_{o_0}]} \tag{1.2.6}$$

(II) The post-measurement state $\rho'(0)$ is then allowed to evolve according to (1.2.2) up to time $t$ when a second projective measurement of $O(t)$ is performed. The outcome of this second measurement will be an eigenvalue of $O(t)$. The conditional probability of obtaining $o_t$ given that the first outcome was $o_0$ is given by

$$P(o_t|o_0) = \mathrm{Tr}\left[\Pi_{o_t}U(t,0)\rho'(0)U^\dagger(t,0)\Pi_{o_t}\right] \tag{1.2.7}$$

From (1.2.5) and (1.2.7) we construct the joint probability to measure $o_0$ at time 0 and $o_t$ at time $t$ as

$$\begin{aligned} P(o_t; o_0) &= P(o_t|o_0)P(o_0) \\ &= \mathrm{Tr}\left[\Pi_{o_t}U(t,0)\Pi_{o_0}\rho(0)\Pi_{o_0}U^\dagger(t,0)\Pi_{o_t}\right]. \end{aligned} \tag{1.2.8}$$

From now on, we will consider the case $[\rho(0), O(0)] = 0$.

The probability distribution (PD) for the difference $\Delta o = o_t - o_0$ between the outputs of the two consecutive measurements is given by

$$P(\Delta o) = \sum_{o_0,o_t} \delta\{\Delta o - (o_t - o_0)\} P(o_t; o_0) \tag{1.2.9}$$

The characteristic function (CF) is given by the Fourier transformation of the PD in (1.2.9),

$$\begin{aligned}
\mathcal{G}(\chi) &= \int d(\Delta o)\, e^{i\chi\,\Delta o}\, P(\Delta o) \\
&= \sum_{o_0,o_t} e^{i\chi(o_t - o_0)} P(o_t; o_0) \\
&= \sum_{o_0,o_t} e^{i\chi(o_t - o_0)}\, \mathrm{Tr}\left[U^\dagger(t,0)\Pi_{o_t} U(t,0)\Pi_{o_0}\rho(0)\Pi_{o_0}\right] \\
&= \sum_{o_0,o_t} \mathrm{Tr}\left[U^\dagger(t,0)\Pi_{o_t} e^{i\chi O(t)} U(t,0) e^{-i\chi O(0)}\Pi_{o_0}\rho(0)\Pi_{o_0}\right] \\
&= \langle e^{i\chi O^H(t)} e^{-i\chi O(0)}\rangle_{\rho(0)},
\end{aligned} \tag{1.2.10}$$

where $O^H(t) = U^\dagger(t,0) O U(t,0)$ is the observable $O$ in the Heisenberg picture, and $\chi$ is known as the counting field. To reach the final form of the characteristic function (CF) in (1.2.10), we utilized the properties of the projection operators (i) $\Pi^2_{o_{0,t}} = \Pi_{o_{0,t}}$, (ii) $\sum_{o_0} \Pi_{o_0} = \sum_{o_t} \Pi_{o_t} = 1$, and (iii) $[\rho(0), \Pi_{o_0}] = 0$.

The Full Counting Statistics (FCS) framework allows us to analyze the complete probability distribution of the observable $\Delta o$, capturing not only the average quantities but also the higher-order moments and fluctuations. The characteristic function $\mathcal{G}(\chi)$ serves as a generating function for these moments. Specifically, the $n$th moment $\langle \Delta o^n \rangle$ of the distribution $P(\Delta o)$ is obtained via

$$\langle \Delta o^n \rangle = (-i)^n \frac{\partial^n}{\partial \chi^n} \mathcal{G}(\chi)\Big|_{\chi=0} \tag{1.2.11}$$

However, to describe the fluctuations more effectively, it is convenient to work with the cumulants rather than moments. The cumulant generating function (CGF) is defined as the natural logarithm of the CF, $\ln \mathcal{G}(\chi)$. The $n$th cumulant $\langle\langle \Delta o^n \rangle\rangle$ is then given by

$$\langle\!\langle \Delta o^n \rangle\!\rangle = (-i)^n \frac{\partial^n}{\partial \chi^n} \ln \mathcal{G}(\chi) \Big|_{\chi=0} \tag{1.2.12}$$

The first cumulant coincides with the first moment, providing the mean $\langle \Delta o \rangle$. Of particular interest in this thesis is the second cumulant, or the variance, $\langle\!\langle \Delta o^2 \rangle\!\rangle = \langle \Delta o^2 \rangle - \langle \Delta o \rangle^2$, which quantifies the fluctuations around the mean.

### 1.2.2 Quantum fluctuation theorems

***Time-reversed probability*:** In the time-reversed evolution, the 'final' density matrix from the forward quantum evolution in (1.2.2) is mapped back to its initial state. The initial condition of the time-reversed evolution is given by $\widetilde{\rho}(0)$. It is important to avoid the assumption that $\widetilde{\rho}(0) = \rho(t)$ because the initial state of the reverse process depends on the specific physical scenario being considered. This distinction will be clarified at the end of this section, and also with particular physical scenarios in the subsequent subsections: such as when work is performed on an isolated system initially in a thermal state, or when heat and matter are exchanged between systems initially prepared in product equilibrium states.

The evolution of the system in the reverse process is described by $\widetilde{\rho}(t) = U_r(t,0)\widetilde{\rho}(0)U_r^\dagger(t,0)$, where $U_r(t,0) = \Theta U^\dagger(t,0)\Theta^\dagger$ with $\Theta$ being the antiunitary time reversal operator. Additionally, we will consider the case where $[O(t), \widetilde{\rho}(0)] = 0$, ensuring the same compatibility between the observable and the initial condition of the reverse process as was assumed for the forward process above.

The joint PD for measuring $o_t$ at time 0 and $o_0$ at time $t$ in the reverse process is denoted by $P_r(o_0; o_t)$. In the previous section, while we discussed two-point measurements and joint probability distributions, we did not explicitly associate them with the forward process. To clarify, we now designate those quantities as part of the forward process by adding the subscript $f$.

Similar to the forward evolution, we define the probability to measure the difference $\Delta o = o_0 - o_t$ between the two successive measurements in the reverse process by

$$P_r(\Delta o) = \sum_{o_0, o_t} \delta\{\Delta o - (o_0 - o_t)\} P_r(o_0; o_t), \tag{1.2.13}$$

which we refer to as the time-reversed probability. The Fourier transform of this probability distribution yields the time-reversed CF:

$$\begin{aligned} \mathcal{G}_r(\chi) &= \int d(\Delta o)\, e^{i\chi\,\Delta o}\, P_r(\Delta o) \\ &= \sum_{o_0, o_t} e^{-i\chi(o_t - o_0)} P_r(o_0; o_t). \end{aligned} \tag{1.2.14}$$

***General quantum FT*:** We define the associated irreversible entropy change for the forward process as

$$\Xi_f(o_t; o_0) = \ln \frac{P_f(o_t; o_0)}{P_r(o_0; o_t)} = \ln \frac{\langle o_0 | \rho(0) | o_0 \rangle}{\langle o_t | \widetilde{\rho}(0) | o_t \rangle}, \tag{1.2.15}$$

and for the reverse process as

$$\Xi_r(o_0; o_t) = \ln \frac{P_r(o_0; o_t)}{P_f(o_t; o_0)} = -\Xi_f(o_t; o_0) \tag{1.2.16}$$

These results follow from (1.2.8) by noting that (i) Joint probabilities factorize as $P_f(o_t; o_0) = P_f(o_t|o_0)P(o_0)$ and $P_r(o_0; o_t) = P_r(o_0|o_t)P(o_t)$; (ii) Microreversibility ensures $P_f(o_t|o_0) = P_r(o_0|o_t)$, reducing the entropy production to the logarithm of ratio of initial probabilities.

Similar to (1.2.9) and (1.2.13), we define the probabilities

$$P_f(\Xi) = \sum_{o_0, o_t} \delta\{\Xi - \Xi_f(o_t; o_0)\}\, P_f(o_t; o_0) \tag{1.2.17}$$

$$P_r(\Xi) = \sum_{o_0, o_t} \delta\{\Xi - \Xi_r(o_0; o_t)\}\, P_r(o_0; o_t) \tag{1.2.18}$$

This leads to the detailed fluctuation theorem

$$P_f(\Xi) = \sum_{o_0, o_t} \delta\{\Xi - \Xi_f(o_t; o_0)\}\, e^{\Xi_f(o_t; o_0)} P_r(o_t; o_0)$$

$$
\begin{aligned}
&= e^{\Xi} \sum_{o_0, o_t} \delta\{\Xi + \Xi_r(o_0; o_t)\}\, P_r(o_0; o_t) \\
&= e^{\Xi}\, P_r(-\Xi), \qquad (1.2.19)
\end{aligned}
$$

or equivalently

$$
\frac{P_f(\Xi)}{P_r(-\Xi)} = e^{\Xi}. \qquad (1.2.20)
$$

From this detailed FT (1.2.20) we can derive the integral FT,

$$
\langle e^{-\Xi} \rangle_f = 1, \qquad (1.2.21)
$$

which, according to Jensen's inequality, leads to a second law-type inequality $\langle \Xi \rangle_f \geq 0$.

It should be noted that the FTs expressed in equations (1.2.20) and (1.2.21) are physically meaningful only if the quantity $\Xi$ is a measurable physical observable. In this context, the assumptions $[O(0), \rho(0)] = 0$ and $[O(t), \widetilde{\rho}(0)] = 0$ play a crucial role. For example, under these assumptions, we find that

$$
\begin{aligned}
\langle \Xi \rangle_f &= \sum_{o_0, o_t} \Xi_f(o_t, o_0) P_f(o_t, o_0) \\
&= \sum_{o_0, o_t} \ln \frac{\langle o_0 | \rho(0) | o_0 \rangle}{\langle o_t | \widetilde{\rho}(0) | o_t \rangle} |\langle o_t | U(t, 0) | o_0 \rangle|^2 \langle o_0 | \rho(0) | o_0 \rangle \\
&= \sum_{o_0} \langle o_0 | \rho(0) | o_0 \rangle \ln \langle o_0 | \rho(0) | o_0 \rangle - \sum_{o_t} \langle o_t | \rho(t) | o_t \rangle \ln \langle o_t | \widetilde{\rho}(0) | o_t \rangle \\
&= \mathrm{Tr}[\rho(0) \ln \rho(0)] - \mathrm{Tr}[\rho(t) \ln \widetilde{\rho}(0)] \\
&= \mathrm{Tr}[\rho(t) \{\ln \rho(t) - \ln \widetilde{\rho}(0)\}] \\
&\geq 0, \qquad (1.2.22)
\end{aligned}
$$

which is recognized as the Kullback-Leibler divergence, or relative entropy, between $\rho(t)$ and $\widetilde{\rho}(0)$. Since relative entropy is always non-negative, this ensures the second law of thermodynamics is satisfied.

### Crooks FT and Jarzynski equality

The stochastic work done on an isolated driven quantum system, initialized at a thermal state with respect to inverse temperature $\beta$, is determined by measuring the energy of the system $H(t)$ at the initial time $t = 0$ and then at the final time $t$, yielding $w = E_t - E_0$. In this context, the observable $O(t)$ coincides with $H(t)$. The initial density matrices for the forward and the reverse processes are given by

$$\rho(0) = \frac{e^{-\beta H(0)}}{\mathrm{Tr}[e^{-\beta H(0)}]} = e^{-\beta[H(0)-F(0)]} \quad \text{and} \quad \widetilde{\rho}(0) = \frac{e^{-\beta H(t)}}{\mathrm{Tr}[e^{-\beta H(t)}]} = e^{-\beta[H(t)-F(t)]}, \tag{1.2.23}$$

where the free energy $F(t) = -\beta^{-1} \ln Z(t)$and the partition function is $Z(t) = \mathrm{Tr}[e^{-\beta H(t)}]$. Given that $[H(0), \rho(0)] = 0$ and $[H(t), \widetilde{\rho}(0)] = 0$, the CF corresponding to the work-PD is is derived from (1.2.10),

$$\mathcal{G}(\chi) = \langle e^{i\chi H^H(t)}\, e^{-i\chi H(0)} \rangle_{\rho(0)} \tag{1.2.24}$$

Additionally, from (1.2.15), we can identify

$$\Xi_f(E_t; E_0) = \beta[(E_t - E_0) - \Delta F] = \beta w_d, \tag{1.2.25}$$

where, the free energy difference is $\Delta F = F(t) - F(0)$, and $w_d = w - \Delta F$ represents the dissipated work. The Crooks FT [106, 107] follows from (1.2.20),

$$\frac{P_f(+\beta w_d)}{P_r(-\beta w_d)} = e^{\beta w_d}. \tag{1.2.26}$$

This relation can be reformulated in terms of the total work $w$ [126],

$$\frac{P_f(+w)}{P_r(-w)} = e^{\beta(w-\Delta F)}. \tag{1.2.27}$$

The corresponding integrated FT, as presented in (1.2.21), is known as the Jarzynski equality [104, 125, 128],

$$\langle e^{-\beta(w-\Delta F)} \rangle_f = 1, \tag{1.2.28}$$

Furthermore, by applying Jensen's inequality, we obtain a second law-type inequality: $\langle w \rangle_f \geq \Delta F$. Note that for a cyclic process, where $\Delta F = 0$, this result reduces to the standard Kelvin statement of the second law.

### Quantum exchange FT

We consider a system with the total Hamiltonian $H = H_A + H_B + V$, where the total system is partitioned into two subsystems $A$ and $B$, and $V$ represents a weak interaction between them. No external driving is present. The energy $E_A$ and the number of particles $N_A$ of subsystem $A$ are measured at times 0 and $t$. Initially, both subsystems are assumed to be in grand canonical equilibrium, with $\beta_i$ and $\mu_i$ being their respective inverse temperatures and chemical potentials ($i = A, B$). The initial density matrix for both forward and reverse processes is given by:

$$\rho(0) = \widetilde{\rho}(0) = \frac{e^{-\beta_A(H_A - \mu_A N_A)}}{\mathrm{Tr}\left[e^{-\beta_A(H_A - \mu_A N_A)}\right]} \cdot \frac{e^{-\beta_B(H_B - \mu_B N_B)}}{\mathrm{Tr}\left[e^{-\beta_B(H_B - \mu_B N_B)}\right]}. \tag{1.2.29}$$

This assumption is valid when the interaction $V$ is initially negligible. At time $t = 0$, the first measurement is performed, then the interaction $V$ is turned on, allowing for energy and particle exchange between the subsystems. After evolving under the total Hamiltonian $H$ for a time $t$, the interaction $V$ is turned off, and the second measurement is made.

In the absence of interaction, the particle numbers in each subsystems are conserved, allowing simultaneous measurement of energy and particle number. When measuring both subsystems, the joint PDs for the forward and reverse processes are:

$$P_f(\Phi_t^{\{A,B\}}; \Phi_0^{\{A,B\}}) = |\langle \Phi_t^{\{A,B\}} | U(t,0) | \Phi_0^{\{A,B\}} \rangle|^2 \langle \Phi_0^{\{A,B\}} | \rho(0) | \Phi_0^{\{A,B\}} \rangle, \tag{1.2.30}$$

and

$$\begin{aligned} P_r(\Phi_0^{\{A,B\}}; \Phi_t^{\{A,B\}}) &= |\langle \Phi_0^{\{A,B\}} | \Theta U^\dagger(t,0) \Theta^\dagger | \Phi_t^{\{A,B\}} \rangle|^2 \langle \Phi_t^{\{A,B\}} | \widetilde{\rho}(0) | \Phi_t^{\{A,B\}} \rangle \\ &= |\langle \Phi_t^{\{A,B\}} | U(t,0) | \Phi_0^{\{A,B\}} \rangle|^2 \langle \Phi_t^{\{A,B\}} | \widetilde{\rho}(0) | \Phi_t^{\{A,B\}} \rangle \end{aligned} \tag{1.2.31}$$

where $\Phi^{\{A,B\}}$ represents the measurement outcomes $\{E_A, N_A, E_B, N_B\}$. The irreversible entropy exchange between subsystems, as follows from (1.2.15), is given by

$$\begin{aligned}\Xi[\Phi_t^{\{A,B\}};\Phi_0^{\{A,B\}}] = &-\beta_A\big[E_A^0 - E_A^t - \mu_A(N_A^0 - N_A^t)\big]\\ &-\beta_B\big[E_B^0 - E_B^t - \mu_B(N_B^0 - N_B^t)\big]\end{aligned} \tag{1.2.32}$$

Under the weak coupling assumption, energy conservation holds approximately, allowing the change in energy of each subsystem to be interpreted as heat,

$$E_A^0 - E_A^t \approx -(E_B^0 - E_B^t). \tag{1.2.33}$$

For strong couplings, this interpretation breaks down as system-environment correlations become non-negligible. Additionally, particle number conservation,

$$N_A^0 + N_B^0 = N_A^t + N_B^t \tag{1.2.34}$$

holds true.

Using these conservation laws, the entropy production given in (1.2.32) can be further simplified in terms of the measured quantities $E_A$ and $N_A$ for subsystem $A$,

$$\begin{aligned}\Xi[\Phi_t^{\{A\}};\Phi_0^{\{A\}}] \approx &-(\beta_B - \beta_A)(E_A^t - E_A^0) - (\mu_A\beta_A - \mu_B\beta_B)(N_A^t - N_A^0)\\ = &-\mathcal{A}_h(E_A^t - E_A^0) - \mathcal{A}_m(N_A^t - N_A^0)\\ = &-\mathcal{A}_h\Delta E_A - \mathcal{A}_m\Delta N_A,\end{aligned} \tag{1.2.35}$$

where $\Delta E_A = E_A^t - E_A^0$ and $\Delta N_A = N_A^t - N_A^0$ denote the changes in energy and particle number of subsystem $A$, and $\mathcal{A}_h = \beta_B - \beta_A$, $\mathcal{A}_m = \mu_A\beta_A - \mu_B\beta_B$ are the nonequilibrium constraints for heat and particle exchange, respectively. These correspond to the thermodynamic affinities in response theory. From this, using (1.2.20), the detailed fluctuation theorem follows:

$$\frac{P(\Delta E_A, \Delta N_A)}{P(-\Delta E_A, -\Delta N_A)} = e^{\mathcal{A}_h\Delta E_A + \mathcal{A}_m\Delta N_A} \tag{1.2.36}$$

The above relation is known as quantum exchange FT [114]. The $f$ and $r$ subscripts are dropped because the forward and reversed probabilities are identical in this case, $P_f(\Delta E_A, \Delta N_A) = P_r(\Delta E_A, \Delta N_A)$. Note that, $\mathcal{A}_h = \mathcal{A}_m = 0$ corresponds to an equilibrium situation, where the detailed balance $P(\Delta E_A, \Delta N_A) = P(-\Delta E_A, -\Delta N_A)$

is satisfied. In terms of CF, the exchange FT is expressed as

$$\mathcal{G}(\chi_h, \chi_m) = \mathcal{G}(-\chi_h + i\mathcal{A}_h, -\chi_m + i\mathcal{A}_m), \tag{1.2.37}$$

where $\chi_h$ and $\chi_m$ are the counting fields for heat and matter exchange, respectively.

### Steady-state FT

We now present some qualitative arguments to show how the quantum exchange fluctuation theorem (FT) derived in equation (1.2.36) can be extended to obtain a quantum steady-state FT for heat and particle exchange between two macroscopic reservoirs through a mesoscopic system.

To this end, we consider subsystems $A$ and $B$ as macroscopic reservoirs, with their respective Hamiltonians denoted by $H_A$ and $H_B$. The interaction term $V$ now consists of $V = H_S + H_{AS} + H_{BS}$, where $H_S$ represents a finite mesoscopic system, and $H_{AS}$ and $H_{BS}$ are weak interaction terms coupling the system to reservoirs $A$ and $B$, respectively. The energy $E_A$ and the number of particles $N_A$ of reservoir $A$ are measured at times 0 and $t$.

In the $t \to \infty$ limit, the system $S$ is assumed to reach a NESS. Due to the finiteness of the system $S$ and the weak system-bath couplings $H_{AS}$ and $H_{BS}$, the energy and particles lost (or gained) by the reservoir $A$ are transferred to (or lost from) the reservoir $B$, with negligible contribution from the system itself. Therefore, for the total irreversible entropy production, equation (1.2.32) approximately holds:

$$\begin{aligned}\Xi[\Phi_t^{\{S,A,B\}}; \Phi_0^{\{S,A,B\}}] \approx &-\beta_A\big[E_A^0 - E_A^t - \mu_A(N_A^0 - N_A^t)\big] \\ &-\beta_B\big[E_B^0 - E_B^t - \mu_B(N_B^0 - N_B^t)\big] \\ &+ O(E_S^t - E_S^0) + O(N_S^t - N_S^0),\end{aligned} \tag{1.2.38}$$

Since energy and particle number conservation approximately hold [cf. (1.2.33) and (1.2.34)], the irreversible entropy production can be further simplified in terms of the measured quantities $E_A$ and $N_A$ for reservoir $A$ [cf. (1.2.35)], leading to

$$\Xi[\Phi_t^{\{A\}}; \Phi_0^{\{A\}}] \approx -\mathcal{A}_h\Delta E_A - \mathcal{A}_m\Delta N_A + O(E_S^t - E_S^0) + O(N_S^t - N_S^0) \tag{1.2.39}$$

where $\Delta E_A = E_A^t - E_A^0$ and $\Delta N_A = N_A^t - N_A^0$ denote the changes in energy and particle number of reservoir $A$, and $\mathcal{A}_h = \beta_B - \beta_A$, $\mathcal{A}_h = \mu_A\beta_A - \mu_B\beta_B$ are the nonequilibrium constraints for heat and particle exchange, respectively.

For long times, a universal steady-state FT for the heat and particle currents emerges, which is independent of system-specific properties [35, 164]:

$$\lim_{t\to\infty} \frac{1}{t} \ln \frac{P(\Delta E_A, \Delta N_A)}{P(-\Delta E_A, -\Delta N_A)} = \mathcal{A}_h\, j_h + \mathcal{A}_m\, j_m \tag{1.2.40}$$

where $j_h = \Delta E_A/t$ and $j_m = \Delta N_A/t$ are the heat and matter fluxes flowing between the system and reservoir $A$. The corresponding scaled cumulant generating function (SCGF), defined as

$$\mathcal{Q}(\chi_h, \chi_m) = \lim_{t\to\infty} \frac{1}{t} \ln \mathcal{G}(\chi_h, \chi_m), \tag{1.2.41}$$

satisfies the symmetry relation

$$\mathcal{Q}(\chi_h, \chi_m) = \mathcal{Q}(-\chi_h + i\mathcal{A}_h, -\chi_m + i\mathcal{A}_m). \tag{1.2.42}$$

It should be noted that cumulants of steady state currents can be directly computed from $\mathcal{Q}(\chi_h, \chi_m)$ by taking derivatives with respect to the counting fields $\chi_h$ and $\chi_m$,

$$\langle\langle j_h^k j_m^l \rangle\rangle = \frac{\partial^k \partial^l}{\partial(i\chi_h)^k \partial(i\chi_m)^l} \mathcal{Q}(\chi_h, \chi_m)\Big|_{\{\chi\}=0}. \tag{1.2.43}$$

### 1.2.3 Linear response and Fluctuation-Dissipation from Fluctuation Theorem

In this section, we provide a straightforward derivation of Onsager's linear response theory using the steady-state fluctuation theorem (FT), leading to Onsager's reciprocity relations and the fluctuation-dissipation theorem.

We begin with an abstract formulation of the symmetry relation given by equation (1.2.42),

$$\mathcal{Q}^{\mathcal{A}_1,\mathcal{A}_2}(\chi_1, \chi_2) = \mathcal{Q}^{\mathcal{A}_1,\mathcal{A}_2}(-\chi_1 + i\mathcal{A}_1, -\chi_2 + i\mathcal{A}_2), \tag{1.2.44}$$

which directly reflects a steady-state FT of the form

$$\lim_{t\to\infty} \frac{1}{t} \ln \frac{P^{\mathcal{A}_1,\mathcal{A}_2}(\Delta I_1, \Delta I_2)}{P^{\mathcal{A}_1,\mathcal{A}_2}(-\Delta I_1, -\Delta I_2)} = \mathcal{A}_1\, j_1 + \mathcal{A}_2\, j_2, \tag{1.2.45}$$

where $j_1 = \Delta I_1/t$ and $j_2 = \Delta I_2/t$ are two independent currents and $\mathcal{A}_1$, $\mathcal{A}_2$ are the two corresponding nonequilibrium constraints–or affinities. $\Delta I_1$ and $\Delta I_2$ are the net amount of charges of type 1 and 2 transferred through the system during time $t$ [cf. (1.2.40)]. The SCGF $\mathcal{Q}(\chi_h, \chi_m)$ in (1.2.44) is defined as

$$\begin{aligned}\mathcal{Q}^{\mathcal{A}_1,\mathcal{A}_2}(\chi_1, \chi_2) &= \lim_{t\to\infty} \frac{1}{t} \ln \mathcal{G}^{\mathcal{A}_1,\mathcal{A}_2}(\chi_1, \chi_2) \\ &= \lim_{t\to\infty} \frac{1}{t} \ln \int d(\Delta I_1) \int d(\Delta I_2) e^{i\chi_1 \Delta I_1} e^{i\chi_2 \Delta I_2} P^{\mathcal{A}_1,\mathcal{A}_2}(\Delta I_1, \Delta I_2)\end{aligned} \tag{1.2.46}$$

We note down some important properties of this SCGF:

(i) $\mathcal{Q}^{\mathcal{A}_1,\mathcal{A}_2}(0,0) = 0$, arises from the normalization of the probability distribution $P^{\mathcal{A}_1,\mathcal{A}_2}(\Delta I_1, \Delta I_2)$ in (1.2.46).

(ii) $\mathcal{Q}^{\mathcal{A}_1,\mathcal{A}_2}(i\mathcal{A}_1, i\mathcal{A}_2) = 0$, arises from the symmetry relation (1.2.44).

(iii) In equilibrium (i.e. in absence of the affinities) $\mathcal{Q}^{0,0}(\chi_1, \chi_2) = \mathcal{Q}^{0,0}(-\chi_1, -\chi_2)$.

(iv) The cumulants of the currents are calculated via via

$$\langle\langle j_1^k j_2^l \rangle\rangle = \frac{\partial^k \partial^l}{\partial(i\chi_1)^k \partial(i\chi_2)^l} \mathcal{Q}^{\mathcal{A}_1,\mathcal{A}_2}(\chi_1, \chi_2)\Big|_{\{\chi\}=0}, \tag{1.2.47}$$

which is abbreviated as

$$\langle\langle j_1^k j_2^l \rangle\rangle = (-i)^{k+l} \partial_{\chi_1}^k \partial_{\chi_2}^l \mathcal{Q}^{\mathcal{A}_1,\mathcal{A}_2}(0,0). \tag{1.2.48}$$

Differentiating both sides of equation (1.2.44) with respect to counting field $\chi_\alpha$ ($\alpha$ can take values 1 and 2) and using the definition given in (1.2.46) and the FT in (1.2.45) yields

$$\frac{\partial}{\partial \chi_\alpha} \mathcal{Q}^{\mathcal{A}_1,\mathcal{A}_2}(\chi_1, \chi_2) = -\frac{\partial}{\partial \chi_\alpha} \mathcal{Q}^{\mathcal{A}_1,\mathcal{A}_2}(-\chi_1 + i\mathcal{A}_1, -\chi_2 + i\mathcal{A}_2), . \tag{1.2.49}$$

In the equilibrium limit, this leads to the expected result $\partial_{\chi_\alpha} \mathcal{Q}^{0,0}(0,0) = 0$, indicating that, on average, no current flows.

In the small affinity limit (linear response), we can express the average current as a Taylor expansion:

$$\begin{aligned}
\langle j_\alpha \rangle &= -i\partial_{\chi_\alpha} \mathcal{Q}^{\mathcal{A}_1,\mathcal{A}_2}(0,0) \\
&= -i\partial_{\chi_\alpha} \mathcal{Q}^{0,0}(0,0) - i \sum_{\gamma=1,2} \mathcal{A}_\gamma \, \partial_{\chi_\alpha} \partial_{\mathcal{A}_\gamma} \mathcal{Q}^{0,0}(0,0) + O(\mathcal{A}^2) \\
&= \sum_{\gamma=1,2} L_{\alpha\gamma} \mathcal{A}_\gamma, \qquad (1.2.50)
\end{aligned}$$

where we identify the response coefficients as

$$L_{\alpha\gamma} = -i\partial_{\chi_\alpha} \partial_{\mathcal{A}_\gamma} \mathcal{Q}^{0,0}(0,0). \qquad (1.2.51)$$

The right hand side of the above identity should be interpreted as (i) first, differentiate with respect to $\mathcal{A}_\gamma$, (ii) then take the limit $\{\mathcal{A}\} \equiv \{\mathcal{A}_1, \mathcal{A}_2\} \to 0$ (iii) next, differentiate with respect to $\chi_\alpha$, and (iv) finally, take the limit $\{\chi\} \equiv \{\chi_1, \chi_2\} \to 0$. Steps (ii) and (iii) are interchangeable.

Now, differentiating equation (1.2.44) with respect to affinity $\mathcal{A}_\gamma$ (where $\gamma = 1, 2$) yields

$$\frac{\partial}{\partial \mathcal{A}_\gamma} \mathcal{Q}^{\mathcal{A}_1,\mathcal{A}_2}(\chi_1, \chi_2) = \frac{\partial}{\partial \mathcal{A}_\gamma} \mathcal{Q}^{\mathcal{A}_1,\mathcal{A}_2}(-\chi_1, -\chi_2) - i\frac{\partial}{\partial \chi_\gamma} \mathcal{Q}^{\mathcal{A}_1,\mathcal{A}_2}(-\chi_1, -\chi_2). \qquad (1.2.52)$$

The above relation we have exploits the definition of SCGF in (1.2.46) and the FT in (1.2.45).

Next, we differentiate equation (1.2.52) with respect to $\chi_\alpha$, while taking into account (1.2.49), and then we take the limit $\{\chi\} \to 0$:

$$2\,\frac{\partial^2}{\partial \chi_\alpha \partial \mathcal{A}_\gamma} \mathcal{Q}^{0,0}(0,0) = -i\frac{\partial^2}{\partial \chi_\alpha \partial \chi_\gamma} \mathcal{Q}^{0,0}(0,0), \qquad (1.2.53)$$

Therefore, we can establish that the response coefficients are symmetric and can be expressed as follows:

$$\begin{aligned}
L_{\alpha\gamma} = L_{\gamma\alpha} =& - i\frac{\partial^2}{\partial\chi_\alpha\partial\mathcal{A}_\gamma}\mathcal{Q}^{0,0}(0,0)\\
=&\frac{(-i)^2}{2}\frac{\partial^2}{\partial\chi_\alpha\partial\chi_\gamma}\mathcal{Q}^{0,0}(0,0)\\
=&\frac{1}{2}\langle\langle j_\alpha j_\gamma\rangle\rangle
\end{aligned}\tag{1.2.54}$$

This concludes our proof.

These results establish the foundational framework for analyzing nonequilibrium quantum systems in this thesis. The derived fluctuation relations and response coefficients will underpin our investigation of performance bounds for quantum thermal machines (Chapters 2 to 5) in diverse operating regimes.

## 1.3 Main Research Questions Addressed

The central aim of this thesis is to quantify the constraints on the performance of a broad class of small-scale thermodynamic machines by examining fluctuations. Specifically, we explore how nonequilibrium fluctuations influence the efficiency, power, and reliability of thermal machines, and provide universal bounds on these fluctuations. In Chapter 2, we investigate autonomous continuous thermal machines, focusing on quantum absorption refrigerators with time-reversal symmetry. In Chapter 3, we extend our study of continuous machines where time-reversal symmetry is broken, exemplified by non-autonomous continuous machines, specifically, a Brownian heat engine. In both cases, we work within the linear response regime and apply the principles of linear irreversible thermodynamics to derive universal bounds on fluctuations. In Chapter 4 and Chapter 5, we delve into the study of discrete four-stroke Otto cycles. First, we analyze asymmetrically driven Otto cycles with specific working fluids such as a single qubit and a harmonic oscillator, noting that these cycles lack a well-established linear response formalism, unlike continuous machines. We explore the bounds on fluctuations far from equilibrium, revealing distinctive behavior compared to their continuous counterparts. In Chapter 5, we address the absence of a linear response framework for generic Otto cycles by employing the Schwinger-Keldysh nonequilibrium Green's function (NEGF) technique.

This allows us to explain the observed differences in fluctuation bounds between discrete and continuous machines.

Our analysis establishes connections between various proposed bounds, such as thermodynamic uncertainty relations (TURs), and evaluates their applicability across different scenarios for both quantum and classical thermal machines.

Key contributions of this thesis include:

- Deriving new bounds on the cooling efficiency and power of a continuous absorption refrigerator in the linear response regime, with a focus on how fluctuations limit performance.
- Extending these bounds to systems where time-reversal symmetry is broken.
- Investigating a discrete four-stroke Otto cycle with a two-level system and harmonic oscillator working medium, showing that bounds on fluctuation behave differently compared to continuous machines.
- Developing a rigorous linear-response formalism for the discrete Otto cycle using the Schwinger-Keldysh nonequilibrium Green's function (NEGF) technique, explaining the distinct behavior of discrete machines compared to continuous ones.

This work advances our understanding of the performance of nanoscale machines, providing theoretical insights that may inform the design and optimization of next-generation thermodynamic devices.

### 1.3.1 Outline

This thesis is organized as follows:

**Chapter 2:** We begin with a study of three-terminal quantum absorption refrigerators, that falls into the category of autonomous continuous machines, operating in the linear response regime. We derive bounds on cooling power and efficiency by exploring the hierarchy in current fluctuations. Our analysis relies on the principles of linear irreversible thermodynamics and Onsager reciprocity. Furthermore, we establish a hierarchy in the TURs of different currents. As a consequence of this hierarchy, the seemingly independent bounds on cooling power derived from the TURs are, in fact, interconnected and follow a similar hierarchy. Publication related to this project– (iii).

**Chapter 3:** We extend our study to continuous machines with broken time-reversal symmetry, by focusing on non-autonomous continuous machines, specifically Brownian heat engines. The chapter establishes universal bounds on fluctuations even in the absence of Onsager reciprocity. Crucially, a proper symmetrization of the operational regime is pivotal for understanding performance limitations. Publication related to this project– (iv).

**Chapter 4:** We transition to discrete machines, investigating the quantum Otto cycle with a single qubit and a harmonic oscillator as working fluids. We consider the case of broken time-reversal symmetry for the sake of generality. Unlike continuous machines, these systems lack a robust linear response formalism. We explore the bounds on fluctuations far from equilibrium and highlight how these bounds behave differently compared to continuous machines. Additionally, we derived generalized thermodynamic uncertainty relations (GTURs) for the qubit-Otto cycle valid in far from equilibrium regime. Publication related to this project– (ii).

**Chapter 5:** We address the lack of a linear response framework for Otto cycles by systematically applying the Schwinger-Keldysh nonequilibrium Green's function (NEGF) technique. Importantly, we report robust Onsager reciprocity even when drivings are asymmetric. This is a distinctive feature of the Otto cycle, attributed to the clear separation between the work and heat exchange strokes. This chapter also explains the observed differences in bounds on fluctuation between discrete and continuous machines, linking them to violation of the work-fluctuation-dissipation relation due to presence of external drivings. Publication related to this project– (i).

**Chapter 6:** Finally, we conclude this thesis with closing remarks and discussing some future prospects.

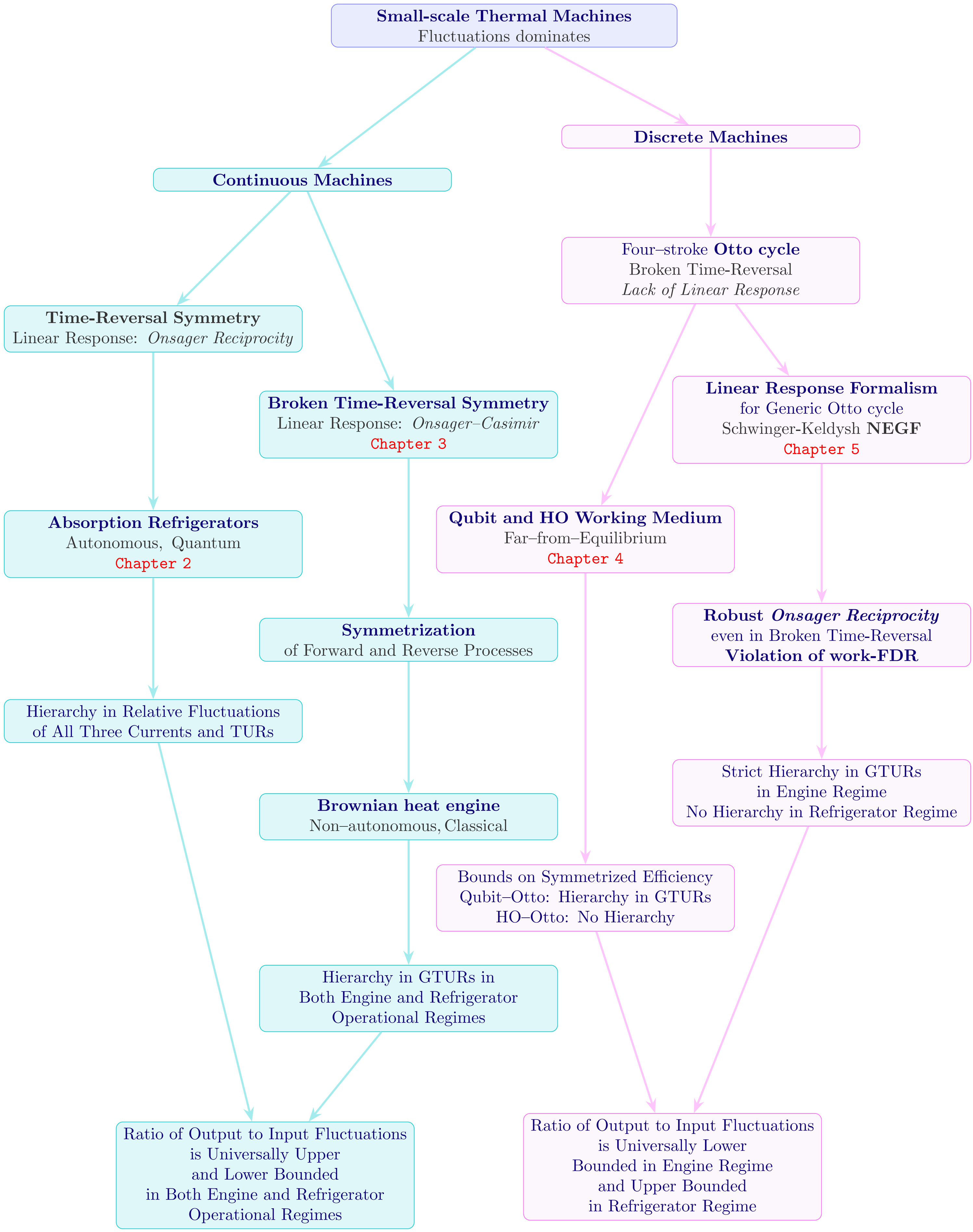

Small-scale Thermal Machines
Fluctuations dominates
Continuous Machines
Discrete Machines
Time-Reversal Symmetry
Linear Response: Onsager Reciprocity
Broken Time-Reversal Symmetry
Linear Response: Onsager–Casimir
Chapter 3
Four–stroke Otto cycle
Broken Time-Reversal
Lack of Linear Response
Linear Response Formalism
for Generic Otto cycle
Schwinger-Keldysh NEGF
Chapter 5
Absorption Refrigerators
Autonomous, Quantum
Chapter 2
Qubit and HO Working Medium
Far–from–Equilibrium
Chapter 4
Symmetrization
of Forward and Reverse Processes
Robust Onsager Reciprocity
even in Broken Time-Reversal
Violation of work-FDR
Hierarchy in Relative Fluctuations
of All Three Currents and TURs
Strict Hierarchy in GTURs
in Engine Regime
No Hierarchy in Refrigerator Regime
Brownian heat engine
Non–autonomous, Classical
Bounds on Symmetrized Efficiency
Qubit–Otto: Hierarchy in GTURs
HO–Otto: No Hierarchy
Hierarchy in GTURs in
Both Engine and Refrigerator
Operational Regimes
Ratio of Output to Input Fluctuations
is Universally Upper
and Lower Bounded
in Both Engine and Refrigerator
Operational Regimes
Ratio of Output to Input Fluctuations
is Universally Lower
Bounded in Engine Regime
and Upper Bounded
in Refrigerator Regime

# 2

# Bounds on performance for autonomous absorption refrigerators

The second law of thermodynamics forbids spontaneous heat flow from a cold to a hot reservoir. Refrigerators, however, remove heat from the cold reservoir and dump heat into the hot reservoir by utilizing external work. The absorption refrigerators (ARs) are a special type of autonomous cooling system that transfer heat from a cold reservoir to a hot reservoir, utilizing a third thermal reservoir, often referred to as the "work reservoir", instead of relying on a mechanical work source. A typical autonomous AR is a three-terminal setup that operates in a non-equilibrium steady state, continuously directing energy flow from the cold ($c$) terminal to the hot ($h$) terminal by absorbing energy from the work ($w$) terminal [73, 165–182], and therefore, fall into the class of continuous thermal machines (see Fig. 2.1). It should be noted that in order to achieve refrigeration, the temperature of the work reservoir must be the highest among the three. In other words, the inverse temperatures ($\beta_\alpha = 1/k_B T_\alpha$) of the three reservoirs must follow the sequence $\beta_c > \beta_h > \beta_w$.

The first useful absorption refrigerator (AR) for industrial applications was realized in the 19th century by the Carré brothers [183, 184]. With rapid advancements in quantum technologies, intense efforts are now directed toward understanding and realizing the smallest possible ARs [166–172, 178, 179, 181] that can operate with maximum cooling efficiency and power by leveraging quantum resources. Various

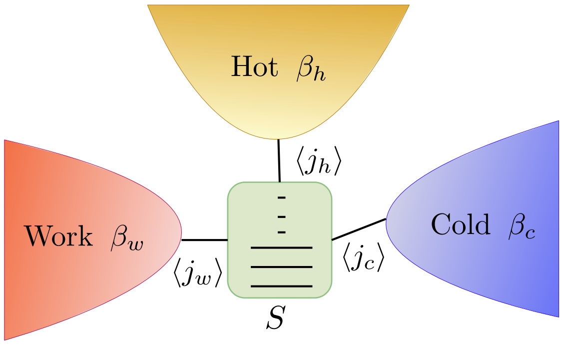


Figure 2.1: Schematic for a generic three-terminal quantum autonomous absorption refrigerator. The inverse temperatures of three reservoirs follow the sequence $\beta_c > \beta_h > \beta_w$.

proposals to realize quantum ARs using platforms such as superconducting qubits, arrays of quantum dots have been put forward [185–188], with one successful experimental implementation using trapped ions achieved very recently [11].

Notably, as the system size shrinks, fluctuations—both quantum and thermal—can significantly impact the performance of thermal machines. In this context, thermodynamic uncertainty relations (TURs) [42, 129, 130, 132, 134–139, 142–144], which represent a trade-off between the relative fluctuations of currents (precision) and the entropy production rate (cost), have provided universal upper bounds on the performance of thermal machines in terms of current fluctuations. For multi-affinity-driven thermal machines, it has been demonstrated that TURs for different currents can impose distinct bounds on output power [42]. However, the relationship between these different bounds has not been clearly established.

In this chapter, we show that for time-reversal symmetric ARs, the relative fluctuations of the three different currents (cold, hot and work) are not truly independent but follow a strict hierarchy in the linear response regime. Consequently, the different universal bounds on cooling power (i.e., the cold current) derived from TURs also follow a similar hierarchy. Furthermore, we report novel bounds on both cooling power and its associated efficiency (quantified as the ratio of cold–to–work currents), which can be tighter than those derived from the TURs.

We organize this chapter as follows: In section 2.1, we introduce a generic AR setup and provide a proof for the hierarchy in the relative fluctuations of currents.

In section 2.2, we discuss the bounds on cooling efficiency and cooling power derived from the TURs and connect these findings with bounds derived from the hierarchy. In sections 2.4 and 2.5, we provide numerical results and discuss these bounds for two paradigmatic quantum AR models.

## 2.1 Hierarchy in the relative fluctuations of currents

A generic setup for an autonomous AR consists of a working medium (classical or quantum) connected to three thermal reservoirs, namely the cold ($c$), hot ($h$) and work ($w$) reservoirs. The inverse temperatures ($\beta_\alpha = 1/k_B T_\alpha$) of the three reservoirs follow the sequence $\beta_c > \beta_h > \beta_w$. The average current from reservoir $\alpha$ is denoted as $\langle j_\alpha \rangle$, and the fluctuation of current about the mean is denoted by $\langle\langle j_\alpha^2 \rangle\rangle = \langle j_\alpha^2 \rangle - \langle j_\alpha \rangle^2$. We adhere to the sign convention: Energy flowing into the working medium is considered positive. Since, the purpose of an AR is to cool down the cold reservoir by absorbing energy from the work reservoir and dumping heat into the hot reservoir, we characterize the refrigeration operational regime as $\langle j_c \rangle > 0$, $\langle j_w \rangle > 0$ and $\langle j_h \rangle < 0$. In this section we will show that the relative fluctuations of the three different currents, defined as $\langle\langle j_\alpha^2 \rangle\rangle / \langle j_\alpha \rangle^2$ for $\alpha = c, h, w$, follow a strict hierarchy in the linear response regime,

$$\frac{\langle\langle j_c^2 \rangle\rangle}{\langle j_c \rangle^2} \geq \frac{\langle\langle j_h^2 \rangle\rangle}{\langle j_h \rangle^2} \geq \frac{\langle\langle j_w^2 \rangle\rangle}{\langle j_w \rangle^2}. \tag{2.1.1}$$

The equality in the above relation corresponds to the tight-coupling limit, i.e., all mean currents are proportional to each other.

First, we will prove the first inequality in equation (2.1.1). For this, we focus on the cold and the hot currents, i.e., $j_c$ and $j_h$. In the linear response limit, we can express the currents in terms of the Onsager's response coefficients as

$$\begin{aligned} \langle j_c \rangle &= L_{cc}\, \mathcal{A}_c^w + L_{ch}\, \mathcal{A}_h^w, \\ \langle j_h \rangle &= L_{hc}\, \mathcal{A}_c^w + L_{hh}\, \mathcal{A}_h^w, \end{aligned} \tag{2.1.2}$$

where $\mathcal{A}_\alpha^w = (\beta_w - \beta_\alpha)$, $\alpha = c, h$, represent the thermodynamic affinities, defined with respect to the inverse temperature of the work reservoir $\beta_w$, which is set as the reference in this particular case. Notice that these affinities can be identified from the expression of average entropy production rate,

$$\begin{aligned}
\langle\sigma\rangle &= -\sum_{i=c,h,w} \beta_i \langle j_i\rangle \\
&= (\beta_w - \beta_c)\langle j_c\rangle + (\beta_w - \beta_h)\langle j_h\rangle \\
&= \sum_{\alpha=c,h} \mathcal{A}^w_\alpha \langle j_\alpha\rangle,
\end{aligned} \tag{2.1.3}$$

where, in order to go from first to second line, we used the first law of thermodynamics, $\sum_{\alpha=c,h,w}\langle j_\alpha\rangle = 0$. We focus on time-reversal symmetric scenario. Therefore, Onsager raciprocity holds true, i.e., the off-diagonal Onsager coefficients satisfy $L_{ch} = L_{hc}$. To prove the first inequality given in (2.1.1), we consider an alternative expression $\langle j_h\rangle^2 \langle\langle j_c^2\rangle\rangle - \langle j_c\rangle^2 \langle\langle j_h^2\rangle\rangle$.

$$\begin{aligned}
\langle j_h\rangle^2 \langle\langle j_c^2\rangle\rangle - \langle j_c\rangle^2 \langle\langle j_h^2\rangle\rangle &= 2L_{cc}\langle j_h\rangle^2 - 2L_{hh}\langle j_c\rangle^2 \\
&= 2(L_{cc}L_{hh} - L_{ch}^2)\big(L_{hh}\mathcal{A}_h^{w2} - L_{cc}\mathcal{A}_c^{w2}\big) \\
&= 2\det(L)\big(\langle j_h\rangle\mathcal{A}_h^w - \langle j_c\rangle\mathcal{A}_c^w\big) \\
&\geq 0.
\end{aligned} \tag{2.1.4}$$

Here, in the first line we have used fluctuation-dissipation relation (FDR), $\langle\langle j_i^2\rangle\rangle = 2L_{ii}$, for $i = c, h$, and for the last line we have used:

(i) The determinant of Onsager matrix is non-negative, $\det(L) \geq 0$, reminiscent of second law of thermodynamics,

(ii) In the refrigeration operational regime, $\langle j_c\rangle > 0$ and $\langle j_h\rangle < 0$, and $\mathcal{A}^w_\alpha < 0$ for both $\alpha = c$ and $h$ (since $\beta_c > \beta_h > \beta_w$). Therefore, both $\langle j_h\rangle\mathcal{A}^w_h$ and $-\langle j_c\rangle\mathcal{A}^w_c$ are positive (non-negative) quantities.

We emphasize that the above argument is independent of the sign convention taken; e.g., if one chooses the convention that current flowing into the reservoirs be positive, both the signs of fluxes, $\langle j_c\rangle$, $\langle j_h\rangle$, and the (revised) affinities, $\mathcal{A}_c^{\alpha\prime} = (\beta_\alpha - \beta_w)$, $\alpha = c, h$, will be reversed and as a result the signs of the products $\langle j_c\rangle\mathcal{A}^w_c$ and

$\langle j_h \rangle \mathcal{A}_h^w$ will remain the same. From (2.1.4), we conclude

$$\frac{\langle\langle j_c^2 \rangle\rangle}{\langle j_c \rangle^2} \geq \frac{\langle\langle j_h^2 \rangle\rangle}{\langle j_h \rangle^2}. \tag{2.1.5}$$

Notice that the equality in the above relation corresponds to vanishing determinant of the Onsager's matrix, which is achieved in the tight-coupling limit (when all mean currents are proportional to each other).

Next, we prove the second inequality in equation (2.1.1). For this, we take inverse temperature of the cold reservoir $\beta_c$ as reference and write down the expressions for average hot and work currents, $\langle j_h \rangle$, $\langle j_w \rangle$, up to linear order in affinities

$$\begin{aligned} \langle j_h \rangle &= \tilde{L}_{hh}\, \mathcal{A}_h^c + \tilde{L}_{hw}\, \mathcal{A}_w^c \\ \langle j_w \rangle, &= \tilde{L}_{wh}\, \mathcal{A}_h^c + \tilde{L}_{ww}\, \mathcal{A}_w^c, \end{aligned} \tag{2.1.6}$$

where $\mathcal{A}_\alpha^c = (\beta_c - \beta_\alpha)$, $\alpha = h, w$, are the thermodynamic affinities identified from the expression of total entropy production rate, $\langle \Sigma \rangle = \sum_{\alpha=h,w} \mathcal{A}_\alpha^c \langle j_\alpha \rangle$. The symbol tilde on the response coefficients indicate that these are now computed with respect to the affinities $\mathcal{A}_\alpha^c$ (i.e., cold reservoir as reference). Similar to the steps followed to prove the first inequality in (2.1.1), we will consider an alternative expression $\langle j_w \rangle^2 \langle\langle j_h^2 \rangle\rangle - \langle j_h \rangle^2 \langle\langle j_w^2 \rangle\rangle$,

$$\begin{aligned} \langle j_w \rangle^2 \langle\langle j_h^2 \rangle\rangle - \langle j_h \rangle^2 \langle\langle j_w^2 \rangle\rangle &= 2\tilde{L}_{hh} \langle j_w \rangle^2 - 2\tilde{L}_{ww} \langle j_h \rangle^2 \\ &= 2(\tilde{L}_{hh}\tilde{L}_{ww} - \tilde{L}_{hw}^2)\big(\tilde{L}_{ww}\mathcal{A}_w^{c\,2} - \tilde{L}_{hh}\mathcal{A}_h^{c\,2}\big) \\ &= 2\det(\tilde{L})\big(\langle j_w \rangle \mathcal{A}_w^c - \langle j_h \rangle \mathcal{A}_h^c\big) \\ &\geq 0, \end{aligned} \tag{2.1.7}$$

where we used:

(i) The standard FDR, $\langle\langle j_i^2 \rangle\rangle = 2\tilde{L}_{ii}$, $i = h, w$.

(ii) The non-negativity of determinant of the onsager matrix, $\det(\tilde{L}) \geq 0$.

(iii) The refrigeration operational regime condition: $\langle j_h \rangle < 0$ and $\langle j_w \rangle > 0$, and $\mathcal{A}_\alpha^c > 0$ for both $\alpha = h$ and $w$ (since $\beta_c > \beta_h > \beta_w$). Thus, both $\langle j_w \rangle \mathcal{A}_w^c$ and $-\langle j_h \rangle \mathcal{A}_h^c$ are positive (non-negative) quantities.

From (2.1.7), we conclude

$$\frac{\langle\langle j_h^2 \rangle\rangle}{\langle j_h \rangle^2} \geq \frac{\langle\langle j_w^2 \rangle\rangle}{\langle j_w \rangle^2}. \tag{2.1.8}$$

It is important to note that the above inequality is valid independent of the direction of current from the cold reservoir, as in this case, imposing the conditions $\langle j_h \rangle < 0$ and $\langle j_w \rangle > 0$ does not fix a definite direction for $\langle j_c \rangle$. Therefore, this particular inequality concerning the work and hot currents, as given in equation (2.1.8), is valid even in the heat pump operational regime, which is characterized by $\langle j_c \rangle < 0$, $\langle j_w \rangle > 0$ and $\langle j_h \rangle < 0$. However, focusing only in the refrigerator regime, equations (2.1.5) and (2.1.8) provide the required hierarchy given in (2.1.1). This hierarchy in the relative fluctuations of currents, as given in equation (2.1.1), represents the first central result of this chapter.

We note an immediate consequence of this hierarchy in (2.1.1): The inequality involving cold and work currents provides a completely different universal upper bounds for the cooling efficiency, defined as $\langle \varepsilon \rangle = \langle j_c \rangle / \langle j_w \rangle$, and average cooling power $\langle j_c \rangle$,

$$\langle \varepsilon \rangle := \frac{\langle j_c \rangle}{\langle j_w \rangle} \leq \sqrt{\frac{\langle\langle j_c^2 \rangle\rangle}{\langle\langle j_w^2 \rangle\rangle}}, \tag{2.1.9}$$

$$\langle j_c \rangle \leq \sqrt{\frac{\langle\langle j_c^2 \rangle\rangle}{\langle\langle j_w^2 \rangle\rangle}}\, \langle j_w \rangle. \tag{2.1.10}$$

Next, we demonstrate that this newly defined upper bound on cooling efficiency [cf. (2.1.9)] is tighter than the standard three-terminal version of maximum cooling efficiency $\varepsilon_\mathrm{c} = \frac{(\beta_h - \beta_w)}{(\beta_c - \beta_h)}$. Note that $\varepsilon_\mathrm{c}$ reduces to the well-known two-terminal cooling efficiency version $(1 - \eta_\mathrm{c})/\eta_\mathrm{c}$, with $\eta_\mathrm{c} = \beta_h / (\beta_c - \beta_h)$, in the limit $\beta_w \ll \beta_h$.

$$\sqrt{\frac{\langle\langle j_c^2 \rangle\rangle}{\langle\langle j_w^2 \rangle\rangle}} \leq \varepsilon_\mathrm{c}. \tag{2.1.11}$$

To prove this inequality in (2.1.11), we will consider the cold and work currents, $\langle j_c \rangle$ and $\langle j_w \rangle$, taking inverse temperature of the hot reservoir $\beta_h$ as the reference. In the linear response regime, the currents $\langle j_c \rangle$ and $\langle j_w \rangle$ are expressed in terms of the Onsager's coefficients $\bar{L}_{\alpha\gamma}$, with $\alpha, \gamma = w, c$, and thermodynamic affinities $\mathcal{A}^h_\alpha = (\beta_h - \beta_\alpha)$, with $\alpha = c, w$,

$$\begin{aligned} \langle j_c \rangle &= \bar{L}_{cc}\,\mathcal{A}^h_c + \bar{L}_{cw}\,\mathcal{A}^h_w, \\ \langle j_w \rangle &= \bar{L}_{wc}\,\mathcal{A}^h_c + \bar{L}_{ww}\,\mathcal{A}^h_w. \end{aligned} \tag{2.1.12}$$

We notice that

$$\langle j_w \rangle \mathcal{A}^h_w - \langle j_c \rangle \mathcal{A}^h_c \geq 0. \tag{2.1.13}$$

This is because (i) $\langle j_c \rangle > 0$ and $\langle j_w \rangle > 0$ in the refrigerator operational regime, and (ii) due to the inverse temperature sequence $\beta_c > \beta_h > \beta_w$, we obtain $\mathcal{A}^h_w > 0$, $\mathcal{A}^h_c < 0$. Now,

$$\begin{aligned} &\langle j_w \rangle \mathcal{A}^h_w - \langle j_c \rangle \mathcal{A}^h_c \geq 0 \\ &\Rightarrow \bar{L}_{cc} {\mathcal{A}^h_c}^2 \leq \bar{L}_{ww} {\mathcal{A}^h_w}^2 \\ &\Rightarrow \frac{\bar{L}_{cc}}{\bar{L}_{ww}} \leq \left( -\frac{\mathcal{A}^h_w}{\mathcal{A}^h_c} \right)^2 \\ &\Rightarrow \frac{\langle\langle j_c^2 \rangle\rangle}{\langle\langle j_w^2 \rangle\rangle} \leq \varepsilon_{\mathrm{c}}^2, \end{aligned} \tag{2.1.14}$$

where, in the last line, we have used the standard FDRs, $\langle\langle j_i^2 \rangle\rangle = 2\bar{L}_{ii}$, for $i = c, w$. This concludes our proof for the inequality given in (2.1.11). The inequalities in equations (2.1.9) and (2.1.10), together with equation (2.1.11), constitute the another central result of this chapter:

$$\langle \varepsilon \rangle \leq \sqrt{\frac{\langle\langle j_c^2 \rangle\rangle}{\langle\langle j_w^2 \rangle\rangle}} \leq \varepsilon_{\mathrm{c}}, \tag{2.1.15}$$

$$\langle j_c \rangle \leq \sqrt{\frac{\langle\langle j_c^2 \rangle\rangle}{\langle\langle j_w^2 \rangle\rangle}}\, \langle j_w \rangle \leq \varepsilon_{\mathrm{c}}\, \langle j_w \rangle. \tag{2.1.16}$$

We have derived new tighter bounds on cooling efficiency and cooling power in terms of fluctuations of the cold and work currents, valid in the linear response regime. The equality in the above relations corresponds to the tight-coupling situation

## 2.2 Bounds on cooling efficiency and cooling power derived from TURs

For an out-of-equilibrium system in steady-state, subjected to multiple thermodynamic affinities, the TURs [42, 129, 130, 132, 134–139, 142–144] represent trade-off relation between the relative fluctuations of individual currents (such as heat, work and particle currents) and the net eRtuations and the dissipation arbitrarily. For the AR setup, the TURs can be can be expressed as

$$\langle\sigma\rangle\frac{\langle\langle j_\alpha^2\rangle\rangle}{\langle j_\alpha\rangle^2}\geq 2,\quad \alpha=c,h,w. \tag{2.2.1}$$

Note that the above TURs hold true in the linear response regime. We now provide a simple proof for the TUR corresponding to the cold current by utilizing the onsager relation given in (2.1.2):

$$\begin{aligned}\langle\sigma\rangle\frac{\langle\langle j_c^2\rangle\rangle}{\langle j_c\rangle^2} &= \frac{2\,L_{cc}}{\langle j_c\rangle^2}\sum_{i,j=c,h}L_{ij}\mathcal{A}_i^w\mathcal{A}_j^w\\ &= 2+\frac{2\,\mathcal{A}_h^{w2}}{\langle j_c\rangle^2}\det(L)\\ &\geq 2.\end{aligned} \tag{2.2.2}$$

Here, the equality corresponds to the tight-coupling limit, i.e., when the determinant of the Onsager's matrix vanishes. A similar approach can be applied to derive the other two TURs.

First, we note that the entropy production rate $\langle\sigma\rangle=-\sum_{\alpha=c,h,w}\beta_\alpha\langle j_\alpha\rangle$ can be expressed as

$$\begin{aligned}\langle\sigma\rangle &= (\beta_c-\beta_h)\Big[\frac{\varepsilon_c}{\langle\varepsilon\rangle}-1\Big]\langle j_c\rangle\\ &\equiv -(\beta_c-\beta_h)\frac{\varepsilon_c-\langle\varepsilon\rangle}{1+\langle\varepsilon\rangle}\langle j_h\rangle\\ &\equiv (\beta_c-\beta_h)\big[\varepsilon_c-\langle\varepsilon\rangle\big]\langle j_w\rangle,\end{aligned} \tag{2.2.3}$$

where we recall that $\varepsilon_c=\frac{(\beta_h-\beta_w)}{(\beta_c-\beta_h)}$, and $\langle\varepsilon\rangle=\langle j_c\rangle/\langle j_w\rangle$. Therefore, the TURs in

(2.2.1) can be exprressed in the following alternative forms:

$$(\beta_c - \beta_h)\left[\frac{\varepsilon_{\rm c}}{\langle\varepsilon\rangle} - 1\right]\frac{\langle\!\langle j_c^2\rangle\!\rangle}{\langle j_c\rangle} \geq 2, \tag{2.2.4}$$

$$(\beta_c - \beta_h)\frac{\varepsilon_{\rm c} - \langle\varepsilon\rangle}{1 + \langle\varepsilon\rangle}\left[\frac{\langle\!\langle j_h^2\rangle\!\rangle}{-\langle j_h\rangle}\right] \geq 2, \tag{2.2.5}$$

$$(\beta_c - \beta_h)\left[\varepsilon_{\rm c} - \langle\varepsilon\rangle\right]\frac{\langle\!\langle j_w^2\rangle\!\rangle}{\langle j_w\rangle} \geq 2. \tag{2.2.6}$$

In the refrigerator operational regime, characterized by $\langle j_c\rangle > 0$, $\langle j_w\rangle > 0$ and $\langle j_h\rangle < 0$, we highlight that these alternative expressions of the TURs enable us to derive novel upper bounds on cooling efficiency $\langle\varepsilon\rangle$, which are tighter than $\varepsilon_{\rm c}$.

$$\langle\varepsilon\rangle \leq \varepsilon_{\rm c}\Big/\left(1 + \frac{2\,\langle j_c\rangle}{(\beta_c - \beta_h)\,\langle\!\langle j_c^2\rangle\!\rangle}\right) := \mathcal{E}_{\rm cold}, \tag{2.2.7}$$

$$\langle\varepsilon\rangle \leq \left(\varepsilon_{\rm c} + \frac{2\,\langle j_h\rangle}{(\beta_c - \beta_h)\,\langle\!\langle j_h^2\rangle\!\rangle}\right)\Big/\left(1 - \frac{2\,\langle j_h\rangle}{(\beta_c - \beta_h)\,\langle\!\langle j_h^2\rangle\!\rangle}\right) := \mathcal{E}_{\rm hot}, \tag{2.2.8}$$

$$\langle\varepsilon\rangle \leq \varepsilon_{\rm c} - \frac{2\,\langle j_w\rangle}{(\beta_c - \beta_h)\,\langle\!\langle j_w^2\rangle\!\rangle} := \mathcal{E}_{\rm work}. \tag{2.2.9}$$

One can alternatively express the above bounds on the cooling efficiency as bounds on the cooling power,

$$\langle j_c\rangle \leq (\beta_c - \beta_h)\frac{\varepsilon_{\rm c} - \langle\varepsilon\rangle}{2\langle\varepsilon\rangle}\,\langle\!\langle j_c^2\rangle\!\rangle := \mathcal{P}_{\rm cold}, \tag{2.2.10}$$

$$\langle j_c\rangle \leq (\beta_c - \beta_h)\frac{\varepsilon_{\rm c} - \langle\varepsilon\rangle}{2(1 + \langle\varepsilon\rangle)^2}\langle\varepsilon\rangle\,\langle\!\langle j_h^2\rangle\!\rangle := \mathcal{P}_{\rm hot}, \tag{2.2.11}$$

$$\langle j_c\rangle \leq (\beta_c - \beta_h)\,\frac{\varepsilon_{\rm c} - \langle\varepsilon\rangle}{2}\langle\varepsilon\rangle\,\langle\!\langle j_w^2\rangle\!\rangle := \mathcal{P}_{\rm work}. \tag{2.2.12}$$

Next, we study the implication of the hierarchy of the relative fluctuations, as given in equation (2.1.1) on the the above-mentioned bounds on cooling efficiency and cooling power, derived from the TURs.

## 2.3 Comparison of the bounds

First of all, we notice that, (2.1.1) immediately indicates that the TURs for different currents [cf. (2.2.1)] are not truly independent of each other but follow a strict hierarchy. Therefore, we infer that in the linear response regime, among the three different currents, the work current provides the best estimate for entropy production rate compared to the other two currents [189, 190].

As a consequence, the three separate and seemingly independent bounds on cooling power derived from TURs [cf. (2.2.10) to (2.2.12)], are also not truly independent but follow a similar strict hierarchy. Since

$$\langle\langle j_w^2 \rangle\rangle \leq \frac{\langle\langle j_h^2 \rangle\rangle}{(1+\langle\varepsilon\rangle)^2} \leq \frac{\langle\langle j_c^2 \rangle\rangle}{\langle\varepsilon\rangle^2}, \tag{2.3.1}$$

we obtain,

$$\langle j_c \rangle \leq \mathcal{P}_{\text{work}} \leq \mathcal{P}_{\text{hot}} \leq \mathcal{P}_{\text{cold}}, \tag{2.3.2}$$

We conclude that, due to this hierarchy, the cooling power gets most tightly bounded when the bound is derived from the work-TUR. However, the bound on cooling power given in (2.1.16) does not fall within this hierarchy, and potentially can become tighter compared to the bounds derived from the TURs, making it important to consider.

Finally, we also notice that the bounds on cooling efficiency derived from the TURs [cf. (2.2.7) to (2.2.9)], and as well as the bound given in (2.1.15) do not follow such a hierarchy. However, we can prove that

$$\langle\varepsilon\rangle \leq \sqrt{\frac{\langle\langle j_c^2 \rangle\rangle}{\langle\langle j_w^2 \rangle\rangle}} \leq \mathcal{E}_{\text{cold}} \leq \varepsilon_{\text{c}}. \tag{2.3.3}$$

To prove the above relation, we note that in the linear response regime, we can express the currents $\langle j_c \rangle$ and $\langle j_w \rangle$ in terms of the Onsager's coefficients $\bar{L}_{\alpha\gamma}$, with $\alpha, \gamma = w, c$.

$$\begin{aligned} \langle j_c \rangle =& \bar{L}_{cc}\left(\beta_h - \beta_c\right) + \bar{L}_{cw}\left(\beta_h - \beta_w\right), \\ \langle j_w \rangle =& \bar{L}_{wc}\left(\beta_h - \beta_c\right) + \bar{L}_{ww}\left(\beta_h - \beta_w\right). \end{aligned} \tag{2.3.4}$$

We recall that in the refrigeration regime we must have $\langle j_c \rangle \geq 0$. Notice that, because of the temperature sequence $\beta_c > \beta_h > \beta_w$, and the fact that $\bar{L}_{cc} = \langle\langle j_c^2 \rangle\rangle/2 \geq 0$, we can conclude that $\bar{L}_{cw} \geq 0$. We will need this for our proof. Next, we express

(2.2.7) as

$$\begin{aligned}\mathcal{E}_{\text{cold}} =& \frac{\beta_h - \beta_w}{\beta_c - \beta_h} \Big/ \left(1 + \frac{\bar{L}_{cc}\left(\beta_h - \beta_c\right) + \bar{L}_{cw}\left(\beta_h - \beta_w\right)}{\left(\beta_c - \beta_h\right)\bar{L}_{cc}}\right) \\ =& \frac{\bar{L}_{cc}}{\bar{L}_{cw}}\end{aligned} \tag{2.3.5}$$

Now,

$$\sqrt{\frac{\langle\langle j_c^2 \rangle\rangle}{\langle\langle j_w^2 \rangle\rangle}} = \sqrt{\frac{\bar{L}_{cc}}{\bar{L}_{ww}}} = \sqrt{\frac{\bar{L}_{cc}^2}{\bar{L}_{ww}\bar{L}_{cc}}} \leq \sqrt{\frac{\bar{L}_{cc}^2}{\bar{L}_{cw}^2}} = \mathcal{E}_{\text{cold}} \tag{2.3.6}$$

where, in the last step, we have utilized the constraint on time-reversal symmetric Onsager coefficients steaming form the non-negativity of the entropy production rate, $\det(\bar{L}) = \bar{L}_{cc}\bar{L}_{ww} - \bar{L}_{cw}^2 \geq 0$. This completes our proof for equation (2.3.3).

**Equality in tight-coupling**– It should be noted that, as the equality for the TURs and the hierarchy of relative fluctuations is achieved in the tight-coupling limit, all the above mentioned bounds saturate, and we can write

$$\begin{aligned}\langle \varepsilon \rangle &= \sqrt{\frac{\langle\langle j_c^2 \rangle\rangle}{\langle\langle j_w^2 \rangle\rangle}} = \mathcal{E}_{\text{cold}} = \mathcal{E}_{\text{hot}} = \mathcal{E}_{\text{work}} \leq \varepsilon_{\text{c}}, \\ \langle j_c \rangle &= \sqrt{\frac{\langle\langle j_c^2 \rangle\rangle}{\langle\langle j_w^2 \rangle\rangle}}\, \langle j_w \rangle = \mathcal{P}_{\text{cold}} = \mathcal{P}_{\text{hot}} = \mathcal{P}_{\text{work}}.\end{aligned} \tag{2.3.7}$$

In what follows, we test the validity of these bounds for two paradigmatic absorption refrigerator setups.

## 2.4 Example I: Weak (additive) system-reservoir coupling

### 2.4.1 Four-level working medium

As a first model example, we consider a four-level working medium which is weakly connected to three thermal reservoirs $(c, h, w)$ (see Fig. 2.2). We restrict our discussion to the weak system-bath coupling regime with Markovian bath dynamics, described by the quantum maser equation (QME) for the reduced density matrix

[174]. Under the secular/rotating wave approximation and assuming non-degenerate energy levels, the coherence and population dynamics decouple.

The joint dynamics of populations and energy transfers can be compactly represented by the counting-field dressed population vector $|\mathcal{Z}(\chi,t)\rangle$, where the counting fields $\chi = (\chi_w, \chi_h, \chi_c)$ track energy exchange with each reservoir. Note that, $|\mathcal{Z}(\chi = 0,t)\rangle$ corresponds to the standard population vector, while finite $\chi$ encodes the full counting statistics of energy quanta exchanged with reservoir $\alpha = w, h, c$.

Mathematically, $|\mathcal{Z}(\chi,t)\rangle$ generates the statistics of energy transfers via:

$$\frac{d|\mathcal{Z}(\chi,t)\rangle}{dt} = \hat{\mathcal{W}}(\chi)|\mathcal{Z}(\chi,t)\rangle, \tag{2.4.1}$$

where $\hat{\mathcal{W}}(\chi)$ generalizes the standard rate matrix $\hat{\mathcal{W}}(0)$. The cumulant generating function

$$\mathcal{G}(\chi) = \lim_{t\to\infty} \frac{1}{t} \ln\langle I|\mathcal{Z}(\chi,t)\rangle \tag{2.4.2}$$

then extracts all current statistics through derivatives at $\chi = 0$. Here, the unit vector $\langle I| = \langle 1,\dots,1|$ performs the trace over system states.

Notice that, although the three-level setup is the minimal model to realize a Quantum AR in the weak-coupling limit [73, 169, 170], it always satisfies the tight-coupling condition. This condition corresponds to the equality in the bounds.

***Three-level AR and the tight-coupling situation*:**

The dressed rate matrix corresponding to a three-level AR is given by

$$\hat{\mathcal{W}}(\chi) = \begin{pmatrix} -k^c_{1\to2} - k^h_{1\to3} & k^c_{2\to1}e^{-i\chi_c\omega_c} & k^h_{3\to1}e^{-i\chi_h\omega_h} \\ k^c_{1\to2}e^{i\chi_c\omega_c} & -k^c_{2\to1} - k^w_{2\to3} & k^w_{3\to2}e^{-i\chi_w\omega_w} \\ k^h_{1\to3}\,e^{i\chi_h\omega_h} & k^w_{2\to3}e^{i\chi_w\omega_w} & -k^w_{3\to2} - k^h_{3\to1} \end{pmatrix}, \tag{2.4.3}$$

with $k^\alpha_{i\to j}$ being the transition rates between states $i$ and $j$ due to presence of reservoir $\alpha = w, h, c$. However, for this three level setup, we obtain analytical forms for the mean currents and the fluctuations of currents, without requiring the explicit forms for the incoherent transition rates induced by the baths. The energy states are labeled from bottom to top by 1,2,3, with energies $\epsilon_{1,2,3} =$

$(0,\, \omega_c,\, \omega_c+\omega_w)$. The statistics for all three currents is determined by the (real part) largest eigenvalue of the characteristic polynomial. Notice that, the largest eigenvalue satisfies the characteristic polynomial,

$$\lambda_{\max}^3 - a_1\,\lambda_{\max}^2 + a_2\,\lambda_{\max} - a_3(\chi) = 0 \tag{2.4.4}$$

with the condition that $\lambda_{\max}(\chi=0)=0$. Here,

$$\begin{aligned}
a_1 =& w_{0,0} + w_{1,1} + w_{2,2},\\
a_2 =& w_{0,0}w_{1,1} + w_{0,0}w_{2,2} + w_{1,1}w_{2,2} - w_{0,1}(\chi_c)\,w_{1,0}(\chi_c)\\
&- w_{0,2}(\chi_h)\,w_{2,0}(\chi_h) - w_{1,2}(\chi_w)\,w_{2,1}(\chi_w),\\
a_3(\chi) =& w_{0,0}\,w_{1,1}\,w_{2,2} - w_{0,0}\,w_{1,2}(\chi_w)\,w_{2,1}(\chi_w)\\
&- w_{0,1}(\chi_c)w_{1,0}(\chi_c)\,w_{2,2} + w_{0,1}(\chi_c)\,w_{1,2}(\chi_w)\,w_{2,0}(\chi_h)\\
&+ w_{0,2}(\chi_h)\,w_{2,1}(\chi_w)\,w_{1,0}(\chi_c) - w_{0,2}(\chi_h)\,w_{2,0}(\chi_h)\,w_{1,1},
\end{aligned} \tag{2.4.5}$$

where $w_{i,j}$ are the elements of the rate matrix $\hat{\mathcal{W}}(\chi)$ [174]. Notice that, $a_1$ is counting field independent. Moreover, the counting field dependent phase factors exactly cancels out in $a_2$. As a result, $a_3$ is the only counting field dependent term in (2.4.4). We can obtain analytical expression for the mean current corresponding to reservoir $\alpha$ as

$$\langle j_\alpha \rangle = \frac{1}{a_2}\,\frac{\partial a_3}{\partial(i\chi_\alpha)}\Big|_{\chi=0}, \qquad \alpha = h, c, w. \tag{2.4.6}$$

The obtained currents are proportional to each other:

$$\begin{aligned}
\langle j_c \rangle =& \frac{\omega_c}{a_2}\Big[w_{0.2}\,w_{2,1}\,w_{1,0} - w_{0,1}\,w_{1,2}\,w_{2,0}\Big],\\
\langle j_w \rangle =& \frac{\omega_w}{\omega_c}\,\langle j_c \rangle,\\
\langle j_h \rangle =& -\,\frac{\omega_c+\omega_w}{\omega_c}\,\langle j_c \rangle.
\end{aligned} \tag{2.4.7}$$

Therefore, tight-coupling always holds for this three-level quantum AR setup in the weak system-bath coupling limit. The fluctuation of current corresponding to bath $\alpha$ is given by

$$\langle\!\langle j_\alpha^2 \rangle\!\rangle = \frac{1}{a_2}\left[\frac{\partial^2 a_3}{\partial(i\chi_\alpha)^2} + \frac{2a_1}{a_2^2}\left(\frac{\partial a_3}{\partial(i\chi_\alpha)}\right)^2\right]_{\chi=0}. \tag{2.4.8}$$

As a result, the relative fluctuations simplify to

$$\frac{\langle\!\langle j_\alpha^2 \rangle\!\rangle}{\langle j_\alpha \rangle^2} = \frac{2\,a_1}{a_2} + a_2\,\frac{a_3''(0)}{[a_3'(0)]^2}, \tag{2.4.9}$$

where the primes indicate the order of the derivative with respect to the respective counting field $\chi_\alpha$. Notice that, $a_1$ and $a_2$ remains the same for any current. Interestingly, it turns out that $a_3''(0)/[a_3'(0)]^2$ is also the same for any current,

$$\frac{a_3''(0)}{[a_3'(0)]^2} = \frac{w_{0,2}\,w_{2,1}\,w_{1,0} + w_{0,1}\,w_{1,2}\,w_{2,0}}{\left(w_{0,2}\,w_{2,1}\,w_{1,0} - w_{0,1}\,w_{1,2}\,w_{2,0}\right)^2}. \tag{2.4.10}$$

Therefore, we conclude that the relative fluctuations of currents for all three baths are the same:

$$\frac{\langle\!\langle j_c^2 \rangle\!\rangle}{\langle j_c \rangle^2} = \frac{\langle\!\langle j_h^2 \rangle\!\rangle}{\langle j_h \rangle^2} = \frac{\langle\!\langle j_w^2 \rangle\!\rangle}{\langle j_w \rangle^2}. \tag{2.4.11}$$

Because of the above relation, the bounds on cooling efficiency and cooling power coalesce, as given in (2.3.7).

The four-level model was recently studied in Refs [53, 176] by employing full-counting analysis for cold and work currents. This analysis can be easily extended to study statistics of all three currents involved. The dressed rate matrix $\hat{\mathcal{W}}(\chi)$ is given as

$$\hat{\mathcal{W}}(\chi) = \begin{pmatrix} -k^c_{1\to2} - k^c_{1\to3} - k^h_{1\to4} & k^c_{2\to1}e^{-i\chi_c(\omega_c-g)} & k^c_{3\to1}e^{-i\chi_c(\omega_c+g)} & k^h_{4\to1}e^{-i\chi_h(\omega_c+\omega_w)} \\ k^c_{1\to2}e^{i\chi_c(\omega_c-g)} & -k^c_{2\to1} - k^w_{2\to4} & 0 & k^w_{4\to2}e^{-i\chi_w(\omega_w+g)} \\ k^c_{1\to3}e^{i\chi_c(\omega_c+g)} & 0 & -k^c_{3\to1} - k^w_{3\to4} & k^w_{4\to3}e^{-i\chi_w(\omega_w-g)} \\ k^h_{1\to4}e^{i\chi_h(\omega_c+\omega_w)} & k^w_{2\to4}e^{i\chi_w(\omega_w+g)} & k^w_{3\to4}e^{i\chi_w(\omega_w-g)} & -k^h_{4\to1} - k^w_{4\to2} - k^w_{4\to3} \end{pmatrix}, \tag{2.4.12}$$

with $k^\alpha_{i\to j}$ being the transition rates between states $i$ and $j$ due to presence of reservoir $\alpha = w, h, c$. Due to the weak system-bath coupling, these transition rates

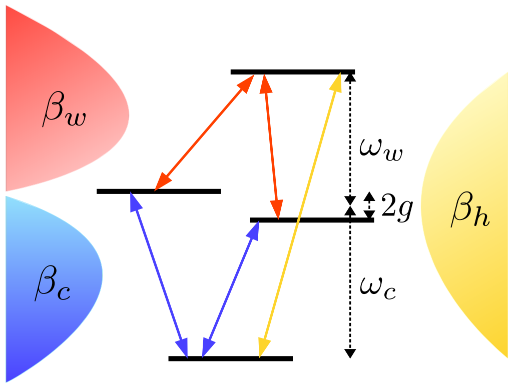


Figure 2.2: Schematic of a four-level AR coupled weakly with all the three reservoirs. Bath-induced incoherent transitions are shown by the solid arrows. Energy gaps between the states are indicated by dotted lines.

appear additively in the population dynamics. The energy levels are labeled from bottom to top as 1 to 4, with energies given by $\epsilon_{1,2,3,4} = (0, \omega_c - g, \omega_c + g, \omega_c + \omega_w)$. For simplicity, in this example, we ignore the possible presence of quantum coherence in the system. This, however, does not affect the main message presented in this chapter.

In Fig. 2.3, we display the different bounds for cooling power and cooling efficiency. We choose the transition rates as $k^{\alpha}_{i\to j} = \Gamma_\alpha(\varepsilon_j - \varepsilon_i)\, n_\alpha(\varepsilon_j - \varepsilon_i)$, with $n_\alpha(\Delta) = \left(e^{\beta_\alpha \Delta} - 1\right)^{-1}$ being the Bose-Einstein distribution function at inverse temperature $\beta_\alpha$ and $\Gamma_\alpha(\Delta) = \gamma_\alpha\, \Delta\, e^{-|\Delta|/\Lambda}$ being the Ohomic spectral density function of reservoir $\alpha$ [53], with $\Lambda$ being the cutoff frequency, which is assumed to be large, $\Lambda \gg \omega_\alpha, 1/\beta_\alpha$. Figs. 2.3 (a) and (b) shows results beyond the tight-coupling regime, which corresponds to values of $g$ comparable to $\omega_\alpha$. The hierarchy in the bounds for cooling power ( $\mathcal{P}_{\text{work}} < \mathcal{P}_{\text{hot}} < \mathcal{P}_{\text{cold}}$ ) is clearly observed with the tightest bound being $\mathcal{P}_{\text{work}}$. Notice that, as mentioned earlier, the additional bound given in (2.1.16) do not follow the above hierarchy and can become a tighter bound, which can be clearly seen for $\omega_c > 0.4$. Notice that, the additional bound for cooling efficiency, as given in (2.1.15), is also tighter than the bound predicted from the cold-TUR in (2.2.7). Figs. 2.3 (c) and (d) shows results in the tight-coupling limit corresponding to closing of the gap between the states 2 and 3 ($g = 1 \times 10^{-4} \ll \omega_\alpha$). In this case, as predicted in (2.3.7), all the bounds on cooling efficiency and cooling power saturate and coalesce with their respective exact mean values.

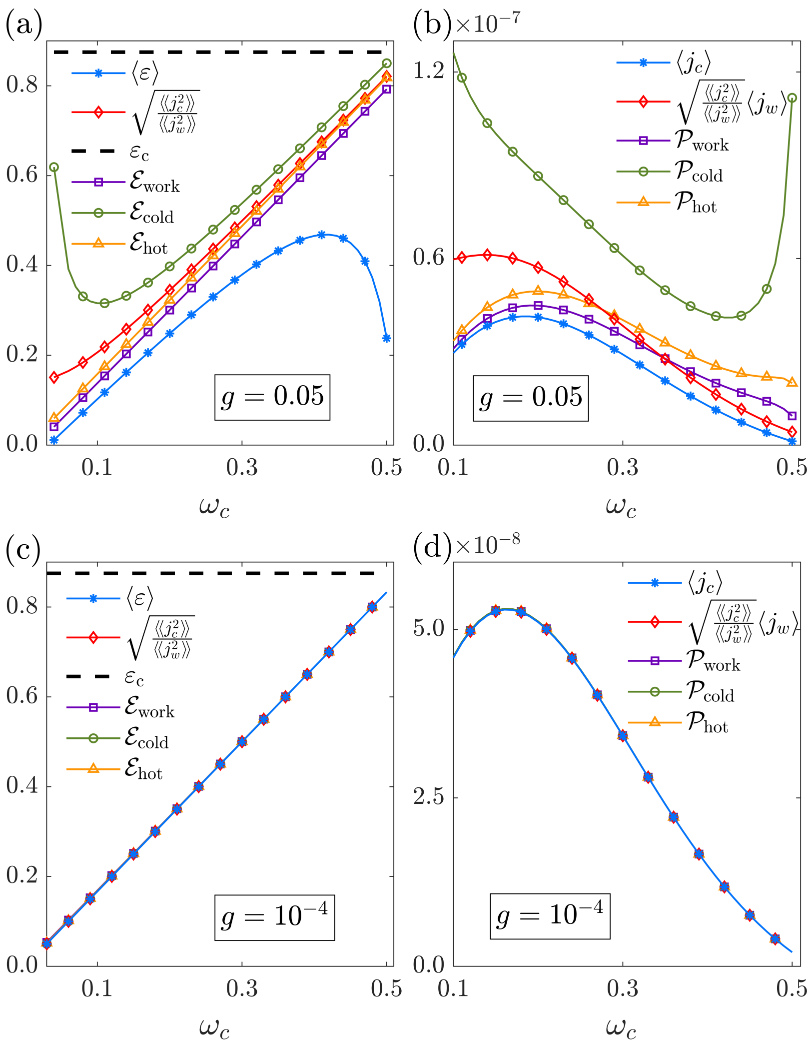


Figure 2.3: Comparison between different bounds on cooling efficiency $\langle \varepsilon \rangle$ [(a) and (c)], and cooling power $\langle j_c \rangle$ [(b) and (d)] for the four-level AR as a function of $\omega_c$. The parameters chosen here are: $T_c = 0.14$, $T_h = 0.15$, $T_w = 0.16$, $\omega_w = 0.6$, $\gamma_c = \gamma_h = \gamma_w = 10^{-3}$, $\Lambda = 50$. For (a) and (b) $g = 5 \times 10^{-2}$. For (c) and (d) $g = 1 \times 10^{-4}$, which correspond to the tight-coupling situation. For these parameters, $\varepsilon_c = 0.8750$.

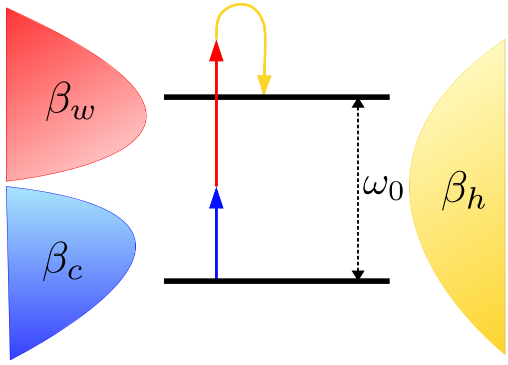


Figure 2.4: Schematic of a two-level AR coupled strongly with all the three baths. The bath-induced incoherent transitions are shown by the solid arrows. In the population dynamics, the different baths induced transition rates contribute in a multiplicative manner.

## 2.5 Example II: Strong (multiplicative) system-reservoir coupling

### 2.5.1 Two-level working medium

The bounds on cooling efficiency and cooling power obtained in our study are not limited to the nature of the system-bath coupling. In order to see this, we choose another central model for quantum AR, where the working medium consists of a two-level system coupled strongly to all three reservoirs (see Fig. 2.4) as a second example. We note that, a qubit coupled weakly to three reservoirs fails to work as a quantum AR [172] , thanks to the non-additive nature of the transition rates in the rate equations, leading to a collective and simultaneous effect involving all the three reservoirs. The full Hamiltonian, which mimics a strong system-bath interaction, can be written as [172],

$$H = \frac{\omega_0}{2}\sigma_z + \frac{\sigma_x}{2} \otimes \big(B_c \otimes B_h \otimes B_w\big) + \sum_{\alpha=c,h,w} H_{B,\alpha}, \tag{2.5.1}$$

where the crucial second term involves the bath operators in a multiplicative manner and is responsible for inducing a collective effect. This term induces transition between the system states with energy being shared or supplied by all three baths simultaneously. Here, $\sigma_z = |1\rangle\langle 1| - |0\rangle\langle 0|$ and $\sigma_x = |1\rangle\langle 0| + |0\rangle\langle 1|$ are the standard

Pauli spin operators with $|0\rangle$ ($|1\rangle$) representing the ground (excited) state of the qubit, and

$$B_\alpha = \sum_j \frac{g_{\alpha,j}}{\omega_{\alpha,j}} (b^\dagger_{\alpha,j} + b_{\alpha,j}) \tag{2.5.2}$$

is the bath operator with coupling strength $g_{\alpha,j}$, corresponding to reservoir $\alpha$. $H_{B,\alpha} = \sum_j \omega_{\alpha,j} b^\dagger_{\alpha,j} b_{\alpha,j}$ is the standard bosonic bath Hamiltonian. The individual baths are in equilibrium with a fixed temperature. Note that the Hamiltonian appearing in (2.5.1) can be rigorously derived by performing a polaron transformation to the standard spin-boson Hamiltonian, which is bilinearly coupled to bosonic baths [172]. Similar to previous method, one can obtain the mean currents and associated fluctuations using a full-counting statistics approach. Following Ref. [172], the counting field dressed rate matrix can be written as,

$$\hat{\mathcal{W}}(\chi) = \begin{pmatrix} -k_{0\to1} & k^\chi_{1\to0} \\ k^\chi_{0\to1} & -k_{1\to0} \end{pmatrix}, \tag{2.5.3}$$

with the dressed transition rates given by

$$\begin{aligned} k^\chi_{1\to0} = \int_{-\infty}^{\infty} \frac{d\omega}{2\pi} \int_{-\infty}^{\infty} \frac{d\omega'}{2\pi} \, M_h(\omega)\, M_c(\omega')\, M_w(\omega_0 - \omega - \omega') \\ e^{-i\chi_h\omega}\, e^{-i\chi_c\omega'}\, e^{-i\chi_w(\omega_0-\omega-\omega')}, \end{aligned} \tag{2.5.4}$$

where $k^\chi_{0\to1} = k^\chi_{1\to0}(\omega_0 \to -\omega_0)$. Here, $M_\alpha(t) = \langle B_\alpha(t) B_\alpha(0)\rangle$ is the two-time bath correlation function, with $B_\alpha(t) = e^{iH_{B,\alpha}t}\, B_\alpha\, e^{-iH_{B,\alpha}t}$ being the bath operator in the interaction picture. $M_\alpha(\omega) = \int_{-\infty}^{\infty} ds\, M_\alpha(s)\, e^{iws}$ is the Fourier transformed two-time bath correlation function, which satisfies the detailed balance condition $M_\alpha(-\omega) = e^{-\beta_\alpha\omega}\, M_\alpha(\omega)$. As shown in Ref. [172], various possible choices of $M_\alpha(\omega)$ can give rise to refrigeration, and the optimal cooling efficiency $\varepsilon_c$ is achieved in the tight-coupling limit, which corresponds to highly engineered baths with $M_\alpha(\omega)$ being described by a single frequency component. Here, we make the following

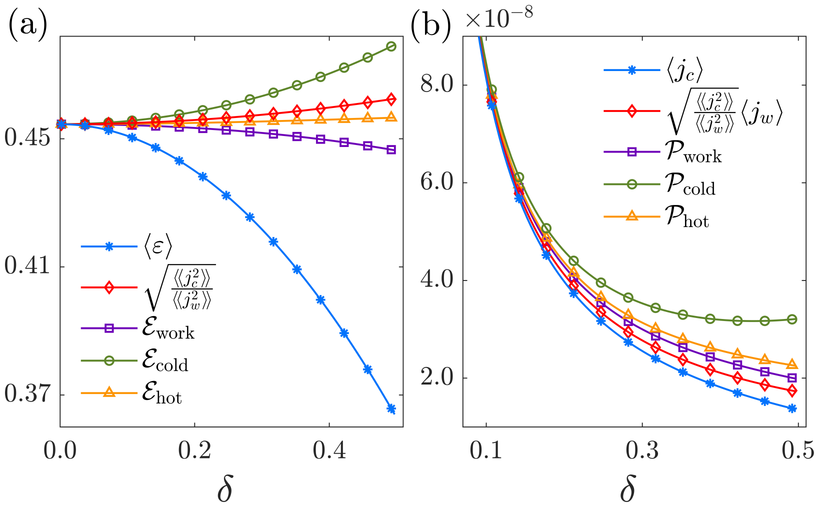


Figure 2.5: Comparison between different bounds for (a) cooling efficiency $\langle \varepsilon \rangle$ and (b) cooling power $\langle j_c \rangle$ for two-level quantum AR operating under strong system-bath coupling as a function of $\delta$, as defined in (2.5.5) . The parameters chosen here are $\omega_0 = 0$, $T_c = 1$, $T_h = 1.3$, $T_w = 1.6$, $\omega_c = 0.5$, $\omega_w = 1.1$, $\omega_h = \omega_c + \omega_w = 1.6$, $\gamma_h = \gamma_w = 10^{-2}$ and $\gamma_c = 1$. For these set of parameters, $\varepsilon_c = 0.6250$.

choice for $M_\alpha(\omega)$ for $\omega > 0$,

$$\begin{aligned} M_c(\omega) =& \gamma_c \, \delta(\omega - \omega_c), \\ M_h(\omega) =& \frac{\gamma_h}{2\delta} \Big[ \Theta(\omega - \omega_h + \delta) - \Theta(\omega - \omega_h - \delta) \Big], \\ M_w(\omega) =& \frac{\gamma_w}{2\delta} \Big[ \Theta(\omega - \omega_w + \delta) - \Theta(\omega - \omega_w - \delta) \Big]. \end{aligned} \tag{2.5.5}$$

The negative frequency parts for the rates are fixed by the detailed balance equations. Here, $\gamma_\alpha > 0$ is a dimensionless parameter, $\Theta(x)$ ($\delta(x)$) is the Heaviside step (Dirac Delta) function. $\omega_\alpha$ is the central characteristic frequency for the reservoir $\alpha$. We set the central frequencies such that the resonant condition $\omega_c + \omega_w = \omega_h$ is satisfied. The parameter $\delta$ appearing in $M_h$ and $M_w$ in (2.5.5) is the width parameter around central frequencies $\omega_h$ and $\omega_w$. Notice that, $\delta \to 0$ corresponds to the tight-coupling or the optimal cooling limit. In Fig. 2.5 we display our results for the bounds on cooling efficiency and cooling power as a function of $\delta$. For small values of $\delta$ ($\delta \ll \omega_\alpha$), corresponding to the tight-coupling limit, all the bounds saturate and exactly predict the values for both the mean cooling power and mean cooling efficiency. For large $\delta$, i.e., beyond the tight-coupling limit, the hierarchy in the bounds on cooling power become transparent, and within this hierarchy $\mathcal{P}_{\text{work}}$ provides the tightest bound for the power. Moreover, for these choice of parameters, the additional bounds in equations (2.1.15) and (2.1.16) for the cooling power and the cooling efficiency become tighter than the bounds obtained from the TURs.

## 2.6 Summary

In this chapter, we have demonstrated that for three-terminal autonomous absorption refrigerators operating in the linear response regime, a strict hierarchy exists in the relative fluctuations of the three currents involved. This result stems from the Onsager's reciprocity relations, with the additional requirement that direction of the mean currents aligns with the refrigeration conditions. As a consequence, the seemingly independent bounds on cooling power derived from the TURs are, in fact, interconnected and follow a similar hierarchy. Within this framework, the most accurate estimate of cooling power is achieved when the bound is derived from the work-TUR. However, the bounds on cooling efficiency derived from TURs do not adhere to this hierarchy.

Additionally, we provide independent, universal bounds on both cooling efficiency and cooling power, expressed in terms of ratio of output to input current fluctuations. In the example section, through the analysis of two paradigmatic absorption refrigerators, we have shown that these universal bounds can be tighter than those obtained from the TURs.

# 3

# Fate of bounds on fluctuations for continuous machines with broken time-reversal symmetry

In the previous chapter, we studied linear response regime of autonomous ARs, which fall into the continuous thermal machine category, and reported a strict hierarchy in the relative fluctuation of the three different currents involved. Let us first highlight two crucial points:

(i) Since, the purpose of an AR is to extract heat from the cold reservoir by absorbing energy from the work reservoir, we identify the output current as $\langle j_{\text{out}} \rangle = \langle j_c \rangle$, and the input current as $\langle j_{\text{in}} \rangle = \langle j_w \rangle$ of this setup. From the hierarchy in (2.1.1), it is evident that

$$\frac{\langle\langle j_{\text{out}}^2 \rangle\rangle}{\langle j_{\text{out}} \rangle^2} \geq \frac{\langle\langle j_{\text{in}}^2 \rangle\rangle}{\langle j_{\text{in}} \rangle^2}. \tag{3.0.1}$$

The above inequality concerning the relative fluctuation of output and input currents was first reported in Ref. [53], and was shown to be valid for any continuous thermal machine ( e.g., engine, refrigerator and heat pump) that respects time-reversal symmetry, and operates in the linear response regime. An intriguing outcome of the above relation is that

$$\langle \eta \rangle^2 \leq \eta^{(2)} := \frac{\langle\langle j_{\text{out}}^2 \rangle\rangle}{\langle\langle j_{\text{in}}^2 \rangle\rangle} \leq \eta_{\mathcal{C}}^2, \tag{3.0.2}$$

where, $\langle \eta \rangle = |\langle j_{\rm out} \rangle| / \langle j_{\rm in} \rangle$ represents the efficiency of the machine, and $\eta_{\mathcal{C}}$ denotes the maximum efficiency permissible under the second law of thermodynamics [such as Carnot efficiency for engines and Carnot coefficient of performance (COP) for refrigerators]. Notice that, equation (2.1.15) in the previous chapter is equivalent to (3.0.2). The profound implication of the above relation is that it offers a stricter universal bound on the performance (efficiency) of a small-scale continuous thermal machine in terms of fluctuation of the currents.

(ii) We observe that the underlying time-reversal symmetry played a pivotal role in deriving the results presented both in the previous chapter and in Ref. [53]. To be more specific, in the linear response regime where Onsager formalism is applicable, this symmetry leads to the famous Onsager reciprocity relation $L_{ij} = L_{ji}$, indicating that the off-diagonal elements of the Onsager matrix are equal. Our derivations heavily relied on these reciprocity relations.

A natural question that immediately arises is what happens to the aforementioned results when the time-reversal symmetry is not respected. In fact, breakdown of time-reversal symmetry is quite common in many scenarios, such as thermoelectric transport in presence of magnetic field $\mathcal{B}$ [38, 191–195] and cyclic heat engines driven in a time-asymmetric manner [196, 197] (see Fig. 3.1). In this chapter, we address this gap by generalizing the earlier findings to cases where time-reversal symmetry is broken.

The structure of this chapter is as follows: In Section 3.1, we extend the time-reversal symmetric results [cf. (3.0.1) and (3.0.2)] to the broken time-reversal symmetry scenario. We also explore the implications of our findings on the recently reported generalized thermodynamic uncertainty relations (GTURs) for time-reversal symmetry-broken systems [160]. In Section 3.2, we illustrate these results with a paradigmatic example: a classical cyclic Brownian heat engine.

## 3.1 Broken time-reversal symmetry: Bounds on symmetrized fluctuations

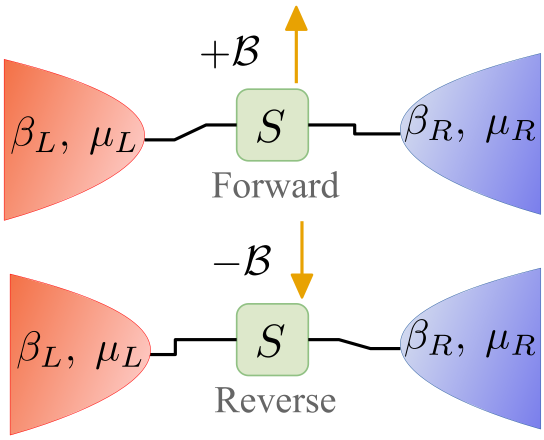


Figure 3.1: Schematic for broken time-reversal symmetric situation in a thermoelectric transport set up in presence of magnetic field $\mathcal{B}$. Note that in the reverse process sign of $\mathcal{B}$ is altered, $\mathcal{B} \to -\mathcal{B}$.

### 3.1.1 Distinct forward and reverse processes

In systems where time-reversal symmetry is broken, it is essential to distinguish between forward $(f)$ and reverse $(r)$ processes. The $(f)$ process typically refers to the system's evolution in the presence of external driving forces (such as magnetic field $\mathcal{B}$ and other time-dependent parameter in the system Hamiltonian), while the $(r)$ process is its evolution when these forces are reversed (see Fig. 3.1). Notice, this distinction can lead to different statistical properties and fluctuation behaviors, necessitating a more comprehensive framework to describe systems where time-reversal symmetry is broken.

We consider here a generic out-of-equilibrium setup with broken time-reversal symmetry, characterized by two independent stochastic currents. For notational convenience, we denote these currents as $j_1$ and $j_2$, with the corresponding conjugate affinities $\mathcal{A}_1$ and $\mathcal{A}_2$, respectively. Without any loss of generality, the thermodynamic affinities are assumed to be time-reversal symmetric, and positive, $\mathcal{A}_1, \mathcal{A}_2 > 0$. In our context, $j_1$ refers to the input current $(j_{\text{in}})$, and $j_2$ refers to the output current $(j_{\text{out}})$. Similar to previous chapter, we restrict our discussions to the linear response regime. In this regime, the currents in $f$ and $r$ processes can be expressed as

$$\langle j_\alpha \rangle_f = \sum_{\gamma=1,2} L^f_{\alpha\gamma} \mathcal{A}_\gamma, \tag{3.1.1}$$

$$\langle j_\alpha \rangle_r = \sum_{\gamma=1,2} L^r_{\alpha\gamma} \mathcal{A}_\gamma, \tag{3.1.2}$$

with $\alpha = 1, 2$ [98, 99]. It is important to note that when time-reversal symmetry is preserved, the forward and reverse processes become identical.

### 3.1.2 Breakdown of Onsager reciprocity: Onsager-Cashimir relation

In the presence of time-reversal symmetry, the Onsager reciprocity states that the off-diagonal elements of the Onsager matrix are equal ($L_{\alpha\gamma} = L_{\gamma\alpha}$). However, when time-reversal symmetry is broken, this relation no longer holds. Instead, the Onsager-Casimir relations come into play, which generalizes the reciprocity to $L_{\alpha\gamma}(B) = L_{\gamma\alpha}(-B)$, where $B$ represents the magnetic field [198]. This modification accounts for the effects of external magnetic fields or other time-reversal symmetry-breaking factors. In our context, this relation translates to $L^f_{\alpha\gamma} = L^r_{\gamma\alpha}$ [38, 193, 194, 199], or equivalently, $L^f = (L^r)^T$, where $T$ denotes the transpose of the matrix. We notice that, the non-negativity of the entropy production rate for individual $f$ and $r$ processes ensures that the determinant of the symmetric part of the Onsager matrix is non-negative,

$$L^i_{11}, L^i_{22} \geq 0, \qquad \det(L^s) = L^i_{11} L^i_{22} - \frac{(L^i_{12} + L^i_{21})^2}{4} \geq 0, \tag{3.1.3}$$

for $i = f, r$, where $L^s = [L^f + (L^f)^T]/2 = [L^r + (L^r)^T]/2 = [L^f + L^r]/2$.

### 3.1.3 Symmetrization of the operational regime conditions

An immediate consequence of the breakdown of conventional Onsager reciprocity is that (3.0.2) may not hold for individual forward or reverse processes. Moreover, we recall specifying the operational regime of the machine was crucial when deriving (3.0.2). In the case of broken time-reversal symmetry, however, the forward and reverse cycles can operate in different operational regimes. We observe that specifying operational regime for individual forward or reverse processes does not lead us to a useful bound like the one given in (3.0.2). Instead, by constraining both the forward and reverse process es to operate in the same operational regime, we derive the following inequality between the symmetrized relative fluctuation of the two currents

$$\frac{\langle\langle j_2^2\rangle\rangle_f + \langle\langle j_2^2\rangle\rangle_r}{\left(\langle j_2\rangle_f + \langle j_2\rangle_r\right)^2} \geq \frac{\langle\langle j_1^2\rangle\rangle_f + \langle\langle j_1^2\rangle\rangle_r}{\left(\langle j_1\rangle_f + \langle j_1\rangle_r\right)^2}. \tag{3.1.4}$$

### 3.1.4 Generalized thermodynamic uncertainty relations

Before presenting the proof for (3.1.4), we motivate the choice of this particular form of symmetrized relative fluctuation. Recently, in Ref. [160] a generalized version of the conventional TURs was reported, which is applicable in the scenario of broken time-reversal symmetry. In the linear response regime, the generalized thermodynamic uncertainty relations (GTURs) provide universal lower bounds on the symmetrized relative fluctuation of individual currents in terms of the symmetrized entropy production rate,

$$\left(\langle\sigma\rangle_f + \langle\sigma\rangle_r\right)\frac{\langle\langle j_\alpha^2\rangle\rangle_f + \langle\langle j_\alpha^2\rangle\rangle_r}{\left(\langle j_\alpha\rangle_f + \langle j_\alpha\rangle_r\right)^2} \geq 2, \qquad \text{for } \alpha = 1, 2. \tag{3.1.5}$$

Here, the entropy production rate is denoted as $\langle\sigma\rangle_i = \sum_{\alpha=1,2}\langle j_\alpha\rangle_i \mathcal{A}_\alpha \geq 0$, with $i = f, r$ representing the forward and reverse processes, respectively [38, 116]. The proof of GTURs in the linear response regime relies solely on the non-negativity condition of the determinant of the symmetric part of the Onsager matrix. From the inequality in (3.1.4), it is evident that under the condition that both the forward and reverse processes operate in the same regime, the GTURs for different currents exhibit a strict hierarchy:

$$\left(\langle\sigma\rangle_f + \langle\sigma\rangle_r\right)\frac{\langle\langle j_2^2\rangle\rangle_f + \langle\langle j_2^2\rangle\rangle_r}{\left(\langle j_2\rangle_f + \langle j_2\rangle_r\right)^2} \geq \left(\langle\sigma\rangle_f + \langle\sigma\rangle_r\right)\frac{\langle\langle j_1^2\rangle\rangle_f + \langle\langle j_1^2\rangle\rangle_r}{\left(\langle j_1\rangle_f + \langle j_1\rangle_r\right)^2} \geq 2,$$

$$\text{or equivalently,} \qquad \mathrm{GTUR}(j_{\mathrm{out}}) \geq \mathrm{GTUR}(j_{\mathrm{in}}) \geq 2. \tag{3.1.6}$$

### 3.1.5 Bounds on symmetrized efficiency

Let us first demonstrate a brief proof for (3.1.4). Notice that:

$$\langle j_\alpha\rangle_f + \langle j_\alpha\rangle_r = 2\sum_{\gamma=1,2} L^s_{\alpha\gamma}\mathcal{A}_\gamma, \qquad \langle\langle j_\alpha^2\rangle\rangle_f + \langle\langle j_\alpha^2\rangle\rangle_r = 4\,L^s_{\alpha\alpha}, \tag{3.1.7}$$

where we have used the modified Onsager reciprocity $L^f = (L^r)^T$, and the standard fluctuation-dissipation relation $\langle\langle j_\alpha^2 \rangle\rangle_f = \langle\langle j_\alpha^2 \rangle\rangle_r = 2\, L_{\alpha\alpha}^s \equiv 2\, L_{\alpha\alpha}^{f(r)}$ [76, 80, 85–87]. We adhere to the sign convention introduced in the previous chapter: Energy flowing into the working fluid is positive. Using a similar method as in the previous chapter, we obtain

$$\begin{aligned}&\big(\langle\langle j_2^2 \rangle\rangle_f + \langle\langle j_2^2 \rangle\rangle_r\big)\big(\langle j_1 \rangle_f + \langle j_1 \rangle_r\big)^2 - \big(\langle\langle j_1^2 \rangle\rangle_f + \langle\langle j_1^2 \rangle\rangle_r\big)\big(\langle j_2 \rangle_f + \langle j_2 \rangle_r\big)^2 \\ &= 8 \det(L^s)\left[\big(\langle j_1 \rangle_f + \langle j_1 \rangle_r\big)\mathcal{A}_1 - \big(\langle j_2 \rangle_f + \langle j_2 \rangle_r\big)\mathcal{A}_2\right] \geq 0 \end{aligned} \tag{3.1.8}$$

Here, to reach the inequality in the last line, we used:

(i) $\det(L^s) \geq 0$, which manifests from the second law, as given in (3.1.3).

(ii) Under the symmetrized operational regime condition, where both the forward and reverse processes operate in the same regime, we argue that $\langle j_1 \rangle_f \mathcal{A}_1$ and $\langle j_1 \rangle_r \mathcal{A}_1$ are both positive, while $\langle j_2 \rangle_f \mathcal{A}_2$ and $\langle j_2 \rangle_r \mathcal{A}_2$ are both negative. Here, note that $j_1$ represents the input current and $j_2$ represents the output current of the thermal machine. To physically endorse this claim, we observe that thermodynamic currents and affinities appear in such product form in the expression for the entropy production rate, $\langle \sigma \rangle_i = \sum_{\alpha=1,2} \langle j_\alpha \rangle_i \mathcal{A}_\alpha$, with $i = f, r$. According to the second law of irreversible thermodynamics, any spontaneous energy flow (such as the dissipation of electrical, mechanical, or chemical energy into a heat bath, or the transfer of heat from a hot to a cold body) is accompanied by a positive entropy production. Thermodynamic machines, however, are designed to perform tasks that are not spontaneous in nature. For example, engines convert heat into useful work, refrigerators extract heat from a cold reservoir, and heat pumps transfer heat to a hot bath. These processes involve channeling energy in a non-spontaneous manner. Consequently, the entropy production rate $\langle j_2 \rangle \mathcal{A}_2$ associated with the output current is expected to be negative, reflecting the non-spontaneous nature of the output of a thermal machine. Conversely, the entropy production rate $\langle j_1 \rangle \mathcal{A}_1$ associated with the input current is expected to be positive, ensuring that the total entropy production rate remains positive.

(3.1.8) concludes the proof for (3.1.4). A straightforward outcome of (3.1.4) is a symmetrized version of (3.0.2), applicable for the time-reversal symmetry-broken case,

$$\langle\eta\rangle_s^2 := \left(\frac{|\langle j_2\rangle_f + \langle j_2\rangle_r|}{\langle j_1\rangle_f + \langle j_1\rangle_r}\right)^2 \leq \eta^{(2)} = \frac{\langle\!\langle j_2^2\rangle\!\rangle_f + \langle\!\langle j_2^2\rangle\!\rangle_r}{\langle\!\langle j_1^2\rangle\!\rangle_f + \langle\!\langle j_1^2\rangle\!\rangle_r} \equiv \frac{\langle\!\langle j_2^2\rangle\!\rangle_{f(r)}}{\langle\!\langle j_1^2\rangle\!\rangle_{f(r)}} \leq \eta_C^2, \tag{3.1.9}$$

where $\langle\eta\rangle_s$ represents the symmetrized efficiency of the machine.

### 3.1.6 Symmetrized tight-coupling condition

The equality in equations (3.1.4) and (3.1.6) corresponds to the symmetrized tight-coupling condition: $\big(\langle j_1\rangle_f + \langle j_1\rangle_r\big) \propto \big(\langle j_2\rangle_f + \langle j_2\rangle_r\big)$. When time-reversal symmetry is preserved, this symmetrized tight-coupling condition reduces to the usual tight-coupling limit, $\langle j_1\rangle \propto \langle j_2\rangle$. Notably, for individual forward or reverse processes, the usual tight-coupling limit cannot be attained. To substantiate this claim, we present a proof by contradiction. First, we assume that the usual tight-coupling condition holds in the forward process, $\langle j_1\rangle_f = \mathrm{c}\langle j_2\rangle_f$, with c being a proportionality constant. From (3.1.1), this condition implies: (i) $L_{11}^f = \mathrm{c}L_{21}^f$, and (ii) $L_{12}^f = \mathrm{c}L_{22}^f$. Using conditions (i) and (ii), one can show that $\det[L^s] = -(L_{12}^f - L_{21}^f)^2/4 \leq 0$, which directly contradicts the second law of thermodynamics, as given in (3.1.3). Therefore, we conclude that, in the time-reversal symmetry-broken case, the tight-coupling limit for individual forward (or reverse) processes is an impossible situation.

In what follows, we illustrate the results obtained in this section using a paradigmatic example that exhibits broken time-reversal symmetry: a classical cyclic Brownian heat engine, which falls into the class of non-autonomous continuous thermal machine.

## 3.2 Example: Cyclic Brownian heat engine

We consider a one-dimensional cyclic heat engine, consisting of an overdamped Brownian particle in a harmonic trap with a periodically varying trap strength $\kappa(t)$. The particle diffuses within a thermal bath whose temperature $T(t)$ also varies periodically with the same cycle duration $\tau_{cyc}$. In the overdamped limit, where inertial effects are negligible, the Hamiltonian governing the system is given by

$$\begin{aligned} H(x,t) &= \frac{1}{2}\kappa(t)x^2 = \frac{1}{2}\big(\kappa_0 + \Delta\kappa\gamma_w(t)\big)x^2 \\ &= H_0(x) + \Delta H g_w(x,t), \end{aligned} \tag{3.2.1}$$

where $\kappa_0$ is the static component of the trap strength, and $\Delta\kappa$ represents the modulation amplitude. The dimensionless periodic function $\gamma_w(t)$ modulates the trap strength, satisfying $0 \leq \gamma_w(t) \leq 1$. The characteristic length scale of the system is $x_0 = \sqrt{2T_c/\kappa_0}$, where $T_c$ refers to the minimum temperature of the temperature profile. The static part of the Hamiltonian is $H_0(x) = \kappa_0 x^2/2$. We define $\Delta H = \Delta\kappa x_0^2$ as an energy scale corresponding to the strength of time-dependent perturbation, while the dimensionless function $g_w(x,t) = \gamma_w(t)x^2/2x_0^2$ encodes both spatial and temporal dependencies.

The time-dependent temperature profile $T(t)$ is parameterized in terms of its inverse:

$$\frac{1}{T(t)} = \frac{1}{T_c} - \left(\frac{1}{T_c} - \frac{1}{T_h}\right)\gamma_q(t),$$

or equivalently,

$$\beta(t) = \beta_c - \Delta\beta\gamma_q(t). \tag{3.2.2}$$

The dimensionless function $\gamma_q(t)$, controlling the temperature modulation, satisfies $0 \leq \gamma_q(t) \leq 1$.

The change in the internal energy $U(x,t) = \int dx H(x,t)p(x,t)$, where $p(x,t)$ denotes the probability density to find the system at $x$ at time $t$, is partitioned into work-done on the system and heat input from the reservoir,

$$\begin{aligned} \dot{U} &= \int dx \dot{H}(x,t)p(x,t) + \int dx H(x,t)\dot{p}(x,t) \\ &\equiv \dot{w} + \dot{q}. \end{aligned} \tag{3.2.3}$$

Given that both the Hamiltonian $H(x,t)$ and the temperature $T(t)$ are periodic with cycle time $\tau_{cyc}$, we expect the system's probability density function $p(x,t)$ to eventually reach a periodic steady state after many cycles. In this periodic steady state, the probability distribution $p_{\rm pss}(x,t)$ is expected to share the same periodicity as the external driving, $p_{\rm pss}(x,t) = p_{\rm pss}(x,t+\tau_{cyc})$. Assuming that $p_{\rm pss}(x,t)$ is reached, and, therefore, no entropy generation in the system in a full cycle, the total entropy production rate per cycle is given by

$$\begin{aligned}\dot{\Sigma} &= -\frac{1}{\tau_{cyc}}\int_0^{\tau_{cyc}} dt\,\frac{\dot{q}(t)}{T(t)} \\ &= \beta_c \Delta H\,\frac{1}{\tau_{cyc}}\int_0^{\tau_{cyc}} dt \int dx\,\dot{g}_w(x,t)\,p_{\rm pss}(x,t) \\ &\quad + \Delta\beta\,\frac{1}{\tau_{cyc}}\int_0^{\tau_{cyc}} dt \int dx\,\gamma_q(t) H(x,t)\,\dot{p}_{\rm pss}(x,t) \\ &= \mathcal{A}_w \langle j_w \rangle_f + \mathcal{A}_q \langle j_q \rangle_f . \end{aligned} \tag{3.2.4}$$

Here, to in the second line we have used (3.2.2) and (3.2.3), and carried out integration by parts with respect to time. In the last line, we have identified the thermodynamic affinities $\mathcal{A}_w = \beta_c \Delta H$ and $\mathcal{A}_q = \Delta\beta$, and the corresponding thermodynamic fluxes $\langle j_w \rangle_f$ and $\langle j_q \rangle_f$, respectively. Note that the angular bracket $\langle\,\cdot\,\rangle$ stands for both spacial averaging and time averaging over one cycle. In the following, we focus in the linear response regime and seek for a linear expansion of the fluxes with respect to the affinities:

$$\begin{aligned}\langle j_w \rangle_f &= L_{ww}\mathcal{A}_w + L_{wq}\mathcal{A}_q, \\ \langle j_q \rangle_f &= L_{qw}\mathcal{A}_w + L_{qq}\mathcal{A}_q. \end{aligned} \tag{3.2.5}$$

The time-dependent driving protocols $\gamma_w(t)$ and $\gamma_q(t)$ in this model are chosen to be sinusoidal,

$$\begin{aligned}\gamma_w(t) &= \sin\big(2\pi t/\tau_{cyc} + \phi\big), \\ \gamma_q(t) &= \big(1 + \sin\left(2\pi t/\tau_{cyc}\right)\big)/2, \end{aligned} \tag{3.2.6}$$

where the phase $\phi$ introduces asymmetry between the driving protocols and breaks the underlying time-reversal symmetry.

The time evolution of the probability density $p(x,t)$ is governed by the Fokker-

Planck equation

$$\frac{\partial}{\partial t} p(x,t) = \frac{1}{\gamma}\Big([\kappa_0 + \Delta\kappa\gamma_w(t)]\partial_x x + \beta^{-1}(t)\partial_x^2\Big) p(x,t)$$
$$\equiv \mathcal{L}(x,t)\, p(x,t), \tag{3.2.7}$$

where $\gamma$ is the friction. The Fokker-Planck generator $\mathcal{L}(x,t)$ is expressed as the following expansion:

$$\begin{aligned}\mathcal{L}(x,t) &= \gamma^{-1}\big(\kappa_0\partial_x x + \beta_c^{-1}\partial_x^2\big) + \beta_c\Delta H\,\frac{\kappa_0}{2\gamma}\,\gamma_w(t)\partial_x x \\ &\quad + \Delta\beta\beta_c^{-2}\gamma^{-1}\gamma_q(t)\,\partial_x^2 + O(\Delta^2) \\ &\approx \mathcal{L}_0(x) + \mathcal{A}_w\mathcal{L}^w(x,t) + \mathcal{A}_q\mathcal{L}^q(x,t).\end{aligned} \tag{3.2.8}$$

The free (unperturbed) Fokker-Planck generator $\mathcal{L}_0$ results in equilibrium situation in the long time,

$$\mathcal{L}_0(x)\, p_{\mathrm{eq}}(x) = 0, \qquad \text{with} \quad p_{\mathrm{eq}}(x) = \frac{e^{-\beta_c H_0(x)}}{\int dx\, e^{-\beta_c H_0(x)}}. \tag{3.2.9}$$

Moreover, it obeys detailed balance:

$$\mathcal{L}_0(x)[\cdot\, p_{\mathrm{eq}}] = p_{\mathrm{eq}}\mathcal{L}^\dagger(x)[\cdot], \tag{3.2.10}$$

where the adjoint generator is given by

$$\mathcal{L}_0^\dagger(x) = \gamma^{-1}\big(-\kappa_0 x\partial_x + \beta_c^{-1}\partial_x^2\big). \tag{3.2.11}$$

Next, using standard procedure we expand $p_{\mathrm{pss}}(x,t)$ as

$$p_{\mathrm{pss}}(x,t) = p_{\mathrm{eq}}(x) + \sum_{\alpha=w,q}\mathcal{A}_\alpha\int_{-\infty}^{t} dt'\, e^{\mathcal{L}_0(x)(t-t')}\mathcal{L}^\alpha(x,t')\, p_{\mathrm{eq}}(x). \tag{3.2.12}$$

From (3.2.8) and (3.2.9), noticing that

$$\mathcal{L}^\alpha(x,t)p_{\mathrm{eq}}(x) = \zeta_\alpha\gamma_\alpha(t)\frac{\kappa_0}{2\gamma}\big(1 - \beta_c\kappa_0 x^2\big)p_{\mathrm{eq}}(x), \tag{3.2.13}$$

with $\alpha = w, q$, and $\zeta_w = 1$ and $\zeta_q = -2/\beta_c$, and using the detailed balance condition (3.2.10), we obtain

$$\begin{aligned} p_{\rm pss}(x,t) &= p_{\rm eq}(x) + \sum_{\alpha=w,q} \mathcal{A}_\alpha \zeta_\alpha \frac{\kappa_0}{2\gamma} \int_{-\infty}^{t} dt'\, \gamma_\alpha(t')\, p_{\rm eq}(x) e^{\mathcal{L}_0^\dagger(x)(t-t')} \big(1-\beta_c\kappa_0 x^2\big) \\ &= p_{\rm eq}(x) + \sum_{\alpha=w,q} \mathcal{A}_\alpha \zeta_\alpha \frac{\kappa_0}{2\gamma} \int_0^\infty dt'\, \gamma_\alpha(t-t')\, e^{-2\kappa_0\gamma^{-1}t'}\, p_{\rm eq}(x) \big(1-\beta_c\kappa_0 x^2\big). \end{aligned} \tag{3.2.14}$$

In the last line, we have used the fact that $\big(1-\beta_c\kappa_0 x^2\big)$ is a right eigenvector of $\mathcal{L}_o^\dagger$ with eigenvalue $-2\kappa_0\gamma^{-1}$, and changed the variable of the integration $t'$ as $t' \to t-t'$. Finally, we insert (3.2.14) into the expressions of $\langle j_\alpha \rangle$ given in (3.2.4), and obtain the desired expansion (3.2.5). For example,

$$\begin{aligned} \langle j_w \rangle &= \frac{1}{\tau_{cyc}} \int_0^{\tau_{cyc}} dt \int dx\, \dot{g}_w(x,t)\, p_{\rm pss}(x,t) \\ &= \sum_{\alpha=w,q} \mathcal{A}_\alpha \zeta_\alpha \frac{\kappa_0}{2\gamma} \frac{1}{\tau_{cyc}} \int_0^{\tau_{cyc}} dt \int_0^\infty dt'\, \dot{\gamma}_w(t)\, \gamma_\alpha(t-t')\, e^{-2\kappa_0\gamma^{-1}t'} \\ &\qquad\quad \times \int dx\, \frac{x^2}{2x_0^2} \big(1-\beta_c\kappa_0 x^2\big)\, p_{\rm eq}(x) \\ &= \sum_{\alpha=w,q} \mathcal{A}_\alpha \zeta_\alpha \left(-\frac{\kappa_0}{4\gamma}\right) \frac{1}{\tau_{cyc}} \int_0^{\tau_{cyc}} dt \int_0^\infty dt'\, \dot{\gamma}_w(t)\, \gamma_\alpha(t-t')\, e^{-2\kappa_0\gamma^{-1}t'} \\ &= \sum_{\alpha=w,q} \mathcal{A}_\alpha L_{w\alpha}. \end{aligned} \tag{3.2.15}$$

In the second line we have exploited that for our chosen protocols $\int_0^{\tau_{cyc}} \dot{\gamma}_\alpha(t)dt = 0$. Next we compute the time integrals using the explicit forms of $\gamma_w(t)$ and $\gamma_q(t)$, as given in (3.2.6). Similar analysis can be done for $\langle j_q \rangle$. Finally, we obtain

$$\begin{pmatrix} \langle j_w \rangle_f \\ \langle j_q \rangle_f \end{pmatrix} = \frac{\lambda\Omega^2}{16(\lambda^2+\Omega^2)} \begin{pmatrix} 1 & -\beta_c^{-1}(\cos\phi + \frac{\lambda}{\Omega}\sin\phi) \\ -\beta_c^{-1}(\cos\phi - \frac{\lambda}{\Omega}\sin\phi) & \beta_c^{-2} \end{pmatrix} \begin{pmatrix} \mathcal{A}_w \\ \mathcal{A}_q \end{pmatrix}, \tag{3.2.16}$$

where $\lambda = 2\kappa_0/\gamma$ , $\Omega = 2\pi/\tau_{cyc}$.

The reverse process is realized either by substituting $t \to -t$ or $\phi \to -\phi$. The effect on the Onsager matrix is simply to swap the off-diagonal elements.

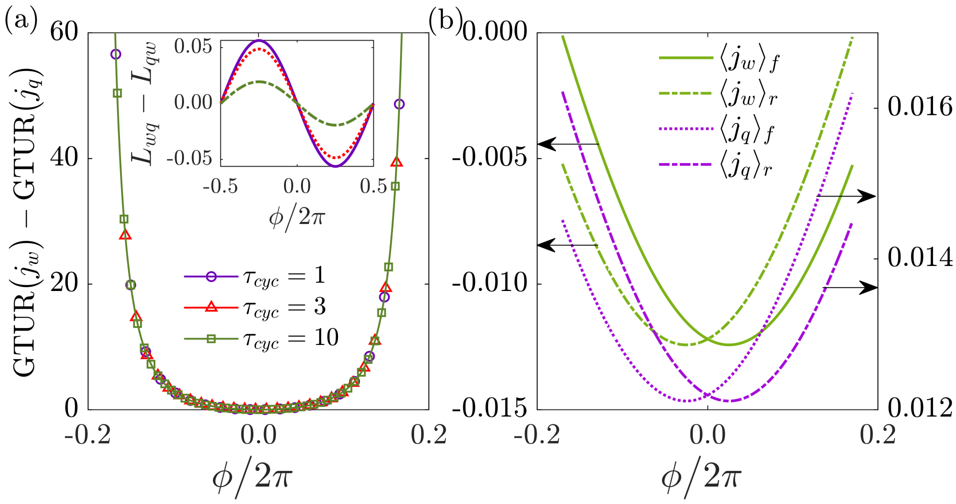


Figure 3.2: Results for a classical cyclic Brownian heat engine: (a) Plot for the difference between GTURs for output work current and GTUR for input heat current, GTUR($j_w$) − GTUR($j_q$), in the engine regime as a function of the asymmetry parameter $\phi$ for three different cycle times $\tau_{cyc} = 1$, 3, and 10. The inset shows the difference between the off-diagonal elements of Onsager matrix ($L_{wq} - L_{qw}$) for the same cycle times. (b) Plot for time-averaged work and heat currents in the engine regime for both F and R processes for $\tau_{cyc} = 1$. As both $\Delta H$ and $\Delta\beta$ are chosen positive here, following our convention an engine is realized when $\langle j_w \rangle_f, \langle j_w \rangle_r < 0$, and $\langle j_q \rangle_f, \langle j_q \rangle_r > 0$. The parameters considered here are $\beta_c = 1$, $\kappa_0 = 1$, $\gamma = 2$, $\Delta\beta = 0.3$, $\Delta H = 0.1$.

**Results in the engine regime**

We demonstrate the results in Fig. 3.2 by focusing on the engine regime and display the GTUR bounds [see Fig. 3.2 (a)] as a function of $\phi$ for three different cycle times. Fig. 3.2 (b) shows the currents (shown only for $\tau_{cyc} = 1$) satisfying the engine conditions in both $f$ and $r$ processes, i.e., $\langle j_w \rangle_{f,r} < 0, \langle j_q \rangle_{f,r} > 0$, for small $\Delta H$ and $\Delta\beta$. As expected, the GTUR for output work current is always upper bounded by the corresponding GTUR for input heat current with the difference (GTUR($j_w$) − GTUR($j_q$)) gets reduced with increasing cycle time $\tau_{cyc}$, corresponds to approaching the generalized tight-coupling limit. Following the positivity of the entropy production rate, it is easy to check that the standard thermodynamic efficiency for the engine, defined as, $\langle \eta \rangle_s := -\frac{\beta_c^{-1} \mathcal{A}_w \langle j_w \rangle_s}{\langle j_q \rangle_s} \leq \eta_C = \frac{\Delta\beta}{\beta_c}$ is bounded by the

Carnot value. Similarly, following (3.2.16), we receive for $\eta^{(2)}$,

$$\eta^{(2)} := \frac{\beta_c^{-2}\,\mathcal{A}_w^2 \langle\langle j_w^2 \rangle\rangle_s}{\langle\langle j_q^2 \rangle\rangle_s}. \tag{3.2.17}$$

Note that here we have used the simplified notations $\langle\, \cdot \,\rangle_s \equiv \langle\, \cdot \,\rangle_f + \langle\, \cdot \,\rangle_r$, and similarly $\langle\langle \cdot \rangle\rangle_s \equiv \langle\langle \cdot \rangle\rangle_f + \langle\langle \cdot \rangle\rangle_r$.

### Results in the refrigerator regime

The cyclic Brownian machine in suitable parameter regime can work as a refrigerator. So-far, in our set-up, we have considered only one bath. The thermal affinity $\mathcal{A}_q$, defined in the main text, is the consequence of a periodically varying temperature of the bath $\beta(t) = \beta_c + \Delta\beta\gamma_q(t)$, where $0 \leq \gamma_q(t) \leq 1$. However, this particular situation can also be looked upon as $\mathcal{A}_q$ created by thermal gradient of two distinct baths: a cold one with inverse temperature $\beta_c$ and a hot bath with inverse temperature $\beta_h$. Then, by definition $\langle j_q \rangle$ provides us the heat flux from the hot bath and the heat flux from the cold reservoir is then given as $\langle j_c \rangle = -\beta_c^{-1}\mathcal{A}_w\langle j_w \rangle - \langle j_q \rangle$. Now to realise a refrigeration regime we should extract heat from the cold reservoir, i.e., $\langle j_c \rangle_f \geq 0$ and $\langle j_c \rangle_r \geq 0$ by applying power from the mechanical controller, $\langle j_w \rangle_f \geq 0$ and $\langle j_w \rangle_r \geq 0$ in both the forward and reversed processes. However, in linear response, the cooling flux becomes $\langle j_c \rangle_{f,r} \approx -\langle j_q \rangle_{f,r}$. Note that the angular bracket here denotes a combined average over the cycle time $\tau_{cyc}$ and over the phase-space.

The coefficient of performance(COP) of the refrigerator, $\langle \varepsilon \rangle_s := \frac{\langle j_c \rangle_s}{\beta^{-1}\mathcal{A}_w\langle j_w \rangle_s} = -\frac{\langle j_q \rangle_s}{\beta^{-1}\mathcal{A}_w\langle j_w \rangle_s} \leq \varepsilon_{\rm c} \approx \frac{\beta_c}{\Delta\beta}$ is upper bounded by the corresponding Carnot value for the refrigerator. Analogous to our engine treatment, one can obtain a tighter bound on COP, given by the ratio of fluctuations of output current to input current.

$$\varepsilon^{(2)} := \frac{\langle\langle j_q^2 \rangle\rangle_s}{\beta^{-2}\mathcal{A}_w^2 \langle\langle j_w^2 \rangle\rangle_s}.$$

In Fig. 3.3 we display the results in the refrigerator regime. In panel (a) we show that in this regime, the GTUR for extracted heat current for the cold bath (output) is always larger than the input work current. Note that, in the linear response regime, as $\langle j_c \rangle_s \approx -\langle j_q \rangle_s$, the GTURs for both the cold and hot currents are the

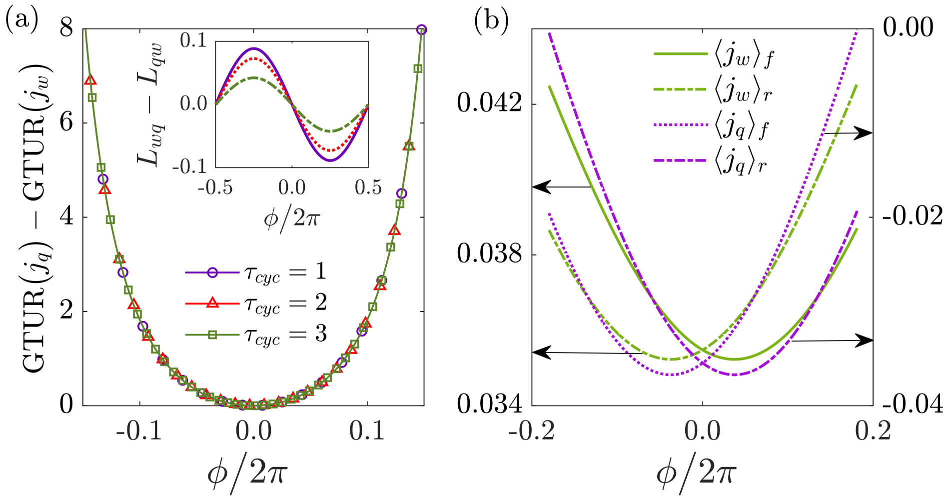


Figure 3.3: (Color o nline:) Results for a classical cyclic Brownian machine in the refrigerator regime: (a) Plot for the difference between GTURs for output heat current extracted from the cold bath and the input work current, GTUR$(j_q)$ − GTUR$(j_w)$, in the refrigerator regime as a function of $\phi$ for three different cycle times $\tau_{cyc} = 1$, 2, and 3. The inset shows the difference between the off-diagonal elements of Onsager matrix $(L_{wq} - L_{qw})$ for the same cycle times. (b) Plot for time-averaged work and heat currents in the refrigerator regime for both $f$ and $r$ processes for $\tau_{cyc} = 1$. As both $\Delta H$ and $\Delta\beta$ are chosen positive here, following our convention a refrigerator is realized when $\langle j_w \rangle_f$, $\langle j_w \rangle_r > 0$, and $\langle j_q \rangle_f$, $\langle j_q \rangle_r < 0$. The parameters considered here are $\beta_c = 1$, $\kappa_0 = 1.5$, $\gamma = 2, \Delta\beta = 0.1$, $\Delta H = 0.5$.

same. In panel (b) we display that the currents satisfy the refrigeration conditions.

## 3.3 Summary

In summary, we have generalised the previous study on universal bounds on fluctuations for machines in a significant way by incorporating time-reversal symmetry breaking situation. We show that even in this general situation non-trivial universal upper and lower bounds for $\eta^{(2)}$ exist whenever a setup operates as a useful machine. However in order to receive such bounds the relative fluctuations of the sum of forward and reversed currents must be taken into account. As a consequence of this bound, we further able to establish the hierarchy in the GTURs between the output and input currents. Future work can be directed towards analysing the validity of these bounds beyond the linear response regime.

# 4

# Bounds on nonequilibrium fluctuations for asymmetrically driven quantum Otto cycle

In the previous two chapters, we explored continuous thermal machines in the linear response regime, deriving novel upper bounds on efficiency in terms of fluctuations. We also extended our analysis to scenarios with broken time-reversal symmetry, highlighting the need to take into account both forward and reverse processes.

In this chapter and the next, we shift our focus to discrete thermal machines, with particular attention to the Otto cycle. The Otto cycle, named after Nikolaus August Otto, consists of four distinct strokes–two isentropic and two isochoric–making it especially suitable for our study of fluctuations in small-scale discrete thermal machines [5, 50, 57, 59, 67, 75, 157, 200–212].

In open-quantum description of a thermodynamic cycle, distinguishing between work and heat can be challenging, particularly when they occur simultaneously (as seen in isothermal processes in Carnot or Stirling cycles). The Otto cycle, however, offers a unique advantage: its isentropic strokes involve no heat exchange, and its isochoric strokes involve no work done. This clear separation allows us to unambiguously distinguish between work and heat, even at the quantum level, enabling us to construct the joint probability distribution of work and heat in a quantum Otto cycle by performing successive projective energy measurements at the start and end of each stroke [47, 54, 128]. We notice that such a treatment is not feasible in other thermodynamic cycles, where the overlap of work and heat exchange processes complicates their separation.

In this chapter, we focus on the paradigmatic qubit-Otto cycle, which has recently been experimentally realized using NMR techniques [5]. We investigate the fundamental relationships between nonequilibrium fluctuations of work and heat across various operational regimes of the Otto cycle and examine their implications for bounding the cycle's performance. Our study addresses the general case of broken time-reversal symmetry, where asymmetric driving is applied during the two unitary (isentropic) work strokes of the Otto cycle. As established in the previous chapter, the results for time-reversal symmetric situation can be viewed as a special limiting case of the broader broken time-reversal symmetry scenario. Additionally, we explore similar constraints on fluctuations in the Otto cycle when a harmonic oscillator serves as the working medium [12, 57, 213].

We organize this chapter as follows: In Section 4.1, we give a brief introduction to the four-stroke quantum Otto cycle that is asymmetrically driven. In Section 4.2, we summarize the two-time measurement scheme to obtain the joint heat and work statistics. In Section 4.3, we consider a single qubit as the working medium and derive bounds on non-equilibrium fluctuations of heat and work, independent of its regime of operation. Following this, we obtain the bounds for the engine regime of operation as well as make connections of the derived bounds with the TURs. In addition, we also discuss the bounds for the refrigerator regime of operation and supplement our analytical calculations with numerical results for better illustration. In Section 4.4, we briefly discuss the results for the parametrically driven harmonic oscillator working medium. Finally we summarize our central results in Section 4.5. Certain details of the calculations are provided in the Appendix A1.

## 4.1 Four-stroke quantum Otto cycle

We begin with a brief overview of the four distinct strokes of an Otto cycle (see Fig. 4.1). The working medium is described by the time-dependent Hamiltonian $H_t$. Initially, at $t=0$, the system Hamiltonian is $H_0$, and the initial state is a thermal state with inverse temperature $\beta_c$. The system then progresses through the following four steps:

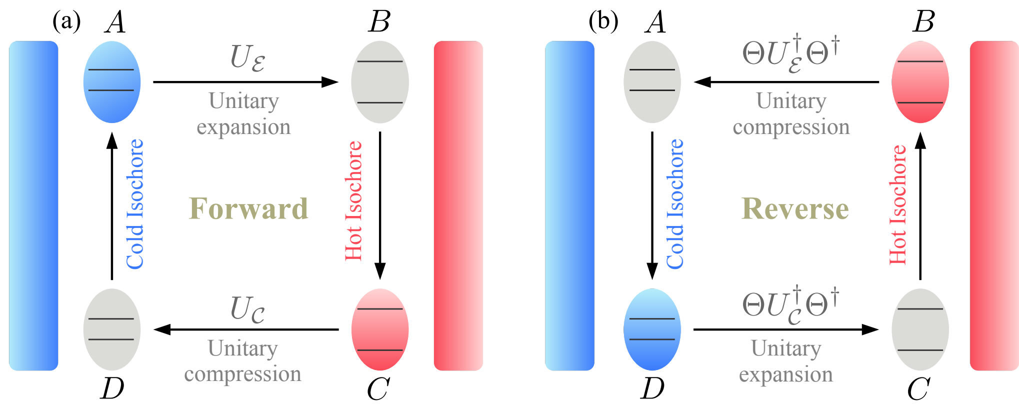


Figure 4.1: Schematic for a four-stroke quantum Otto cycle. The asymmetric driving during the unitary work strokes, $U_{\mathcal{C}} \neq \Theta U_{\mathcal{E}}^{\dagger}\Theta^{\dagger}$, breaks the time-reversal symmetry, and results in distinct (a) forward and (b) reverse processes.

(i) *Unitary expansion* $(A \to B)$. In the first step, the energy levels of the system are expanded through an external drive. The system Hamiltonian evolves unitarily from $H_0$ to $H_\tau$ over a duration $\tau$, governed by the unitary operator $U_{\mathcal{E}}$. During this stroke, the system performs stochastic work $w_1$.

(ii) *Hot isochore* $(B \to C)$. In the second step, the system is brought into weak contact with a hot reservoir at inverse temperature $\beta_h$. During this stroke, the system Hamiltonian $H_\tau$ remains constant, and the system absorbs heat $q_h$ from the hot reservoir over a duration $\tau_h$.

(iii) *Unitary compression* $(C \to D)$. During the third step, the system is decoupled from the hot reservoir, and an external drive causes the system Hamiltonian to transition from $H_\tau$ back to $H_0$ over the time duration $\tau'$. The unitary generator of this stroke is $U_{\mathcal{C}}$. During this stroke, the system's energy levels contract stroke, resulting in stochastic work $w_3$.

(iv) *Cold isochore* $(D \to A)$. In the final step, the system is brought into weak contact with a cold reservoir, at inverse temperature $\beta_c$, while keeping the system Hamiltonian $H_0$ fixed. During this stroke, the system thermalizes over a time $\tau_c$, and heat $q_c$ is exchanged.

Throughout our discussion, we adhere to the sign convention that energy entering the system is positive. We assume that during the heat exchange strokes, the time duration $\tau_h$ and $\tau_c$ are sufficiently long to allow for complete thermalization of the working medium. Additionally, we assume that the energy required to couple and decouple the system from the reservoirs is negligibly small compared to the other energy scales involved in the problem.

It is important to note that the compression stroke in this context is not executed by simply time-reversing the expansion stroke, meaning that $U_\mathcal{C} \neq \Theta U_\mathcal{E}^\dagger \Theta^\dagger$, where $\Theta$ is the anti-unitary time-reversal operator. This breaks the underlying time-reversal symmetry, making the forward and reverse cycles distinct, as illustrated in Figs. 4.1 (a) and (b). In the reverse cycle, the expansion and compression strokes are accomplished by $\widetilde{U}_\mathcal{E} = \Theta U_\mathcal{C}^\dagger \Theta^\dagger$ and $\widetilde{U}_\mathcal{C} = \Theta U_\mathcal{E}^\dagger \Theta^\dagger$, respectively. This distinction results in different joint probability distributions of work and heat in the forward and reverse cycles.

## 4.2 Joint probability distribution of work and heat

To construct the joint probability distribution (PD) of total work output $w = w_1 + w_3$ and heat input $q_h$ from the hot bath for the forward process [see Fig. 4.1 (a)], we employ the projective measurements of the energy of the system at the endpoints of each stroke, i.e., at $A$, $B$, $C$, and $D$, respectively [47]. The joint PD for the forward process is expressed as:

$$\begin{aligned} P_f(w) = \sum_{n,m,k,l} \delta\{w - (\epsilon_m^\tau - \epsilon_n^0) - (\epsilon_l^0 - \epsilon_k^\tau)\}\, \delta\{q_h - (\epsilon_k^\tau - \epsilon_m^\tau)\} \\ \mathcal{T}_{n\to m}^\mathcal{E}\, \mathcal{T}_{k\to l}^\mathcal{C}\, \frac{e^{-\beta_h \epsilon_k^\tau}}{\mathcal{Z}_h^\tau}\, \frac{e^{-\beta_c \epsilon_n^0}}{\mathcal{Z}_c^0}. \end{aligned} \tag{4.2.1}$$

Here, $\mathcal{Z}_c^0 = \sum_n \exp(-\beta_c \epsilon_n^0)$ and $\mathcal{Z}_h^\tau = \sum_k \exp(-\beta_h \epsilon_k^\tau)$ are the canonical partition functions, where the energy eigenvalues $\{\epsilon_n^0\}$ and $\{\epsilon_k^\tau\}$ correspond to Hamiltonians $H_0$ and $H_\tau$, respectively. The transition probabilities are given by

$$\begin{aligned} \mathcal{T}_{n\to m}^\mathcal{E} &= \left|\langle m;\tau|U_\mathcal{E}|n;0\rangle\right|^2, \\ \mathcal{T}_{k\to l}^\mathcal{C} &= \left|\langle l;0|U_\mathcal{C}|k;\tau\rangle\right|^2. \end{aligned} \tag{4.2.2}$$

Similarly, the joint PD for the reverse cycle can be constructed by following the successive projective energy measurements at $D$, $C$, $B$ and $A$,

$$\begin{aligned} P_r(w) = \sum_{n,m,k,l} \delta\{w-(\epsilon_k^\tau-\epsilon_l^0)-(\epsilon_n^0-\epsilon_m^\tau)\}\,\delta\{q_h-(\epsilon_m^\tau-\epsilon_k^\tau)\} \\ \widetilde{\mathcal{T}}^{\mathcal{E}}_{l\to k}\,\widetilde{\mathcal{T}}^{\mathcal{C}}_{m\to n}\,\frac{e^{-\beta_h\epsilon_m^\tau}}{\mathcal{Z}_h^\tau}\,\frac{e^{-\beta_c\epsilon_l^0}}{\mathcal{Z}_c^0}. \end{aligned} \tag{4.2.3}$$

### 4.2.1 Fluctuation symmetry

Given that the expansion and compression strokes in the reverse cycle are governed by the operators $\widetilde{U}_{\mathcal{E}} = \Theta U_{\mathcal{C}}^\dagger \Theta^\dagger$ and $\widetilde{U}_{\mathcal{C}} = \Theta U_{\mathcal{E}}^\dagger \Theta^\dagger$, respectively, the transition probabilities for the forward and reverse cycles are related by

$$\begin{aligned} \widetilde{\mathcal{T}}^{\mathcal{E}}_{l\to k} =& \left|\langle k;\tau|\widetilde{U}_{\mathcal{E}}|l;0\rangle\right|^2 = \left|\langle k;\tau|\Theta U_{\mathcal{C}}^\dagger\Theta^\dagger|l;0\rangle\right|^2 = \left|\langle k;\tau|U_{\mathcal{C}}^\dagger|l;0\rangle^*\right|^2 = \left|\langle l;0|U_{\mathcal{C}}|k;\tau\rangle\right|^2 \\ =& \mathcal{T}^{\mathcal{C}}_{k\to l}, \\ \widetilde{\mathcal{T}}^{\mathcal{C}}_{m\to n} =& \mathcal{T}^{\mathcal{E}}_{n\to m}. \end{aligned} \tag{4.2.4}$$

Using these relationships, one can show that the PDs for the forward and reverse cycles are consistent with the fluctuation symmetry,

$$\frac{P_f(w,q_h)}{P_r(-w,-q_h)} = \exp(\Sigma), \tag{4.2.5}$$

where $\Sigma = \beta_c w + (\beta_c - \beta_h) q_h$ is the stochastic entropy production in the forward cycle. This detailed fluctuation relation, also known as the heat engine fluctuation relation, was previously reported in Ref. [214]. In the time-reversal symmetric situation, when $U_{\mathcal{C}} = \Theta U_{\mathcal{E}}^\dagger \Theta^\dagger$, the forward and reverse cycles become identical, leading to $P_f(w,q_h) = P_r(w,q_h)$ for the PDs.

### 4.2.2 Statistics of work and heat: The cumulant generating function

Since we are interested in the statistics of work and heat, it is more convenient to work with characteristic function (CF) of the total work and heat defined by the

Fourier transformation of joint PD,

$$\mathcal{G}_{f(r)}(\chi_w, \chi_h) = \int\int dw\, dq_h\, P_{f(r)}(w, q_h)\, e^{i\chi_w w} e^{i\chi_h q_h}, \tag{4.2.6}$$

where $\chi_w$ and $\chi_h$ are the conjugate counting parameters for work $w$ and heat $q_h$, respectively. The fluctuation relation in (4.2.5) can be expressed in terms of the CF as $\mathcal{G}_f(\chi_w, \chi_h) = \mathcal{G}_r(-\chi_w + i\beta_c, -\chi_h + i(\beta_c - \beta_h))$. All the cumulants (denoted by double angular brackets) can be obtained from the natural logarithm of this CF in (4.2.6), also known as the cumulant generating function, by taking partial derivatives with respect to $\chi_w$ and $\chi_h$,

$$\langle\langle w^n\, q_h^m \rangle\rangle_{f(r)} = \frac{\partial^n \partial^m}{\partial(i\chi_w)^n \partial(i\chi_h)^m} \ln\mathcal{G}_{f(r)}(\chi_w, \chi_h)\Big|_{\{\chi\}=0}. \tag{4.2.7}$$

In this broken time-reversal symmetric situation, similar to the previous chapter, we define the symmetrization of averages, fluctuations, and relative fluctuations (RF) of work and heat in the following way:

$$\langle \phi \rangle_s := \frac{1}{2}\left(\langle \phi \rangle_f + \langle \phi \rangle_r\right), \tag{4.2.8}$$

$$\langle\langle \phi^2 \rangle\rangle_s := \frac{1}{2}(\langle\langle \phi^2 \rangle\rangle_f + \langle\langle \phi^2 \rangle\rangle_r), \tag{4.2.9}$$

$$\mathcal{R}(\phi) := \frac{\langle\langle \phi^2 \rangle\rangle_s}{\langle \phi \rangle_s^2}, \tag{4.2.10}$$

where $\phi = w, q_h, q_c$ and $\langle \cdot \rangle_{f(r)}$ and $\langle\langle \cdot \rangle\rangle_{f(r)}$ denote the first and second cumulants corresponding to the forward (reverse) PD. In Appendix A1, we demonstrated that, under the perfect thermalization assumption for the heat exchange strokes, statistics of $q_c$ can be obtained from $P(w, q_h)$

In what follows, we start with our first model– asymmetrically driven Otto cycle with single qubit as working medium, and discuss bounds on nonequilibrium fluctuations for heat and work.

## 4.3 Single qubit as a working medium:

We consider a single qubit as the working medium in an Otto cycle. During the unitary expansion stroke ($A \to B$), the system Hamiltonian changes from

$H_0 = H[\omega_0]$, with energy level spacing $\omega_0$, to $H_\tau = H[\omega_1]$, with increased level spacing $\omega_1$ over time $\tau$. The compression stroke ($C \to D$) returns the Hamiltonian to $H[\omega_0]$ in time $\tau'$. The cycle reaches the quasistatic limit when these unitary strokes are driven quantum-adiabatically, meaning no transitions occur between the instantaneous energy eigenstates $|0;\omega_t\rangle, |1;\omega_t\rangle$. From here on, we use "quasistatic" and "quantum-adiabatic" interchangeably. Any deviation from this ideal cycle can be quantified by the transition probabilities between states. For the expansion stroke, we define $u = |\langle 0;\omega_1|U_\mathcal{E}|0;\omega_0\rangle|^2 = |\langle 1;\omega_1|U_\mathcal{E}|1;\omega_0\rangle|^2$ as the probability of no transition between energy states, and similarly, $v = |\langle 0;\omega_0|U_\mathcal{C}|0;\omega_1\rangle|^2 = |\langle 1;\omega_0|U_\mathcal{C}|1;\omega_1\rangle|^2$ for the compression stroke. Note that $u, v \in [0,1]$, and $u = v$ corresponds to the time-reversal symmetric case, with the quasistatic limit at $u = v = 1$.

For the qubit-Otto cycle, the CF for the forward process expressed in a compact form as

$$\begin{aligned}
\mathcal{G}_f(\chi_w,\chi_h) =& \Big(u\cos\Big[\frac{1}{2}\big(\chi_w(\omega_0-\omega_1) + \chi_h\omega_1 - i\beta_c\omega_0\big)\Big] \\
&+ (1-u)\cos\Big[\frac{1}{2}\big(\chi_w(\omega_0+\omega_1) - \chi_h\omega_1 - i\beta_c\omega_0\big)\Big]\Big) \\
&\times\Big(v\cos\Big[\frac{1}{2}\big(\chi_w(\omega_0-\omega_1) + \chi_h\omega_1 + i\beta_h\omega_1\big)\Big] \\
&+ (1-v)\cos\Big[\frac{1}{2}\big(-\chi_w(\omega_0+\omega_1) + \chi_h\omega_1 + i\beta_h\omega_1\big)\Big]\Big) \\
&\times \operatorname{sech}\left(\frac{\beta_c\omega_0}{2}\right)\operatorname{sech}\left(\frac{\beta_h\omega_1}{2}\right).
\end{aligned} \tag{4.3.1}$$

As indicated by (4.2.4), the CF for the reverse cycle, $\mathcal{G}_r(\chi_w,\chi_h)$, can be directly obtained by swapping the probabilites $u$ and $v$ in (4.3.1).

### 4.3.1 Expressions for averages and fluctuations of heat and work

With the CF in (4.3.1), the analytical expressions of the first and second cumulants of work and heat can be expressed as follows:

$$\langle q_h\rangle_f = -\frac{\omega_1}{2}\left[\tanh\left(\frac{\beta_h\omega_1}{2}\right) + (1-2u)\tanh\left(\frac{\beta_c\omega_0}{2}\right)\right], \tag{4.3.2}$$

$$\langle\langle q_h^2\rangle\rangle_f = \frac{\omega_1^2}{4}\left[2 - \tanh^2\left(\frac{\beta_h\omega_1}{2}\right) - (1-2u)^2\tanh^2\left(\frac{\beta_c\omega_0}{2}\right)\right], \tag{4.3.3}$$

$$\begin{aligned}\langle w\rangle_f &= \langle w_1\rangle_f + \langle w_3\rangle_f \\ &= \frac{1}{2}[\omega_0 + (1-2u)\omega_1]\tanh\left(\frac{\beta_c\omega_0}{2}\right) + \frac{1}{2}[\omega_1 + (1-2v)\omega_0]\tanh\left(\frac{\beta_h\omega_1}{2}\right), \end{aligned} \tag{4.3.4}$$

$$\langle\langle w^2\rangle\rangle_f = \frac{(\omega_0+\omega_1)^2}{2} - (u+v)\,\omega_0\,\omega_1 - \langle w_1\rangle_f^2 - \langle w_3\rangle_f^2, \tag{4.3.5}$$

$$\langle q_c\rangle_f = -\frac{\omega_0}{2}\left[\tanh\left(\frac{\beta_c\omega_0}{2}\right) + (1-2v)\tanh\left(\frac{\beta_h\omega_1}{2}\right)\right], \tag{4.3.6}$$

$$\langle\langle q_c^2\rangle\rangle_f = \frac{\omega_0^2}{4}\left[2 - \tanh^2\left(\frac{\beta_c\omega_0}{2}\right) - (1-2v)^2\tanh^2\left(\frac{\beta_h\omega_1}{2}\right)\right]. \tag{4.3.7}$$

Similarly, the first and second cumulants for the reverse cycle can be obtained by interchanging $u$ and $v$.

Depending on the values of $u$ and $v$, the Otto cycle (forward or reverse) can operate in four different regimes: engine, refrigerator, heater, and accelerator [75]. In this time-reversal symmetry-broken scenario, as demonstrated in the previous chapter, we will focus on the symmetrized operational regime condition, where both the forward and reverse cycles operate within the same regime.

### 4.3.2 GTURs in the far-from-equilibrium regime

As our first central result, we present a modified version of the generalized thermodynamic uncertainty relations (GTURs) for the asymmetrically driven qubit-Otto cycle, which remains valid even in the far-from-equilibrium regime. Recently, in the context of a two-qubit swap engine, a modified version of the traditional TUR [42, 129, 130, 134, 157] was derived under time-reversal symmetry, as reported in Ref. [215]:

$$\frac{\langle\langle w^2\rangle\rangle}{\langle w\rangle^2} \geq \frac{2}{\langle\Sigma\rangle} - 1. \tag{4.3.8}$$

We will show that this modified TUR also holds for a symmetrically driven four-stroke qubit-Otto cycle. More generally, we prove a version of this TUR for the asymmetrically driven scenario, leading to a generalized TUR (GTUR):

$$\mathrm{GTUR}(\phi) \coloneqq \langle\Sigma\rangle_s\left(\frac{\langle\langle\phi^2\rangle\rangle_s}{\langle\phi\rangle_s^2} + 1\right) \geq 2, \tag{4.3.9}$$

with $\phi$ can represent the total work $w$ or the heats $q_h$ and $q_c$. In the time-reversal symmetric limit: $u = v$, these GTURs take the form of (4.3.8). To prove (4.3.9), we will consider an alternative expression:

$$\langle\Sigma\rangle_s\big(\langle\langle\phi^2\rangle\rangle_s + \langle\phi\rangle_s^2\big) - 2\,\langle\phi\rangle_s^2 \geq 0, \tag{4.3.10}$$

and demonstrate the proof for $\phi = q_c$. The same reasoning can be extended to the cases of $\phi = w$ and $q_h$.

***Detailed proof*:**

We begin by expressing the left hand side of (4.3.10), as a two-variable function $\boldsymbol{f}(p,q)$, where the two variables are defined as $p = 2 - u - v \ \in [0,2]$, and $q = u - v \ \in [-1,1]$. This formulation corresponds to working with center-of-mass ($p$) and relative ($q$ )coordinates, where $q$ quantifies the asymmetry between the two unitary work strokes of the qubit-Otto cycle, becoming zero in the symmetric driving case.

To streamline the proof, we introduce simplified notations $x_c = \beta_c\omega_0/2$ and $x_h = \beta_h\omega_1/2$, and define $t_c = \tanh(x_c)$ and $t_h = \tanh(x_h)$. These simplified notations are particularly useful for this part of the analysis, but will be discarded later for broader generality. Using these, the function $\boldsymbol{f}(p,q)$ (apart from the positive factor $2\omega_0^2$) is written as

$$\boldsymbol{f}(p,q) = \boldsymbol{c} + \boldsymbol{b}\,p + \boldsymbol{a}\,p^2 - \boldsymbol{g}\,q^2 - \boldsymbol{h}\,pq^2, \tag{4.3.11}$$

where

$$\begin{aligned}
\boldsymbol{c} &= (x_c - x_h)\,(t_c - t_h)\,(1 - t_c t_h) - (t_c - t_h)^2,\\
\boldsymbol{b} &= (x_c - x_h)\,t_c t_h\,(t_c - t_h) + (1 - t_c t_h)\,(x_c t_h + x_h t_c) - 2\,t_h\,(t_c - t_h),\\
\boldsymbol{a} &= t_c t_h\,(x_c t_h + x_h t_c) - t_h^2,\\
\boldsymbol{g} &= \frac{1}{2}\,(x_c - x_h)\,(t_c - t_h)\,t_h^2\\
\boldsymbol{h} &= \frac{1}{2}\,(x_c t_h + x_h t_c)\,t_h^2.
\end{aligned} \tag{4.3.12}$$

The allowed domain of the function $\boldsymbol{f}(p,q)$ is a square in the $pq$–plane: $\mathcal{D} =$

$\{(p,q)\in\mathbb{R}^2 \mid 0\le p\le 2 \text{ and } -1\le q\le 1\}$ (see Fig. 4.2). Our goal is to show that $\boldsymbol{f}(p,q)$ is non-negative for all allowed values of $p$ and $q$.

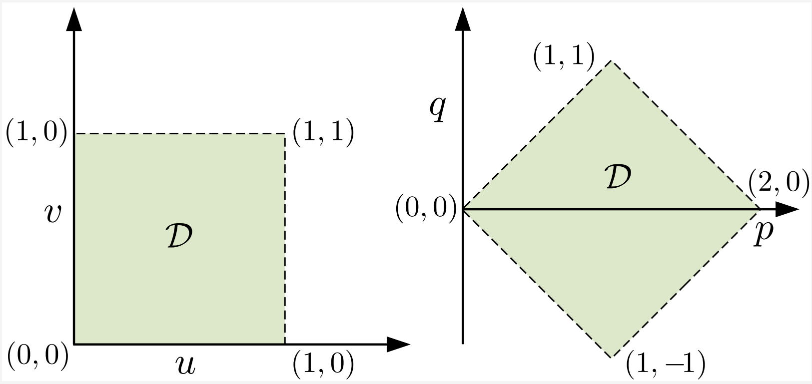


Figure 4.2: The allowed domain of the function $\boldsymbol{f}(p,q)$, where $p=2-u-v$ and $q=u-v$, with $u,v\in[0,1]$.

First, we analyze the signs of the coefficients.

*Sign of* $\boldsymbol{c}$: Notice that the term $\boldsymbol{c}=\boldsymbol{f}(p=0,q=0)$ corresponds to the quasistatic situation, where $u=v=1$. By rearranging the expression for $\boldsymbol{c}$, we obtain

$$\boldsymbol{c}=(t_c-t_h)^2\big[(x_c-x_h)\coth(x_c-x_h)-1\big]\ge 0, \tag{4.3.13}$$

since $x\coth x\ge 1$.

*Sign of* $\boldsymbol{b}$: The first two terms in the expression of $b$ are always non-negative. Moreover, for $x_c\le x_h$, it is straightforward to see that $\boldsymbol{b}\ge 0$. However, determining the sign of $\boldsymbol{b}$ when $x_c>x_h$, requires a more involved analysis:

$$\begin{aligned}
b \ge&(1-t_ct_h)\,(x_ct_h+x_ht_c)-2\,t_h\,(t_c-t_h)\\
=&(t_c-t_h)\big[\coth(x_c-x_h)\,(x_ct_h+x_ht_c)-2\,t_h\big]\\
=&(t_c-t_h)\big[\coth(x_c-x_h)\,(x_ct_h-x_ht_h)+2\big(\coth(x_c-x_h)\,x_h\,t_c-t_h\big)\big]\\
=&(t_c-t_h)\,t_ct_h\big[\coth(x_c-x_h)(x_c\coth x_c-x_h\coth x_h)\\
&\quad+2\,\big(\coth(x_c-x_h)\,(x_h\coth x_h)-\coth x_c\big)\big]\\
\ge&0.
\end{aligned} \tag{4.3.14}$$

In the first step, we omitted the first term of $\boldsymbol{b}$, which is always positive. In the last step, we utilize the fact that we are considering the $x_c > x_h$ case, and used the following identities: (i) $t_c \geq t_h$, (ii) $x_c \coth x_c \geq x_h \coth x_h \geq 1$, and (iii) $\coth(x_c - x_h) \geq \coth x_c \geq 1$. Thus, from (4.3.14), we conclude that $b \geq 0$, regardless of the operational regime.

It is clear from their expressions that both $\boldsymbol{g}$ and $\boldsymbol{h}$ are always non-negative.

Unfortunately, the coefficient $\boldsymbol{a}$ does not have any definite sign, which necessitates a second step in our analysis: performing a local minima/maxima analysis to determine the minimum value of the function $\boldsymbol{f}(p,q)$ within the allowed domain $\mathcal{D}$ in the $pq$–plane. To carry out this analysis, we first compute the first and second partial derivatives of $\boldsymbol{f}(p,q)$ with respect to $p$ and $q$:

$$\begin{gathered}\boldsymbol{f}^{(p)} = \boldsymbol{b} + 2\boldsymbol{a}\,p - \boldsymbol{h}\,q^2, \quad \boldsymbol{f}^{(q)} = -2\,q(\boldsymbol{g} + \boldsymbol{h}\,p), \\ \boldsymbol{f}^{(pp)} = 2\,\boldsymbol{a}, \quad \boldsymbol{f}^{(qq)} = -2(\boldsymbol{g} + \boldsymbol{h}\,p) \leq 0, \quad \boldsymbol{f}^{(pq)} = \boldsymbol{f}^{(qp)} = -2\boldsymbol{h}\,q. \end{gathered} \tag{4.3.15}$$

To find the local extrema (maxima/minima/saddle point), we solve $\boldsymbol{f}^{(p)} = 0$ and $\boldsymbol{f}^{(q)} = 0$ simultaneously. The solution to $\boldsymbol{f}^{(q)} = 0$ is $q^* = 0$, since $\boldsymbol{g}$, $\boldsymbol{h} \geq 0$ and $p \geq 0$. Substituting $q^* = 0$ in $\boldsymbol{f}^{(p)} = 0$, yields $p^* = -\boldsymbol{b}/(2\boldsymbol{a})$.

If $\boldsymbol{a} > 0$, then $p^* \leq 0$ since $b \geq 0$, implying that there are no extrema within the allowed region $\mathcal{D}$. Moreover, this extrema corresponds to a local minima, $\boldsymbol{f}^{(pp)} > 0$ and $\boldsymbol{f}^{(pp)}\boldsymbol{f}^{(qq)} - {\boldsymbol{f}^{(pq)}}^2 > 0$. Therefore, if $\boldsymbol{a} > 0$,

$$\boldsymbol{f}(p,q) \quad \forall\, p,q \in \mathcal{D} > \boldsymbol{f}(p*,q*) = \boldsymbol{c} + \frac{\boldsymbol{b}^2}{4\boldsymbol{a}} > 0. \tag{4.3.16}$$

If $\boldsymbol{a} < 0$, then $\boldsymbol{f}^{(pp)} < 0$ and $\boldsymbol{f}^{(pp)}\boldsymbol{f}^{(qq)} - {\boldsymbol{f}^{(pq)}}^2 \geq 0$, which indicates the presence of maxima. Therefore, if $\boldsymbol{a} < 0$, the function $\boldsymbol{f}(p,q)$ achieves its minimum value on the boundary of $\mathcal{D}$.

Next, we analyze $\boldsymbol{f}(p,q)$ on the boundary of $\mathcal{D}$. We consider one boundary segment $(0,0) \to (1,1)$, where $p = q$. Thus, on this segment

$$\boldsymbol{f}(p) \equiv \boldsymbol{f}(p, q = p) = \boldsymbol{c} + \boldsymbol{b}\,p + (\boldsymbol{a} - \boldsymbol{g})\,p^2 - \boldsymbol{h}\,p^3. \tag{4.3.17}$$

The first and second derivatives of $\boldsymbol{f}(p)$ are:

$$\boldsymbol{f}'(p) = \boldsymbol{b} + 2(\boldsymbol{a} - \boldsymbol{g})p - 3\boldsymbol{h}\,p^2, \qquad \boldsymbol{f}''(p) = 2(\boldsymbol{a} - \boldsymbol{g}) - 6\boldsymbol{h}\,p. \tag{4.3.18}$$

To find minima/maxima on this boundary we solve $\boldsymbol{f}'(p) = 0$, which is quadratic in $p$. Since negative values of $p$ are not allowed, the only feasible solution is

$$p^* = \frac{(\boldsymbol{a} - \boldsymbol{g}) + \sqrt{(\boldsymbol{a} - \boldsymbol{g})^2 + 3\boldsymbol{h}\boldsymbol{b}}}{3\boldsymbol{h}}. \tag{4.3.19}$$

For this $p*$, we find that

$$\boldsymbol{f}''(p^*) = -2\sqrt{(\boldsymbol{a} - \boldsymbol{g})^2 + 3\boldsymbol{h}\boldsymbol{b}} < 0, \tag{4.3.20}$$

indicating a maxima. Thus, the function $\boldsymbol{f}(p)$ reaches its minimum value at one of the endpoints of this segment, $(0,0)$ or $(1,1)$. Repeating the same analysis for the other three boundary segments, we confirm that finding the minimum value of this two-variable function ultimately reduces to evaluating its values at the vertices of the allowed square $\mathcal{D}$ in the $pq$–plane. It is straightforward to show that

$$\boldsymbol{f}(0,0) = (t_c - t_h)^2 \big[(x_c - x_h)\coth(x_c - x_h) - 1\big] \geq 0, \tag{4.3.21}$$

$$\boldsymbol{f}(1,1) = \boldsymbol{f}(1,-1) = \frac{1}{2}(x_c t_c + x_h t_h)(2 - t_h^2) - t_c^2 \geq 0, \tag{4.3.22}$$

$$\boldsymbol{f}(2,0) = (t_c + t_h)^2 \big[(x_c + x_h)\coth(x_c + x_h) - 1\big] \geq 0, \tag{4.3.23}$$

where we have used the identity $x \geq \tanh x$ for $x > 0$. We also note that $\boldsymbol{f}(2,0) \geq \boldsymbol{f}(0,0)$, with $\boldsymbol{f}(0,0)$ representing the quasistatic situation. However, $\boldsymbol{f}(1,1)$, though positive, can become smaller than $\boldsymbol{f}(0,0)$ under certain parameter values. This contrasts with the symmetric driving case, where non-quasistatic TUR values can never fall below the quasistatic TUR value.

In conclusion, the function $\boldsymbol{f}(p,q)$ achieves its minimum value either at $(0,0)$ or at $(1,1)$ and $(1,-1)$, with this minimum value being non-negative. This completes our proof for (4.3.10).

### 4.3.3 General bounds on work to heat fluctuations

We now introduce novel bounds on the nonequilibrium fluctuations of work and heat in a qubit-Otto cycle. Specifically, we derive the following lower bounds on the, which hold regardless of the operational regime of the cycle:

$$\frac{\langle\langle w^2\rangle\rangle_s}{\langle\langle q_h^2\rangle\rangle_s} \geq \left(\frac{\omega_1-\omega_0}{\omega_1}\right)^2, \tag{4.3.24}$$

$$\frac{\langle\langle w^2\rangle\rangle_s}{\langle\langle q_c^2\rangle\rangle_s} > \left(\frac{\omega_1-\omega_0}{\omega_1}\right)^2. \tag{4.3.25}$$

Here, we notice that the ratios of nonequilibrium fluctuations of work and heat (from both hot and cold reservoirs) are not arbitrary but constrained by the parameters of the qubit-Otto cycle. We now provide a proof for these results.

To prove (4.3.24), our strategy will be to consider a modified version of (4.3.24): $\omega_1^2\langle\langle w^2\rangle\rangle_s - (\omega_1-\omega_0)^2\langle\langle q_h^2\rangle\rangle_s \geq 0$. The left hand side of this inequality can be written as

$$\begin{aligned}
&\omega_1^2\langle\langle w^2\rangle\rangle_s - (\omega_1-\omega_0)^2\langle\langle q_h^2\rangle\rangle \\
&\quad= \frac{\omega_0\omega_1^3}{2}(2-u-v)\left[2-\tanh^2\left(\frac{\beta_c\omega_0}{2}\right)-\tanh^2\left(\frac{\beta_h\omega_1}{2}\right)\right] \\
&\qquad+\frac{\omega_0\omega_1^2}{2}\left[\omega_0\tanh^2\left(\frac{\beta_h\omega_1}{2}\right)+(2\omega_1-\omega_0)\tanh^2\left(\frac{\beta_c\omega_0}{2}\right)\right]\left[u(1-u)+v(1-v)\right] \\
&\quad\geq 0.
\end{aligned} \tag{4.3.26}$$

Noticing that $u, v \in [0,1]$ and $\omega_1 > \omega_0$, we immediately conclude that both the terms on the right hand side of the above equation are individually non-negative. The equality occurs in the quasistatic limit: $u=v=1$.

Repeating the same approach for (4.3.25), we obtain:

$$\begin{aligned}
&\omega_1^2\langle\langle w^2\rangle\rangle_s - (\omega_1-\omega_0)^2\langle\langle q_c^2\rangle\rangle_s \\
&= \frac{1}{2}\left[\frac{(\omega_1-\omega_0)^3}{2}(\omega_1+\omega_0)+\omega_0\,\omega_1^3\,(2-u-v)\right]\left[2-\tanh^2\left(\frac{\beta_c\omega_0}{2}\right)-\tanh^2\left(\frac{\beta_h\omega_1}{2}\right)\right] \\
&\quad+\frac{1}{2}\left[u(1-u)+v(1-v)\right]\left[\omega_1^4\tanh^2\left(\frac{\beta_c\omega_0}{2}\right)+\omega_0^3\,(2\omega_1-\omega_0)\tanh^2\left(\frac{\beta_h\omega_1}{2}\right)\right] \\
&> 0,
\end{aligned} \tag{4.3.27}$$

where both terms on the right hand side of the above equation are individually always greater than zero, since $u, v \in [0,1]$ and $\omega_1 > \omega_0$.

In what follows, we will show that once we specify that the qubit-Otto cycle operates in the symmetrized engine or refrigerator regime, the fluctuations of heat and work receive additional universal bounds.

### 4.3.4 Engine regime: Bounds on symmetrized efficiency

The symmetrized engine operational regime, where both the forward and reverse cycles of the qubit-Otto cycle function as engines, is characterized by the conditions $\langle w \rangle_{f(r)} \leq 0$, $\langle q_h \rangle_{f(r)} \geq 0$ and $\langle q_c \rangle_{f(r)} \leq 0$. These conditions impose specific constraints on the parameters $u$ and $v$. In the quasistatic limit, when $u = v = 1$, the engine condition simplifies to $\beta_c \omega_0 \geq \beta_h \omega_1$.

A previous study in Ref. [54] has shown that for a symmetrically driven qubit-Otto cycle operating as an engine, the square of the average efficiency is upper bounded by the ratio of work fluctuation to input heat fluctuation: $\eta^{(2)} = \langle\langle w^2 \rangle\rangle / \langle\langle q_h^2 \rangle\rangle \geq \langle \eta \rangle^2$, where $\langle \eta \rangle = -\langle w \rangle / \langle q_h \rangle$ represents the average efficiency.

For asymmetric work protocols ($u \neq v$), we symmetrize the quantities $\eta^{(2)}$ and $\langle \eta \rangle$ by taking into account both the forward and reverse cycles as

$$\langle \eta \rangle_s := -\frac{\langle w \rangle_s}{\langle q_h \rangle_s}, \tag{4.3.28}$$

$$\eta^{(2)} := \frac{\langle\langle w^2 \rangle\rangle_s}{\langle\langle q_h^2 \rangle\rangle_s}, \tag{4.3.29}$$

and report the following sequence of bounds on the symmetrized average efficiency:

$$1 > \eta^{(2)} \geq \eta_{\mathcal{O}}^2 \geq \langle \eta \rangle_s^2, \tag{4.3.30}$$

where the "Otto efficiency" $\eta_{\mathcal{O}} = (\omega_1 - \omega_0)/\omega_1$ is achieved in the quasistaic limit $u = v = 1$.

Notice that, the inequality $\eta^{(2)} \geq \eta_{\mathcal{O}}^2$ directly follows from (4.3.24). Notably, $\eta_{\mathcal{O}}^2$ establishes a tighter lower bound on $\eta^{(2)}$ compared to what was reported in Ref. [54]. This bound is determined entirely by the chosen parameter values for the engine-cycle. In the quasistatic limit, the lower bounds on $\eta^{(2)}$ converge, resulting in $\eta^{(2)} = \eta_{\mathcal{O}}^2 = \langle\eta\rangle_s^2$.

The upper bound on $\eta^{(2)}$ reveals another fundamental relationship between the symmetrized fluctuations: the fluctuation of input heat is always greater than that of output work, $\langle\langle q_h^2\rangle\rangle_s > \langle\langle w^2\rangle\rangle_s$. To prove this upper bound, we begin with a modified version of this inequality: $\langle\langle q_h^2\rangle\rangle_s - \langle\langle w^2\rangle\rangle_s > 0$. The left hand side of this inequality can be expressed as

$$\langle\langle q_h^2\rangle\rangle_s - \langle\langle w^2\rangle\rangle_s = \omega_0\Big[2-\tanh^2\Big(\frac{\beta_c\omega_0}{2}\Big)-\tanh^2\Big(\frac{\beta_h\omega_1}{2}\Big)\Big]\mathcal{C} + \mathcal{B}_1 - \mathcal{B}_2, \tag{4.3.31}$$

where

$$\begin{aligned} \mathcal{C} &= -\big[\omega_0 + (1-2u)\omega_1\big] - \big[\omega_0 + (1-2v)\omega_1\big], \\ \mathcal{B}_1 &= \omega_0^2\Big[2-\tanh^2\Big(\frac{\beta_c\omega_0}{2}\Big)-\tanh^2\Big(\frac{\beta_h\omega_1}{2}\Big)\Big], \\ \mathcal{B}_2 &= 2\,\omega_0^2\big[u(1-u)+v(1-v)\big]\tanh^2\Big(\frac{\beta_h\omega_1}{2}\Big). \end{aligned} \tag{4.3.32}$$

To establish that $\langle\langle q_h^2\rangle\rangle_s - \langle\langle w^2\rangle\rangle$ is strictly positive in the symmetrized engine operational regime, we will demonstrate that $\mathcal{C} > 0$ and $\mathcal{B}_1 - \mathcal{B}_2 \geq 0$.

First, we note that $\min(1-2u) = \min(1-2v) = -1$, since $u, v \in [0,1]$. Given that $\omega_1 > \omega_0$, from (4.3.4), we can conclude that $\langle w_3\rangle_{f(r)} > 0$, irrespective of the operational regime. Thus, to satisfy the symmetrized engine condition $\langle w\rangle_{f(r)} = \langle w_1\rangle_{f(r)} + \langle w_3\rangle_{f(r)} \leq 0$, we must have $\langle w_1\rangle_{f(r)} < 0$. This immediately implies that $\big(\omega_0 + (1-2u)\omega_1\big) < 0$ and $\big(\omega_0 + (1-2v)\omega_1\big) < 0$. These are precisely the terms appearing in the expression for $\mathcal{C}$, with an additional negative sign. Therefore, we conclude that quantity $\mathcal{C}$ is always positive.

Next, to show that $\mathcal{B}_1 - \mathcal{B}_2 \geq 0$, we first maximize $\mathcal{B}_2$ under the symmetrized engine condition $\langle q_h\rangle_{f(r)} \geq 0$. Notice that, these constraints impose stricter lower limits on $u$ and $v$, where $0 \leq u, v \leq 1$. These lower limits are expressed as

$$\frac{1}{2} + \frac{1}{2}\frac{\tanh\Big(\frac{\beta_h\omega_1}{2}\Big)}{\tanh\Big(\frac{\beta_c\omega_0}{2}\Big)} \leq u, v \leq 1. \tag{4.3.33}$$

These lower bounds, in turn, set an upper limit on the quantity $u(1-u) + v(1-v)$,

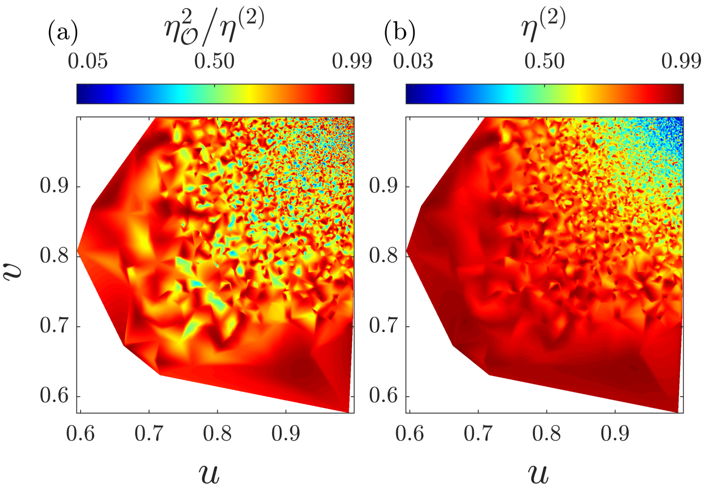


Figure 4.3: Results for (a) lower and (b) upper bounds on $\eta^{(2)}$ for an asymmetrically driven qubit-Otto cycle. $\omega_0$, $\omega_1$, $T_c$ and $T_h$ were chosen from uniform distribution between the interval [0,5]. $u, v$ were chosen between [0,1]. Simulations done over 2.5 million points. The 'white color regions' correspond to situations where the symmetrized engine conditions $\langle w \rangle_{f(r)} \leq 0$, $\langle q_h \rangle_{f(r)} \geq 0$ and $\langle q_c \rangle_{f(r)} \leq 0$ are not satisfied.

which can be expressed as

$$u(1-u) + v(1-v) \leq \frac{1}{2} - \frac{1}{2}\,\frac{\tanh^2\left(\frac{\beta_h\omega_1}{2}\right)}{\tanh^2\left(\frac{\beta_c\omega_0}{2}\right)} \leq \frac{1}{2}\,\frac{\tanh^2\left(\frac{\beta_c\omega_0}{2}\right)}{\tanh^2\left(\frac{\beta_h\omega_1}{2}\right)} - \frac{1}{2}. \tag{4.3.34}$$

Using this inequality to maximize $\mathcal{B}_2$, we finally obtain

$$\mathcal{B}_1 - \mathcal{B}_2 \geq \mathcal{B}_1 - \big[\mathcal{B}_2\big]_{\max} = 2\,\omega_0^2\left[1 - \tanh^2\left(\frac{\beta_h\omega_1}{2}\right)\right] \geq 0. \tag{4.3.35}$$

Since we have established that $\mathcal{C} > 0$ and $\mathcal{B}_1 - \mathcal{B}_2 \geq 0$, we immediately infer $\langle\langle q_h^2 \rangle\rangle_s - \langle\langle w^2 \rangle\rangle_s > 0$. This completees the proof of (4.3.30).

In Fig. 4.3, we present a contour plot displaying the upper and lower bounds on $\eta^{(2)}$ with various parameters chosen arbitrarily from uniform distributions. The plot confirms that both bounds are respected in the asymmetrically driven case, consistent with our theoretical predictions.

### 4.3.5 Engine regime: Hierarchy in the symmetrized relative fluctuations

In the symmetrized engine operational regime of the asymmetrically driven qubit-Otto cycle, we now establish a strict hierarchy among the symmetrized relative fluctuations of work and heat from both hot and cold reservoirs. This hierarchy is stated as

$$\begin{aligned}\frac{\langle\langle w^2\rangle\rangle_s}{\langle w\rangle_s^2} \geq \frac{\langle\langle q_h^2\rangle\rangle_s}{\langle q_h\rangle_s^2} \geq \frac{\langle\langle q_c^2\rangle\rangle_s}{\langle q_c\rangle_s^2}\\ \equiv \mathcal{R}(w) \geq \mathcal{R}(q_h) \geq \mathcal{R}(q_c).\end{aligned} \tag{4.3.36}$$

Notice that the first inequality, $\mathcal{R}(w) \geq \mathcal{R}(q_h)$, directly follows from the bound $\eta^{(2)} \geq \langle\eta\rangle_s^2$ provided in (4.3.30).

Next, we will prove the second inequality, $\mathcal{R}(q_h) \geq \mathcal{R}(q_c)$, by demonstrating the following modified inequality:

$$\frac{\langle q_c\rangle_s^2}{\langle q_h\rangle_s^2} \geq \frac{\langle\langle q_c^2\rangle\rangle_s}{\langle\langle q_h^2\rangle\rangle_s}. \tag{4.3.37}$$

As the first step, using the bound $\eta_{\mathcal{O}} \geq \langle\eta\rangle_s$ provided in (4.3.30), along with the symmetrized engine constraints $\langle q_c\rangle_{f(r)} \leq 0$, we derive

$$\frac{\langle q_c\rangle_s^2}{\langle q_h\rangle_s^2} \geq \frac{\omega_0^2}{\omega_1^2}. \tag{4.3.38}$$

Next, we show that

$$\frac{\omega_0^2}{\omega_1^2} \geq \frac{\langle\langle q_c^2\rangle\rangle_s}{\langle\langle q_h^2\rangle\rangle_s}. \tag{4.3.39}$$

The proof for a modified version the above inequality, $\omega_0^2\langle\langle q_h^2\rangle\rangle_s - \omega_1^2\langle\langle q_c^2\rangle\rangle_s \geq 0$, proceeds as follows

$$\begin{aligned}\omega_0^2\langle\langle q_h^2\rangle\rangle_s - \omega_1^2\langle\langle q_c^2\rangle\rangle_s &= \omega_0^2\omega_1^2\big[u(1-u) + v(1-v)\big]\left[\tanh^2\left(\frac{\beta_c\omega_0}{2}\right) - \tanh^2\left(\frac{\beta_h\omega_1}{2}\right)\right]\\ &\geq 0,\end{aligned} \tag{4.3.40}$$

since $\beta_c\omega_0 \geq \beta_h\omega_1$ within the engine operational regime. Combining equations

(4.3.38) and (4.3.39) we obtain

$$\frac{\langle q_c\rangle_s^2}{\langle q_h\rangle_s^2} \geq \frac{\omega_0^2}{\omega_1^2} \geq \frac{\langle\langle q_c^2\rangle\rangle_s}{\langle\langle q_h^2\rangle\rangle_s}. \tag{4.3.41}$$

This concludes our proof for $\mathcal{R}(q_h) \geq \mathcal{R}(q_c)$. The equality in equation (4.3.36) corresponds to the quasistatic limit of the qubit-Otto cycle, when $u = v = 1$.

### 4.3.6 Engine regime: Bounds on efficiency derived from the GTURs

In the symmetrized engine operational regime, because of the emerging hierarchy between the relative fluctuations of work and the heat exchanges with both the hot and cold reservoirs, as described by (4.3.36), we infer that a similar hierarchy applies to the GTURs, introduced in (4.3.9):

$$\mathrm{GTUR}(w) \geq \mathrm{GTUR}(q_h) \geq \mathrm{GTUR}(q_c) \geq 2. \tag{4.3.42}$$

This hierarchy in (4.3.42) is exclusive to the engine operational regime. Numerical investigations reveal that in other operational regimes, no such hierarchy among the relative fluctuations is observed. In Fig. 4.4 (a) we display the hierarchy in the GTURs in the engine regime, with each GTUR lower bounded by the value 2.

Importantly, in the symmetrized engine regime, each of the GTURs offers thermodynamically consistent bounds on the symmetrized efficiency, $\langle\eta\rangle_s$. To derive these bounds, we begin by expressing the symmetrized average entropy production as follows:

$$\begin{aligned}\langle\Sigma\rangle_s =& -\beta_c\langle w\rangle_s\big(1-\eta_{\mathrm{c}}/\langle\eta\rangle_s\big),\\ \equiv& \quad \beta_c\langle q_h\rangle_s\big(\eta_{\mathrm{c}}-\langle\eta\rangle_s\big),\\ \equiv& -\beta_c\langle q_c\rangle_s\left(1-\frac{1-\eta_{\mathrm{c}}}{1-\langle\eta\rangle_s}\right),\end{aligned} \tag{4.3.43}$$

where $\eta_{\mathrm{c}} = 1-\beta_h/\beta_c$ denotes the Carnot efficiency. Now, by substituting the appropriate expression for thr entropy production from (4.3.43) into (4.3.9), we can derive independent upper bounds on the symmetrized efficiency. These bounds are

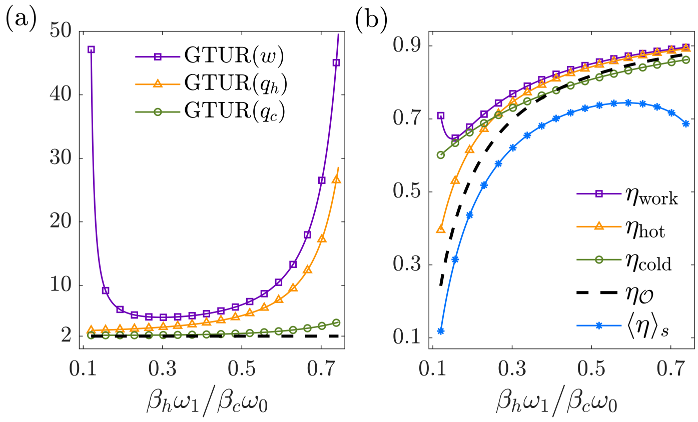


Figure 4.4: (a) Plot for the hierarchy between the three GTURs in the symmetrized engine regime. The black dashed line represents the lower bound 2. (b) Comparison between different bounds on symmetrized efficiency derived from the GTURs. Parameters chosen: $T_c\!=\!0.5$, $T_h\!=\!5.5$, $\omega_0\!=\!0.5$, $u\!=\!0.99$ and $v\!=\!0.9$. The black dashed line represents the quasistatic Otto efficiency $\eta_{\mathcal{O}}$.

listed below:

$$\langle\eta\rangle_s \leq \eta_{\mathrm{c}} \Big/ \left(1 - \frac{2\,\langle w\rangle_s}{\beta_c\left(\langle\!\langle w^2\rangle\!\rangle_s + \langle w\rangle_s^2\right)}\right) := \eta_{\text{work}}, \tag{4.3.44}$$

$$\langle\eta\rangle_s \leq \eta_{\mathrm{c}} - \frac{2\,\langle q_h\rangle_s}{\beta_c\left(\langle\!\langle q_h^2\rangle\!\rangle_s + \langle q_h\rangle_s^2\right)} := \eta_{\text{hot}}, \tag{4.3.45}$$

$$\langle\eta\rangle_s \leq 1 - \frac{\beta_h}{\beta_c}\left(1 + \frac{2\,\langle q_c\rangle_s}{\beta_c\left(\langle\!\langle q_c^2\rangle\!\rangle_s + \langle q_c\rangle_s^2\right)}\right)^{-1} := \eta_{\text{cold}}. \tag{4.3.46}$$

Although the values of GTUR($\phi$), with $\phi = w$, $q_h$ and $q_c$, follow a strict hierarchy within the engine regime, as indicated in (4.3.42), the efficiency bounds derived from these GTURs do not necessarily respect this hierarchical structure. Nevertheless, numerical tests, as shown in Fig. 4.4 (b), reveal that depending on the parameter regime, the bound $\eta_{\text{cold}}$, derived from the tightest GTUR in the engine regime, can, in some cases, be tighter than $\eta_{\mathcal{O}}$ [see equations (4.3.30) and (4.3.46)].

### 4.3.7 Refrigerator regime: Bounds on fluctuation

We now briefly discuss the refrigerator operational regime of the qubit-Otto cycle. The symmetrized refrigerator operational regime, where both the forward and re-

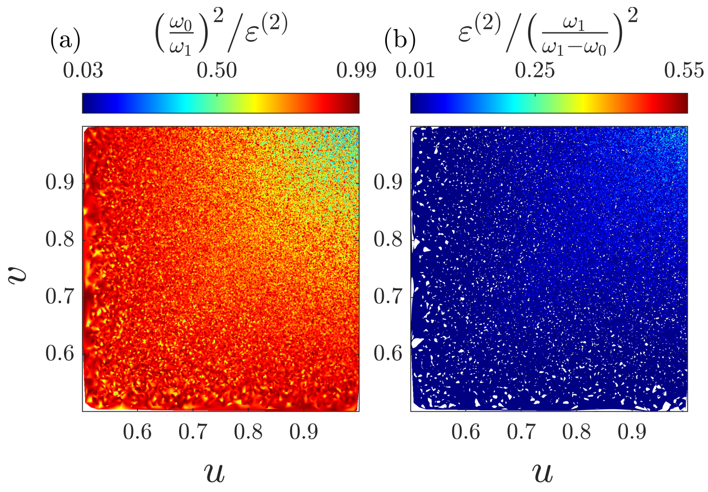


Figure 4.5: Results for (a) upper and (b) lower bounds on $\varepsilon^{(2)}$ in the refrigeration regime for asymmetrically driven qubit-Otto cycle. $\omega_0$, $\omega_1$, $T_c$ and $T_h$ were chosen randomly from uniform distribution between the interval [0,5]. $u, v$ were chosen between [0,1]. Simulations done over 2.5 million points.

verse cycles of the qubit-Otto cycle function as refrigerators, is characterized by the conditions $\langle q_c \rangle_{f(r)} \geq 0$, $\langle w \rangle_{f(r)} \geq 0$ and $\langle q_h \rangle_{f(r)} \leq 0$. In the context of refrigeration, the key quantity to examine is $\varepsilon^{(2)} := \langle\langle q_c^2 \rangle\rangle_s / \langle\langle w^2 \rangle\rangle_s$. It is important to note that (4.3.25) already provides an upper bound on $\varepsilon^{(2)}$. Under symmetrized refrigeration conditions, numerical results further suggest a lower bound on $\varepsilon^{(2)}$:

$$\frac{\omega_1^2}{(\omega_1 - \omega_0)^2} > \varepsilon^{(2)} > \frac{\omega_0^2}{\omega_1^2}. \tag{4.3.47}$$

In Fig. 4.5, we illustrate the validity of both the lower and upper bounds in the refrigeration regime of the qubit-Otto cycle. Note that, unlike the hierarchy of symmetrized relative fluctuations observed in the engine regime as described in (4.3.36), no such hierarchy is found in the refrigerator regime. This absence indicates fundamental differences in nonequilibrium fluctuations across different operational regimes.

In the next section, we consider a parametrically driven harmonic oscillator as the working medium and investigate bounds on fluctuations.

## 4.4 Harmonic oscillator as a working medium

We consider a harmonic oscillator (HO), with unit mass, as the working fluid of the Otto cycle operating between the two thermal reservoirs with inverse temperatures $\beta_c$ and $\beta_h$, with $\beta_c > \beta_h$. The parametric time-dependent Hamiltonian of the HO-working fluid is given by

$$H[\omega_t] = \frac{p^2}{2} + \frac{1}{2}\omega_t^2 x^2 \tag{4.4.1}$$

For the cycle, during the unitary expansion stroke $A \to B$, the time-dependent trapping frequency $\omega_t$ goes from $\omega_0$ at $t = 0$ to $\omega_1$ at time $t = \tau_1$, governed by the expansion protocol $U_{\mathcal{E}}$. During the compression stroke $C \to D$, the compression protocol $U_{\mathcal{C}}$ drives $\omega_1$ back to $\omega_0$ in the time interval $\tau_3$. The heat exchange strokes take place in between and perfect thermalization is achieved in both the heat exchange strokes. To assure time-asymmetric driving, we again consider $U_{\mathcal{E}}^\dagger \neq \Theta U_{\mathcal{C}} \Theta^\dagger$. For HO-Otto cycle, the exact joint CF of output work and input heat can be obtained and much like the qubit case, the non-adiabaticity of asymmetric drivings are captured by the parameters $\mathcal{Q}$ and $\mathcal{Q}^*$. The exact expression of the characteristic function of joint probability distribution of output work and input heat for the time-forward process is given by [216],

$$\begin{aligned} \mathcal{G}_f^{HO}(\chi_w, \chi_h) =& 2(1-e^{-\beta_c\omega_0})(1-e^{-\beta_h\omega_1}) \\ & \times \left[\mathcal{Q}(1-x_1^2)(1-y_1^2) + (1+x_1^2)(1+y_1^2) - 4x_1y_1\right]^{-\frac{1}{2}} \\ & \times \left[\mathcal{Q}^*(1-x_2^2)(1-y_2^2) + (1+x_2^2)(1+y_2^2) - 4x_2y_2\right]^{-\frac{1}{2}}, \end{aligned} \tag{4.4.2}$$

where,

$$\begin{aligned} x_1 &= \exp\left[-\omega_0(\beta_c + i\chi_w)\right], \\ y_1 &= \exp\left[i\omega_1(\chi_w - \chi_h)\right], \\ x_2 &= \exp\left[-\omega_1(\beta_h + i(\chi_w - \chi_h))\right], \\ y_2 &= \exp\left[i\omega_0\chi_w\right], \end{aligned}$$

and $\mathcal{Q}$, $\mathcal{Q}^* \in [1,\infty]$ are the so called adiabaticity parameters for the expansion and compression unitary strokes, respectively. $\mathcal{Q}$ and $\mathcal{Q}^*$ serve as a qualitative indicator of the degree of non-adiabaticity (in the quantum sense) introduced into the unitary work strokes (see Ref. [217] for details). $\mathcal{Q}=\mathcal{Q}^*$ corresponds to the time-symmetric driving case with $\mathcal{Q}=\mathcal{Q}^*=1$ is the quasi-static limit.

Bellow, we list the expressions of the averages and fluctuations of work and heat for the forward cycle.

$$\langle q_h\rangle_f = \frac{\omega_1}{2}\left[\coth\left(\frac{\beta_h\omega_1}{2}\right) - \mathcal{Q}\coth\left(\frac{\beta_c\omega_0}{2}\right)\right], \tag{4.4.3}$$

$$\langle\langle q_h^2\rangle\rangle_f = -\frac{\omega_1^2}{4}\left[2-\coth^2\left(\frac{\beta_h\omega_1}{2}\right) - (2\mathcal{Q}^2-1)\coth^2\left(\frac{\beta_c\omega_0}{2}\right)\right], \tag{4.4.4}$$

$$\begin{aligned}\langle w\rangle_f &= \langle w_1\rangle_f + \langle w_3\rangle_f \\ &= \frac{1}{2}(\mathcal{Q}\omega_1-\omega_0)\coth\left(\frac{\beta_c\omega_0}{2}\right) + \frac{1}{2}(\mathcal{Q}^*\omega_0-\omega_1)\coth\left(\frac{\beta_h\omega_1}{2}\right),\end{aligned} \tag{4.4.5}$$

$$\begin{aligned}\langle\langle w^2\rangle\rangle_f &= \langle w_1\rangle_f^2 + \langle w_3\rangle_f^2 - \frac{(\omega_1-\omega_0)^2}{2} + \frac{\omega_0\omega_1}{2}(\mathcal{Q}+\mathcal{Q}^*-2) \\ &\quad + \frac{\omega_1^2}{4}(\mathcal{Q}^2-1)\coth^2\left(\frac{\beta_c\omega_0}{2}\right) + \frac{\omega_0^2}{4}(\mathcal{Q}^{*2}-1)\coth^2\left(\frac{\beta_h\omega_1}{2}\right),\end{aligned} \tag{4.4.6}$$

$$\langle q_c\rangle_f = \frac{\omega_0}{2}\left[\coth\left(\frac{\beta_c\omega_0}{2}\right) - \mathcal{Q}^*\coth\left(\frac{\beta_h\omega_1}{2}\right)\right], \tag{4.4.7}$$

$$\langle\langle q_c^2\rangle\rangle_f = -\frac{\omega_0^2}{4}\left[2-\coth^2\left(\frac{\beta_c\omega_0}{2}\right) - (2\mathcal{Q}^{*2}-1)\coth^2\left(\frac{\beta_h\omega_1}{2}\right)\right]. \tag{4.4.8}$$

For the reverse cycle, similar expressions for averages and fluctuations of work and heat can be obtained by swapping $\mathcal{Q}$ and $\mathcal{Q}^*$.

In the symmetrized engine operational regime, $\langle w\rangle_f \leq 0$ and $\langle w\rangle_r \leq 0$, the numerical results in Fig. 4.6 suggest that the lower and upper bounds for $\eta^{(2)}$ are given as $1 > \eta^{(2)} \geq \langle\eta\rangle_s^2$. Contrary to (4.3.30) for qubit-Otto cycle, numerical studies suggested that for the HO-Otto engine $\eta_{\mathcal{O}}^2 = \left(1-\omega_0/\omega_1\right)^2$ fails to provide a lower bound on $\eta^{(2)}$ at very low temperatures of the heat reservoirs, specifically for $T_c < 1.0$. This discrepancy in results is caused by the different dimensionalities (number of energy levels) of the working fluids. Note that, $\eta_{\mathcal{O}}$ corresponds to the quantum-adiabatic (quasistatic) cycle's efficiency in both scenarios: $u=v=1$ for the qubit-Otto cycle and $\mathcal{Q}=\mathcal{Q}^*=1$ for the HO-Otto cycle. However, as there are an infinite number of energy levels available for HO-working medium, quantum

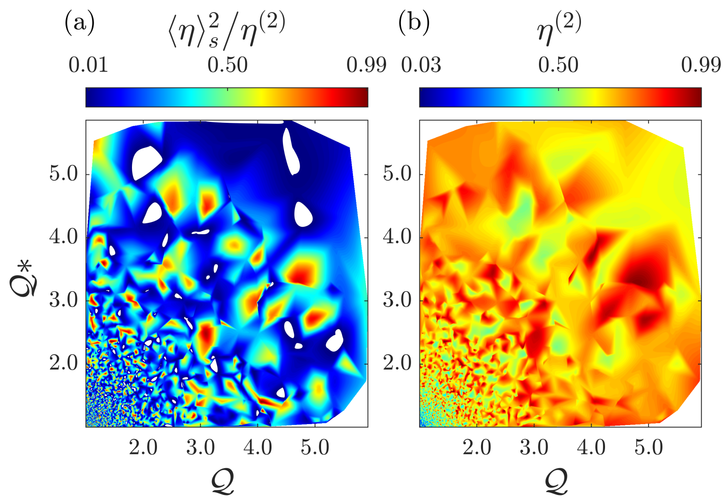


Figure 4.6: For an asymmetrically driven HO-Otto cycle (a) upper and (b) lower bounds on $\eta^{(2)}$ in the engine regime. $\omega_0$, $\omega_1$, $T_c$ and $T_h$ were chosen randomly from uniform distribution between the interval [0,5]. $\mathcal{Q}$, $\mathcal{Q}^*$ were chosen between [1,6]. Simulations done over 2.5 million points.

non-adiabaticity (transitions between the instantaneous eigen basis) plays a more significant role in determining the fluctuations and diminishes the usefulness of the adiabatic (quasistatic) value of efficiency $\eta_O$ in establishing bound on $\eta^{(2)}$.

## 4.5 Summary

In summary, we provide a study of bounds on non-equilibrium fluctuations of heat and work for asymmetrically driven four stroke quantum Otto engine with working fluid consisting of a qubit, or a harmonic oscillator. We show that the non-equilibrium fluctuations are not arbitrary but are restricted. In the engine regime, the ratio of non-equilibrium fluctuations of work and heat from hot reservoir $\eta^{(2)}$ receive both upper and lower bounds. For both the qubit and oscillator case, the upper bound for $\eta^{(2)}$ remains the same whereas the tighter lower bound $\eta_{\text{otto}}^2$, found in qubit-Otto engine, is violated for the oscillator case. For the qubit-Otto cycle, we further make an important connection of our result with the TURs and observe that in the engine regime, the TURs of work and heat for both cold and hot reservoirs follow a strict hierarchy and further lower bounded by the value 2. These results further indicate an interesting possibility to receive a tighter estimate for the thermodynamic efficiency. While preliminary results [212] indicate that some of these bounds may also be satisfied with HO and qubit-Otto engines with finite-time thermalization, it will be interesting to explore the universality of these bounds for more complex working fluids and for other class of finite-time engines.

# 5

# Full statistics of nonequilibrium heat and work for many-body quantum Otto cycle and universal bounds: a NEGF approach

In this work, we consider a generic four-stroke quantum Otto cycle [59, 75, 200–208, 218, 219] consisting of an arbitrary many-body working medium and derive an analytical expression for the joint cumulant generating function (CGF) of total work and input heat, valid up to the second order of the driving amplitude, by employing the rigorous Schwinger-Keldysh nonequilibrium Green's function (NEGF) formalism [220–223]. The CGF obtained for an arbitrary many-body working medium satisfies the nonequilibrium fluctuation relation [214]. Furthermore, we demonstrate the linear response limit characterized by a small driving amplitude and small temperature difference and obtain the expressions for the Onsager's transport coefficients. Notably, we reveal a breakdown of the traditional fluctuation-dissipation relation (FDR) [80, 224–226] for the total work, while, the traditional FDR remains intact for heat. Our findings have remarkable implications for the generic Otto cycle: when operating as an engine, the ratio of output (work) to input (heat from the hot reservoir) fluctuations is bounded from below, while in the refrigerator regime, a similar quantity is bounded from above. Additionally, we also establish connections to the TURs. Finally, we compare the obtained bounds for the discrete Otto cycle with those of autonomous steady-state machines [53, 54, 63, 227].

We organize the paper as follows: Sections 5.1 and 5.2 briefly describes the quantum Otto cycle and the two-point measurement protocol to construct the CGF corresponding to the joint probability distribution of total work and heat. We then demonstrate how to map the CGF on the modified Keldysh contour. In Section 5.3, we obtain the expression for the CGF valid up to the second order of the external driving amplitude. We validate that the CGF respects the fluctuation symmetry. In Sections 5.4 to 5.7, we discuss the linear response limit, obtain the Onsager transport coefficients, and derive universal bounds on nonequilibrium fluctuations in both engine and refrigerator operational regimes. We illustrate the obtained results with a paradigmatic model in Section 5.8. Finally, we summarize our main findings and provide an outlook in Section 5.9.

## 5.1 Quantum Otto cycle with generic many-boday working medium

We consider a generic many-body working medium for the quantum Otto cycle and treat the many-body interaction part as a time-dependent perturbation. The total Hamiltonian of the working medium is given by

$$H(t) = H_0 + \lambda(t) H_1, \tag{5.1.1}$$

where $H_0$ is the non-interacting part, often referred to here as the free Hamiltonian, and $H_1$ represents an arbitrary many-body interaction term. $\lambda(t)$ is an arbitrary driving protocol that drives the system away from equilibrium. Importantly, $\lambda(t)$ serves the purpose of a perturbation parameter, and the values it can take are significantly smaller than those of other dimensionally comparable free parameters. The working medium performs a four-stroke Otto cycle consisting of two unitary and two thermalization strokes with respect to the cold and hot thermal reservoirs with fixed inverse temperatures $\beta_c$ and $\beta_h$, respectively, as illustrated Fig. 5.1. Below we briefly describe these four strokes: (i) ***Unitary expansion*** $(A \to B)$. The system starts at time $t = 0$ from the initial thermal state $A$ characterized by the cold inverse temperature $\beta_c$ and Hamiltonian $H(0) = H_0 + \lambda(0) H_1$, where $\lambda(0) = \lambda_0$. The system is then decoupled from the reservoir and $\lambda(t)$ drives the system out of equilibrium.

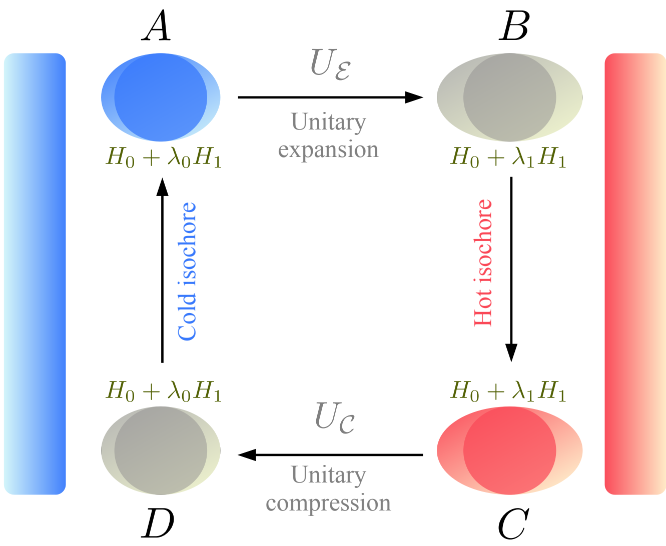


Figure 5.1: Schematic of a four-stroke Otto cycle. We are considering symmetric driving case: $U_{\mathcal{C}} = \Theta U_{\mathcal{E}}^{\dagger} \Theta^{\dagger}$. The final states of the unitary strokes at $B$ and $D$ are non-thermal ones.

The first unitary stroke ends at time $t = \tau$ with $\lambda(\tau) = \lambda_1$. At the end of this stroke, the state of the system $B$ is a non-thermal one. (ii) ***Hot isochore*** $(B \to C)$. During the first heat exchange stroke, the system is brought into weak contact with the hot reservoir while keeping $\lambda_1$ fixed. The system then waits until it reaches a thermal state $C$, parameterized by $(\lambda_1, \beta_h)$ at time $t = \tau + \tau_h$. (iii) ***Unitary compression*** $(C \to D)$. The system is then decoupled from the hot reservoir and the interaction strength $\lambda(t)$ is decreased unitarily from $\lambda_1$ to $\lambda_0$. Consequently, the system ends up in a non-thermal state $D$ at time $t = \tau + \tau_h + \tau'$. (iv) ***Cold isochore*** $(D \to A)$: In the final step, the system is placed in weak contact with the cold reservoir while keeping $\lambda_0$ fixed until it reaches the thermal state parametrized by $(\lambda_0, \beta_c)$ at time $t = \tau + \tau_h + \tau' + \tau_c = \tau_{cyc}$. Here, we assume that the system achieves full thermalization during both hot and cold isochores. This assumption is valid when the heat exchange stroke times $\tau_h$ and $\tau_c$ are much larger than the system relaxation time. Additionally, we consider here the symmetric driving case, meaning the unitary evolution operators, represented by $U_{\mathcal{E}}$ and $U_{\mathcal{C}}$, governing the expansion and compression strokes, respectively, are mirror images of each other, $U_{\mathcal{C}} = \Theta U_{\mathcal{E}}^{\dagger} \Theta^{\dagger}$, where $\Theta$ is the anti-unitary time-reversal operator. As a result, the two unitary stroke duration are equal, $\tau' = \tau$.

Under the complete thermalization assumption, we construct the joint probability distribution (PD) of total work and heat exchange in the hot isochore $P(w, q_h)$ by employing the projective measurements of the energy of the system at the end points of each stroke, i.e., at $A$, $B$, $C$, and $D$, respectively [50]. The characteristic function (CF) corresponding to the joint distribution is given by the Fourier transform of the PD:

$$\begin{aligned}\mathcal{G}(\chi_w, \chi_h) &= \iint dw\, dq_h\, P(w, q_h)\, e^{i\chi_w w}\, e^{i\chi_h q_h} \\ &= \frac{\mathrm{Tr}\big[U_{\mathcal{E}}^{\dagger}\, e^{(i\chi_w - i\chi_h)H(\tau)}\, U_{\mathcal{E}}\, e^{(-i\chi_w - \beta_c)H(0)}\big]}{\mathcal{Z}_c[H(0)]} \frac{\mathrm{Tr}\big[U_{\mathcal{C}}^{\dagger}\, e^{i\chi_w H(0)}\, U_{\mathcal{C}}\, e^{(-i\chi_w + i\chi_h - \beta_h)H(\tau)}\big]}{\mathcal{Z}_h[H(\tau)]},\end{aligned} \tag{5.1.2}$$

where $\chi_w, \chi_h$ are the counting variables associated to the total work $w = w_1 + w_3$ and the heat exchange with the hot reservoir $q_h$, respectively. In (5.1.2), $H(0) = H_0 + \lambda_0 H_1$ and $H(\tau) = H_0 + \lambda_1 H_1$. $\mathcal{Z}_c[H(0)] = \mathrm{Tr}[e^{-\beta_c H(0)}]$ and $\mathcal{Z}_h[H(\tau)] = \mathrm{Tr}[e^{-\beta_h H(\tau)}]$ represent the canonical partition functions with respect to the cold and hot inverse temperatures $\beta_c$ and $\beta_h$, and Hamiltonians $H(0)$ and $H(\tau)$, respectively. We observe that, due to the complete thermalization assumption, the joint PD in (5.1.2) takes a product form. More importantly, under this assumption, the joint PD of total work and heat from the hot reservoir alone suffices to determine the statistics of heat exchange with the cold reservoir $q_c$ (see Appendix A1).

## 5.2 Characteristic function on modified Schwinger-Keldysh contour

In order to obtain a perturbative expression of the CF given in (5.1.2), we utilize the Schwinger-Keldysh formalism. This is a standard approach for systematic calculation of nonequilibrium Green's functions and correlation functions under the influence of time-dependent perturbations by casting the problem on a closed time-ordered contour in the complex time plane, famously known as the Keldysh contour. For the problem considered here, all the unitary evolution operators and the exponential operators, *e.g.*, $e^{(i\chi_w - i\chi_h)H(\tau)}$, appearing in (5.1.2) are mapped on two

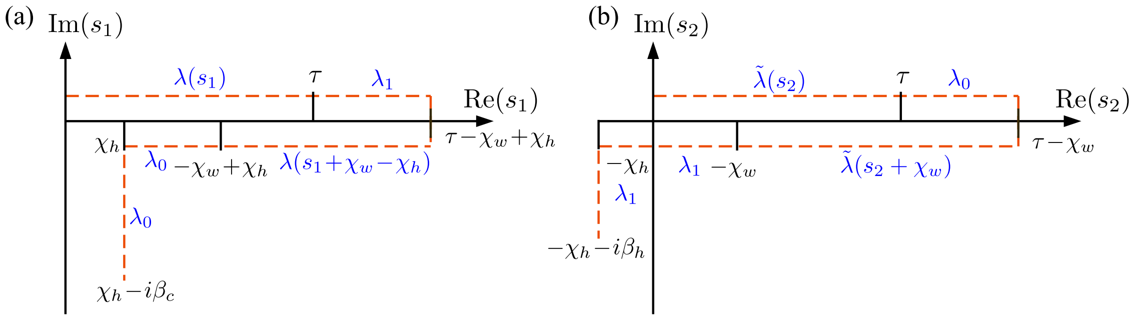


Figure 5.2: The modified Keldysh contour to compute joint work and heat statistics for a generic quantum Otto cycle. (a) Contour $C$ corresponds to the numerator of the first term in (5.1.2). The denominator of this term runs only on the vertical tail. (b) Contour $C'$ corresponds to the numerator of the second term in (5.1.2). The denominator of this term runs only on the vertical tail. In the symmetric driving scenario: $\tilde{\lambda}(s) = \lambda(\tau - s)$. Note that, none of the modified contours $C$ and $C'$ return to $\mathrm{Re}(s) = 0$, and get closed, because of the presence of the non-unitary heat exchange stroke.

modified Keldysh contours. The first trace in (5.1.2) corresponds to the modified contour $C$, as shown in Fig. 5.2 (a), and the second trace gives rise to another modified contour $C'$, as shown in Fig. 5.2 (b). It is important to note that, in the Schwinger-Keldysh formalism, one typically expects closed contours while dealing with time-dependent perturbations. However, here, none of our modified contours are closed, only articulating the fact that both the traces, that are mapped, contain partial information about the non-unitary heat exchange stroke. The tails represent the presence of interaction $H_1$ in the thermal states at $A$ and $C$ (see Fig. 5.1). We express the joint CF on the Keldysh contour in a compact form as

$$\begin{aligned}
\mathcal{G}(\chi_w, \chi_h) =& \frac{\left\langle \mathcal{T}_C \, e^{-\frac{i}{\hbar}\int_C \lambda_C(s_1) H_1^I(s_1) ds_1} \right\rangle_{\widetilde{\beta}_c}}{\left\langle \mathcal{T}_C \, e^{-\frac{i}{\hbar}\int_{\hbar\chi_h}^{\hbar\chi_h - i\hbar\beta_c} \lambda_0 H_1^I(s_1) ds_1} \right\rangle_{\beta_c}} \frac{\left\langle \mathcal{T}_{C'} \, e^{-\frac{i}{\hbar}\int_C \lambda_{C'}(s_2) H_1^I(s_2) ds_2} \right\rangle_{\widetilde{\beta}_h}}{\left\langle \mathcal{T}_{C'} \, e^{-\frac{i}{\hbar}\int_{\tau - \hbar\chi_h}^{\tau - \hbar\chi_h - i\hbar\beta_h} \lambda_1 H_1^I(s_2) ds_2} \right\rangle_{\beta_h}} \\
&\times \langle e^{-i\chi_h H_0} \rangle_{\beta_c} \langle e^{i\chi_h H_0} \rangle_{\beta_h} \\
\equiv& \, \mathcal{G}_C(\chi_w, \chi_h) \, \mathcal{G}_{C'}(\chi_w, \chi_h) \, \langle e^{-i\chi_h H_0} \rangle_{\beta_c} \langle e^{i\chi_h H_0} \rangle_{\beta_h}.
\end{aligned} \tag{5.2.1}$$

Here, crucially, the averages in both the numerators are taken with respect to shifted inverse temperatures $\widetilde{\beta}_c = \beta_c + i\chi_h$ and $\widetilde{\beta}_h = \beta_h - i\chi_h$, which are counting-field dependent. $\mathcal{T}_C$ and $\mathcal{T}_{C'}$ are the contour-time ordered operators defined on the contours $C$ and $C'$, respectively, which orders the time-dependent operators according to their contour-time argument: sorting the operators from left to right with their contour-time arguments decreasing.

***Details of mapping the joint CF on Keldysh contour*:**

We present the details of obtaining the joint CF given in (5.2.1). In time-dependent perturbation theory, we express all the evolution operators in the interaction picture with respect to the free Hamiltonian $H_0$. Here, we consider the first trace of (5.2.1) only. A similar analysis applies to the second trace as well. Exclusively for this proof, we are dropping the $\mathcal{E}$ subscript from $U_{\mathcal{E}}$. In the interaction picture, we obtain

$$U_I(t) = \mathcal{T}_+ \exp\Big[-\frac{i}{\hbar}\int_0^t \lambda(s) H_1^I(s)\, ds\Big], \tag{5.2.2}$$

$$U_I^{(0)}(t) = \mathcal{T}_+ \exp\Big[-\frac{i}{\hbar}\int_0^t \lambda_0 H_1^I(s)\, ds\Big], \tag{5.2.3}$$

$$U_I^{(\tau)}(t) = \mathcal{T}_+ \exp\Big[-\frac{i}{\hbar}\int_0^t \lambda_1 H_1^I(s)\, ds\Big], \tag{5.2.4}$$

where the superscripts $(0)$ and $(\tau)$ in equations (5.2.3) and (5.2.4) indicate interaction picture evolution operator with fixed $\lambda_0$ and $\lambda_1$, respectively. Here $\mathcal{T}_+$ is the time-ordering operator which arranges the operators from left to right with decreasing time. Note that, $H_1^I(s) = U_0^\dagger(s)\, H_1\, U_0(s)$, where $U_0(t) = \exp(-iH_0 t/\hbar)$ represents the free evolution operator. We express the first trace in (5.2.1) as,

$$\begin{aligned}
&\mathrm{Tr}\Big[e^{-i\chi_w H(0)}\, U^\dagger(\tau)\, e^{(i\chi_w - i\chi_h)H(\tau)}\, U(\tau)\, e^{-\beta_c H(0)}\Big] \\
&= \mathrm{Tr}\Big[U^{(0)^\dagger}(-\hbar\chi_w)\, U^\dagger(\tau)\, U^{(\tau)}(-\hbar\chi_w + \hbar\chi_h)\, U(\tau)\, U^{(0)}(-i\hbar\beta_c)\Big] \\
&= \mathrm{Tr}\Big[U_I^{(0)^\dagger}(-\hbar\chi_w)\, U_0^\dagger(-\hbar\chi_w)\, U_I^\dagger(\tau)\, U_0^\dagger(\tau)\, U_0(-\hbar\chi_w + \hbar\chi_h)\, U_I^{(\tau)}(-\hbar\chi_w + \hbar\chi_h) \\
&\qquad U_0(\tau)\, U_I(\tau)\, U_0(-i\hbar\beta_c)\, U_I^{(0)}(-i\hbar\beta_c)\Big] \\
&= \mathrm{Tr}\Big[\overbrace{U_0^\dagger(\hbar\chi_h)\, U_I^{(0)}(-i\hbar\beta_c)\, U_0(\hbar\chi_h)}\, \underbrace{U_0^\dagger(\hbar\chi_h)\, U_I^{(0)^\dagger}(-\hbar\chi_w)\, U_0(\hbar\chi_h)}
\end{aligned}$$

$$
\begin{aligned}
&\overbrace{U_0^\dagger(-\hbar\chi_w+\hbar\chi_h)\,U_I^\dagger(\tau)\,U_0(-\hbar\chi_w+\hbar\chi_h)}\;\underbrace{U_0^\dagger(\tau)\,U_I^{(\tau)}(-\hbar\chi_w+\hbar\chi_h)\,U_0(\tau)}\\
&\quad\overbrace{U_I(\tau)}\;U_0(-i\hbar\beta_c)\,U_0(\hbar\chi_h)\Big]\\
&= \Big\langle \mathcal{T}_+ e^{-\frac{i}{\hbar}\int_{\hbar\chi_h}^{\hbar\chi_h-i\hbar\beta_c}\lambda_0 H_1^I(s)\,ds}\,\mathcal{T}_- e^{-\frac{i}{\hbar}\int_{-\hbar\chi_w+\hbar\chi_h}^{\hbar\chi_h}\lambda_0 H_1^I(s)\,ds}\\
&\quad \mathcal{T}_- e^{-\frac{i}{\hbar}\int_{\tau-\hbar\chi_w+\hbar\chi_h}^{-\hbar\chi_w+\hbar\chi_h}\lambda(s+\chi_w-\chi_h)H_1^I(s)\,ds}\,\mathcal{T}_+ e^{-\frac{i}{\hbar}\int_{\tau}^{\tau-\hbar\chi_w+\hbar\chi_h}\lambda_1 H_1^I(s)\,ds}\\
&\quad \mathcal{T}_+ e^{-\frac{i}{\hbar}\int_0^{\tau}\lambda(s)H_1^I(s)\,ds}\Big\rangle_{\widetilde{\beta}_c}\\
&\quad \times\,\mathrm{Tr}\left[e^{(-\beta_c-i\chi_h)H_0}\right]\\
&= \Big\langle \mathcal{T}_c e^{-\frac{i}{\hbar}\int_c \lambda_C(s)H_1^I(s)\,ds}\Big\rangle_{\widetilde{\beta}_c}\,\mathrm{Tr}\left[e^{(-\beta_c-i\chi_h)H_0}\right].
\end{aligned}
\tag{5.2.5}
$$

In the last line, we map the real-time evolution onto a modified Keldysh contour $C$ [see Fig. 5.2 (a)] by introducing the contour-time ordered operator $\mathcal{T}_C$ with contour-time dependent driving parameter $\lambda_C(s)$. Similarly, we can map the partition function $\mathcal{Z}_c[H(0)]$ appearing in (5.2.1) onto the same contour $C$. For the partition function, we obtain

$$
\begin{aligned}
\mathcal{Z}_c[H(0)] &= \mathrm{Tr}\left[e^{-\beta_c H(0)}\right] = \mathrm{Tr}\left[U_0(-i\hbar\beta_c)\,U_I^{(0)}(-i\hbar\beta_c)\right]\\
&= \mathrm{Tr}\left[U_0(-i\hbar\beta_c)\;\underbrace{U_0^\dagger(\hbar\chi_h)\,U_I^{(0)}(-i\hbar\beta_c)\,U_0(\hbar\chi_h)}\right]\\
&= \Big\langle \mathcal{T}_c\, e^{-\frac{i}{\hbar}\int_{\hbar\chi_h}^{\hbar\chi_h-i\hbar\beta_c}\lambda_0 H_1^I(s)\,ds}\Big\rangle_{\beta_c}\,\mathrm{Tr}\left[e^{-\beta_c H_0}\right],
\end{aligned}
\tag{5.2.6}
$$

where the contour-time dependent first term is mapped onto a Keldysh contour which runs only on the vertical line of Fig. 5.2 (a). The same prescription also applies for the second trace and the partition function $\mathcal{Z}_h[H(\tau)]$ in (5.2.1), resulting in the second modified contour [see Fig. 5.2 (b)].

Next, we expanded the exponential operators in (5.2.1) up to the second order in driving protocol $\lambda(s)$ [220]. Here, we will demonstrate the series expansion for $\mathcal{G}_C(\chi_w,\chi_h)$, mapped on the first contour:

$$
\mathcal{G}_C(\chi_w,\chi_h) \coloneqq \frac{\big\langle \mathcal{T}_C\, e^{-\frac{i}{\hbar}\int_C \lambda_C(s_1)H_1^I(s_1)\,ds_1}\big\rangle_{\widetilde{\beta}_c}}{\big\langle \mathcal{T}_C\, e^{-\frac{i}{\hbar}\int_{\hbar\chi_h}^{\hbar\chi_h-i\hbar\beta_c}\lambda_0 H_1^I(s_1)\,ds_1}\big\rangle_{\beta_c}}
$$

$$= \frac{1+\sum_{n=1}^{\infty}\Big[\prod_{j=1}^{n}\int_C ds_j\lambda_C(s_j)\Theta_C(s_j-s_{j+1})\left(-\frac{i}{\hbar}\right)^n\langle H_1^I(s_1)\cdots H_1^I(s_n)\rangle_{\widetilde{\beta}_c}\Big]}{1+\sum_{n=1}^{\infty}\Big[\prod_{j=1}^{n}\int_{\hbar\chi_h}^{\hbar\chi_h-i\hbar\beta_c} ds_j\lambda_C(s_j)\,\Theta_C(s_j-s_{j+1})\left(-\frac{i}{\hbar}\right)^n\langle H_1^I(s_1)\cdots H_1^I(s_n)\rangle_{\beta_c}\Big]}, \tag{5.2.7}$$

where, the contour step function $\Theta_C(s_j - s_{j+1})$ is appearing because of the contour-time ordering. A more convenient way is to consider the expansion of the cumulant generating function (CGF) $\ln[\mathcal{G}_C(\chi_w, \chi_h)]$, where the series expansion is expressed in terms of $n$-point connected correlation functions (cumulant correlation functions),

$$\ln\,\mathcal{G}_C(\chi_w,\chi_h)=\sum_{n=1}^{\infty}\left[\prod_{j=1}^{n}\int_C d\mathbf{S}_j\widetilde{\mathbb{G}}_c(s_1,...,s_n)-\prod_{j=1}^{n}\int_{\hbar\chi_h}^{\hbar\chi_h-i\hbar\beta_c} d\mathbf{S}_j\mathbb{G}_c(s_1,...,s_n)\right], \tag{5.2.8}$$

where, $d\mathbf{S}_j = ds_j\lambda_C(s_j)\Theta_C(s_j - s_{j+1})$ and

$$\begin{aligned}\widetilde{\mathbb{G}}_c(s_1,...,s_n) &= \left(-\frac{i}{\hbar}\right)^n\langle\!\langle H_1^I(s_1)...H_1^I(s_n)\rangle\!\rangle_{\widetilde{\beta}_c},\\ \mathbb{G}_c(s_1,...,s_n) &= \left(-\frac{i}{\hbar}\right)^n\langle\!\langle H_1^I(s_1)...H_1^I(s_n)\rangle\!\rangle_{\beta_c}.\end{aligned} \tag{5.2.9}$$

Note that, the double angular bracket $\langle\!\langle\,\cdot\,\rangle\!\rangle$ represents cumulant correlation function. The CGF is a very useful quantity as it enables us to calculate all the cumulants of total work and heat exchange with the hot reservoir by taking partial derivatives with respect to $\chi_w$ and $\chi_h$, respectively,

$$\langle\!\langle w^k q_h^l\rangle\!\rangle = \frac{\partial^k\partial^l}{\partial(i\chi_w)^k\partial(i\chi_h)^l}\,\ln\mathcal{G}(\chi_w,\chi_h)\Big|_{\{\chi\}=0}. \tag{5.2.10}$$

## 5.3 Cumulants of work and heat

In this section, we first write down the final expression for the CGF valid up to the second order of the driving protocol $\lambda(s)$:

$$\begin{aligned}
\ln \mathcal{G}(\chi_w,\chi_h) =& \big[-i\chi_w(\lambda_1-\lambda_0)+i\chi_h\lambda_1\big]\,\big[\langle H_1\rangle_{\widetilde{\beta}_h}-\langle H_1\rangle_{\widetilde{\beta}_c}\big] \\
&+\big[-i\hbar\chi_w(\lambda_1^2-\lambda_0^2)+i\hbar\chi_h\lambda_1^2\big]\int\frac{d\omega}{2\pi}\frac{\widetilde{\mathbb{G}}^>_h(\omega)-\widetilde{\mathbb{G}}^>_c(\omega)}{\omega} \\
&-\beta_c\lambda_0\Big[\langle H_1\rangle_{\widetilde{\beta}_c}-\langle H_1\rangle_{\beta_c}+\hbar\lambda_0\int\frac{d\omega}{2\pi}\frac{\widetilde{\mathbb{G}}^>_c(\omega)-\mathbb{G}^>_c(\omega)}{\omega}\Big] \\
&-\beta_h\lambda_1\Big[\langle H_1\rangle_{\widetilde{\beta}_h}-\langle H_1\rangle_{\beta_h}+\hbar\lambda_1\int\frac{d\omega}{2\pi}\frac{\widetilde{\mathbb{G}}^>_h(\omega)-\mathbb{G}^>_h(\omega)}{\omega}\Big] \\
&+\int\frac{d\omega}{2\pi}\frac{1-e^{i\hbar\omega(\chi_w-\chi_h)}}{\omega^2}A(\omega)\widetilde{\mathbb{G}}^>_c(\omega)+\int\frac{d\omega}{2\pi}\frac{1-e^{i\hbar\omega\chi_w}}{\omega^2}A(\omega)\widetilde{\mathbb{G}}^>_h(\omega) \\
&+\ln\langle e^{-i\chi_h H_0}\rangle_{\beta_c}+\ln\langle e^{i\chi_h H_0}\rangle_{\beta_h}.
\end{aligned} \tag{5.3.1}$$

Equation (5.3.1) is the first central result of this chapter. It describes the statistical properties of total work and input heat fluctuations in a generic (many-body) Otto cycle in terms of one-point and two-point correlators of the interaction Hamiltonian $H_1$. In this expression, we suppress the integration limits for $\omega$, which ranges from $-\infty$ to $+\infty$. Here, the nonequilibrium Green's functions are defined as connected two-point correlators of $H_1$ in the interaction picture,

$$\widetilde{\mathbb{G}}^>_\alpha(s)=\left(-\frac{i}{\hbar}\right)^2\langle\langle H_1^I(s)H_1\rangle\rangle_{\widetilde{\beta}_\alpha}, \tag{5.3.2}$$

$$\mathbb{G}^>_\alpha(s)=\left(-\frac{i}{\hbar}\right)^2\langle\langle H_1^I(s)H_1\rangle\rangle_{\beta_\alpha}, \tag{5.3.3}$$

where $\alpha=c,h$. Here, the two-point connected correlation function or cumulant correlation function is given by

$$\langle\langle X^I(s_1)Y^I(s_2)\rangle\rangle_\beta=\langle X^I(s_1)Y^I(s_2)\rangle_\beta-\langle X\rangle_\beta\langle Y\rangle_\beta. \tag{5.3.4}$$

Notably, the shifted inverse temperatures $\widetilde{\beta}_\alpha$, $\alpha=c,h$, appearing in (5.3.1) play a crucial role in calculating the cumulants of the heat exchange. Here, we adopt the

Fourier transformation convention:

$$\mathbb{G}_\alpha^>(\omega) = \int_{-\infty}^{+\infty} ds\, \mathbb{G}_\alpha^>(s)\, e^{i\omega s}. \tag{5.3.5}$$

Crucially, all the information about the time-dependent driving protocol is encapsulated in the quantity $A(\omega)$, defined as

$$A(\omega) = \left| \int_0^\tau \dot{\lambda}(t) e^{i\omega t} dt \right|^2 . \tag{5.3.6}$$

The CGF in (5.3.1) satisfies the normalization condition, $\ln \mathcal{G}(0,0) = 0$. More importantly, it satisfies the universal heat engine fluctuation symmetry [114, 214, 228],

$$\ln \mathcal{G}\big[i\beta_c,\, i(\beta_c - \beta_h)\big] = 0. \tag{5.3.7}$$

This fluctuation symmetry is a direct consequence of the Kubo-Martin-Schwinger (KMS) boundary condition satisfied by the Green's functions introduced in equations (5.3.2) and (5.3.3) [79, 229–231],

$$\widetilde{\mathbb{G}}^>(s - i\hbar\widetilde{\beta}_c) = \widetilde{\mathbb{G}}^>(-s), \tag{5.3.8}$$
$$\mathbb{G}^>(s - i\hbar\beta_c) = \mathbb{G}^>(-s). \tag{5.3.9}$$

***Details of the calculation of joint CGF*:**

Let us begin from (5.2.8). The contour-time dependent driving parameter $\lambda_C(s)$ is piece-wise defined along the contour $C$:

$$\lambda(s) = \begin{cases} \lambda(s) & \text{Part 1}: \; s \in [0, \tau), \\ \lambda_1 & \text{Part 2}: \; s \in [\tau, \tau - \hbar\chi_w + \hbar\chi_h), \\ \lambda(s + \hbar\chi_w - \hbar\chi_h) & \text{Part 3}: \; s \in [\tau - \hbar\chi_w + \hbar\chi_h, -\hbar\chi_w + \hbar\chi_h), \\ \lambda_0 & \text{Part 4}: \; s \in [-\hbar\chi_w + \hbar\chi_h, \hbar\chi_h - i\hbar\beta_c]. \end{cases} \tag{5.3.10}$$

Our goal is to calculate the right-hand side of (5.2.8) up to the second order of the driving parameter $\lambda(s)$.

The contribution to the first order of $\lambda(s)$ is given by

$$O(\lambda) \Rightarrow i\big[\chi_w(\lambda_1-\lambda_0) - \chi_h\lambda_1\big]\langle H_1\rangle_{\widetilde{\beta}_c} - \beta_c\lambda_0\big[\langle H_1\rangle_{\widetilde{\beta}_c} - \langle H_1\rangle_{\beta_c}\big]. \tag{5.3.11}$$

Next, for the contribution to the second order in $\lambda(s)$ we have to calculate double integrals given by

$$\begin{aligned} O(\lambda^2) \Rightarrow & \int_C ds_1\,\lambda_C(s_1)\int_C ds_2\,\lambda_C(s_2)\,\Theta_C(s_1-s_2)\,\widetilde{\mathbb{G}}_c(s_1,s_2) \\ & - \int_{\hbar\chi_h}^{\hbar\chi_h - i\hbar\beta_c} ds_1\,\lambda_C(s_1)\int_{\hbar\chi_h}^{\hbar\chi_h - i\hbar\beta_c} ds_2\,\lambda_C(s_2)\,\Theta_C(s_1-s_2)\,\mathbb{G}_c(s_1,s_2) \\ = & \int_C ds_1\,\lambda_C(s_1)\int_C ds_2\,\lambda_C(s_2)\,\Theta_C(s_1-s_2)\,\widetilde{\mathbb{G}}_c^{>}(s_1-s_2) \\ & - \int_{\hbar\chi_h}^{\hbar\chi_h - i\hbar\beta_c} ds_1\,\lambda_C(s_1)\int_{\hbar\chi_h}^{\hbar\chi_h - i\hbar\beta_c} ds_2\,\lambda_C(s_2)\,\Theta_C(s_1-s_2)\,\mathbb{G}_c^{>}(s_1-s_2). \end{aligned} \tag{5.3.12}$$

Due to (5.3.10), the double integral along the contour $C$ is expressed as a sum of double integrals of parts $(i,j)$, where $i,j \in \{1,2,3,4\}$. Importantly, once we take into account the contour step function $\Theta(s_1 - s_2)$, only 10 out of the possible 16 terms survive in this sum:

$$(i,j) = \begin{cases} (1,1), \\ (2,1),\ (2,2), \\ (3,1),\ (3,2),\ (3,3), \\ (4,1),\ (4,2),\ (4,3),\ (4,4). \end{cases} \tag{5.3.13}$$

Bellow we show details of calculating a few of these double integrations:
(i) For $(i,j) = (4,1)$

$$\int \frac{d\omega}{2\pi} \int_{-\hbar\chi_w+\hbar\chi_h}^{\hbar\chi_h - i\hbar\beta_c} ds_1\,\lambda_0\,e^{-i\omega s_1} \int_0^{\tau} ds_2\,\lambda(s_2)\,e^{i\omega s_2}\widetilde{\mathbb{G}}_c^{>}(\omega)$$

$$
\begin{aligned}
&= \int \frac{d\omega}{2\pi} \lambda_0 \frac{e^{-\hbar\omega(\beta_c + i\chi_h)} \widetilde{\mathbb{G}}_c^{>}(\omega)}{-i\omega} \int_0^\tau ds_2\, \lambda(s_2)\, e^{i\omega s_2} \\
&\quad - \int \frac{d\omega}{2\pi} \lambda_0 \frac{\widetilde{\mathbb{G}}_c^{>}(\omega)}{-i\omega}\, e^{i\hbar\omega(\chi_w - \chi_h)} \int_0^\tau ds_2\, \lambda(s_2)\, e^{i\omega s_2} \\
&= \int \frac{d\omega}{2\pi} \lambda_0 \frac{\widetilde{\mathbb{G}}_c^{>}(-\omega)}{-i\omega} \int_0^\tau ds_2 \lambda(s_2) e^{i\omega s_2} \\
&\quad + \int \frac{d\omega}{2\pi} \lambda_0 \frac{\widetilde{\mathbb{G}}_c^{>}(\omega)}{i\omega}\, e^{i\hbar\omega(\chi_w - \chi_h)} \int_0^\tau ds_2\, \lambda(s_2)\, e^{i\omega s_2} \\
&= \int \frac{d\omega}{2\pi} \frac{\widetilde{\mathbb{G}}_c^{>}(\omega)}{i\omega}\, \lambda_0 \int_0^\tau ds_2\, \lambda(s_2)\, e^{-i\omega s_2} \\
&\quad + \int \frac{d\omega}{2\pi} \frac{\widetilde{\mathbb{G}}_c^{>}(\omega)}{i\omega} \lambda_0\, e^{i\hbar\omega(\chi_w - \chi_h)} \int_0^\tau ds_2\, \lambda(s_2)\, e^{i\omega s_2}.
\end{aligned} \tag{5.3.14}
$$

where to go from the second step to the third step we have used the KMS relation given in (5.3.8).

(ii) For $(i, j) = (4, 2)$

$$
\begin{aligned}
&\int \frac{d\omega}{2\pi} \int_{-\hbar\chi_w + \hbar\chi_h}^{\hbar\chi_h - i\hbar\beta_c} ds_1\, \lambda_0\, e^{-i\omega s_1} \int_\tau^{\tau - \hbar\chi_w + \hbar\chi_h} ds_2\, \lambda_1\, e^{i\omega s_2} \widetilde{\mathbb{G}}_c^{>}(\omega) \\
&= -\int \frac{d\omega}{2\pi} \lambda_0 \lambda_1 \frac{e^{-\hbar\omega(\beta_c + i\chi_h)} \widetilde{\mathbb{G}}_c^{>}(\omega)}{\omega^2} \left(1 - e^{-i\hbar\omega(\chi_w - \chi_h)}\right) e^{i\omega\tau} \\
&\quad - \int \frac{d\omega}{2\pi} \lambda_0 \lambda_1 \frac{\widetilde{\mathbb{G}}_c^{>}(\omega)}{\omega^2} \left(1 - e^{i\hbar\omega(\chi_w - \chi_h)}\right) e^{i\omega\tau} \\
&= -\int \frac{d\omega}{2\pi} \lambda_0 \lambda_1 \frac{\widetilde{\mathbb{G}}_c^{>}(-\omega)}{\omega^2} \left(1 - e^{-i\hbar\omega(\chi_w - \chi_h)}\right) e^{i\omega\tau} \\
&\quad - \int \frac{d\omega}{2\pi} \lambda_0 \lambda_1 \frac{\widetilde{\mathbb{G}}_c^{>}(\omega)}{\omega^2} \left(1 - e^{i\hbar\omega(\chi_w - \chi_h)}\right) e^{i\omega\tau} \\
&= \int \frac{d\omega}{2\pi} \frac{\widetilde{\mathbb{G}}_c^{>}(\omega)}{\omega^2} \left[ -2\lambda_0 \lambda_1 \left(1 - e^{i\hbar\omega(\chi_w - \chi_h)}\right) \cos(\omega\tau) \right],
\end{aligned} \tag{5.3.15}
$$

(iii) For $(i, j) = (4, 3)$

$$
\int \frac{d\omega}{2\pi} \int_{-\hbar\chi_w + \hbar\chi_h}^{\hbar\chi_h - i\hbar\beta_c} ds_1\, \lambda_0\, e^{-i\omega s_1} \int_{\tau - \hbar\chi_w + \hbar\chi_h}^{-\hbar\chi_w + \hbar\chi_h} ds_2\, \lambda(s_2 + \hbar\chi_w - \hbar\chi_h)\, e^{i\omega s_2} \widetilde{\mathbb{G}}_c^{>}(\omega)
$$

$$= -\int \frac{d\omega}{2\pi} \int_{-\hbar\chi_w+\hbar\chi_h}^{\hbar\chi_h - i\hbar\beta_c} ds_1\, \lambda_0\, e^{-i\omega s_1} \int_0^{\tau} ds_2\, \lambda(s_2)\, e^{i\omega(s_2-\hbar\chi_w+\hbar\chi_h)} \widetilde{\mathbb{G}}_c^{>}(\omega)$$
$$= -\int \frac{d\omega}{2\pi} \frac{\widetilde{\mathbb{G}}_c^{>}(\omega)}{i\omega}\, \lambda_0\, e^{i\hbar\omega(\chi_w-\chi_h)} \int_0^{\tau} ds_2\, \lambda(s_2)\, e^{-i\omega s_2}$$
$$- \int \frac{d\omega}{2\pi} \frac{\widetilde{\mathbb{G}}_c^{>}(\omega)}{i\omega}\, \lambda_0 \int_0^{\tau} ds_2\, \lambda(s_2)\, e^{i\omega s_2}. \tag{5.3.16}$$

The intermediate steps are similar to the (4,1) case.
(iv) For $(i, j) = (4, 4)$

$$\int \frac{d\omega}{2\pi} \int_{-\hbar\chi_w+\hbar\chi_h}^{\hbar\chi_h - i\hbar\beta_c} ds_1\, \lambda_0\, e^{-i\omega s_1} \int_{-\hbar\chi_w+\hbar\chi_h}^{s_1} ds_2\, \lambda_0\, e^{i\omega s_2} \widetilde{\mathbb{G}}_c^{>}(\omega)$$
$$- \int \frac{d\omega}{2\pi} \int_{\hbar\chi_h}^{\hbar\chi_h - i\hbar\beta_c} ds_1\, \lambda_0\, e^{-i\omega s_1} \int_{\hbar\chi_h}^{s_1} ds_2\, \lambda_0\, e^{i\omega s_2} \mathbb{G}_c^{>}(\omega)$$
$$= \int \frac{d\omega}{2\pi} \frac{\widetilde{\mathbb{G}}_c^{>}(\omega)}{\omega^2} \lambda_0^2 \big[ - i\hbar\omega\chi_w - \beta_c\hbar\omega + 1 - e^{-\beta_c\hbar\omega} e^{-i\hbar\omega\chi_w} \big]$$
$$- \int \frac{d\omega}{2\pi} \frac{\mathbb{G}_c^{>}(\omega)}{\omega^2} \lambda_0^2 \big[ - \beta_c\hbar\omega + 1 - e^{-\beta_c\omega} \big]$$
$$= \int \frac{d\omega}{2\pi} \lambda_0^2 \Big[ \frac{\widetilde{\mathbb{G}}_c^{>}(\omega)}{\omega^2} \big( - i\hbar\omega\chi_w - \beta_c\hbar\omega + 1 \big) - e^{-i\hbar\omega(\chi_w-\chi_h)} \frac{\widetilde{\mathbb{G}}_c^{>}(-\omega)}{\omega^2} \Big]$$
$$- \int \frac{d\omega}{2\pi} \lambda_0^2 \Big[ \frac{\mathbb{G}_c^{>}(\omega)}{\omega^2} \big( - \beta_c\hbar\omega + 1 \big) - \frac{\mathbb{G}_c^{>}(-\omega)}{\omega^2} \Big]$$
$$= \int \frac{d\omega}{2\pi} \frac{\widetilde{\mathbb{G}}_c^{>}(\omega)}{\omega^2} \lambda_0^2 \big[ - i\hbar\omega\chi_w - \beta_c\hbar\omega + 1 - e^{i\hbar\omega(\chi_w-\chi_h)} \big] + \int \frac{d\omega}{2\pi} \frac{\mathbb{G}_c^{>}(\omega)}{\omega} \lambda_0^2 \beta_c \hbar. \tag{5.3.17}$$

Note that, the second term here is stemming from the canonical partition function $\mathcal{Z}_c[H(0)]$ [second term in (5.3.12)]. The rest of the terms in (5.3.13) can be calculated analogously. Now, following Ref. [220], we will categorize the 10 non-zero terms given in (5.3.13) in 6 groups:

1. $\{(2, 2)\}$:

$$\int \frac{d\omega}{2\pi} \widetilde{\mathbb{G}}_c^{>}(\omega) \Big[ \frac{\lambda_1^2}{\omega^2} \big( i\hbar\omega(\chi_w - \chi_h) + 1 - e^{i\hbar\omega(\chi_w-\chi_h)} \big) \Big]. \tag{5.3.18}$$

2. $\{(1,1)+(3,1)+(3,3)\}$

$$\int \frac{d\omega}{2\pi}\widetilde{\mathbb{G}}_c^{>}(\omega)\left(1-e^{i\hbar\omega(\chi_w-\chi_h)}\right)\int_0^\tau ds_1\int_0^\tau ds_2\,\lambda(s_1)\lambda(s_2)e^{i\omega(s_1-s_2)}. \tag{5.3.19}$$

3. $\{(2,1)+(3,2)\}$

$$\int \frac{d\omega}{2\pi}\widetilde{\mathbb{G}}_c^{>}(\omega)\Big[-\frac{2\lambda_1}{\omega}\left(1-e^{i\hbar\omega(\chi_w-\chi_h)}\right)\int_0^\tau ds\,\lambda(s)\sin\left[\omega(\tau-s)\right]\Big]. \tag{5.3.20}$$

4. $\{(4,3)+(4,1)\}$

$$\int \frac{d\omega}{2\pi}\widetilde{\mathbb{G}}_c^{>}(\omega)\Big[-\frac{2\lambda_0}{\omega}\left(1-e^{i\hbar\omega(\chi_w-\chi_h)}\right)\int_0^\tau ds\,\lambda(s)\sin\left(\omega s\right)\Big]. \tag{5.3.21}$$

5. $\{(4,2)\}$

$$\int \frac{d\omega}{2\pi}\widetilde{\mathbb{G}}_c^{>}(\omega)\Big[-\frac{2\lambda_0\lambda_1}{\omega^2}\left(1-e^{i\hbar\omega(\chi_w-\chi_h)}\right)\cos\left(\omega\tau\right)\Big]. \tag{5.3.22}$$

6. $\{(4,4)\}$

$$\begin{aligned}&\int \frac{d\omega}{2\pi}\widetilde{\mathbb{G}}_c^{>}(\omega)\Big[\frac{\lambda_0^2}{\omega^2}\Big(-i\hbar\omega\chi_w-\beta_c\hbar\omega+1-e^{i\hbar\omega(\chi_w-\chi_h)}\Big)\Big]\\&\qquad+\int \frac{d\omega}{2\pi}\mathbb{G}_c^{>}(\omega)\frac{\hbar\beta_c\lambda_0^2}{\omega}.\end{aligned} \tag{5.3.23}$$

Next, we collect all the terms with $\left(1-e^{i\hbar\omega(\chi_w-\chi_h)}\right)$

$$\begin{aligned}\int \frac{d\omega}{2\pi}\widetilde{\mathbb{G}}_c^{>}(\omega)\frac{1-e^{i\hbar\omega(\chi_w-\chi_h)}}{\omega^2}\Big[&\lambda_1^2+\lambda_0^2-2\lambda_0\lambda_1\cos\left(\omega\tau\right)\\&+\omega^2\int_0^\tau ds_1\int_0^\tau ds_2\,\lambda(s_1)\lambda(s_2)e^{i\omega(s_1-s_2)}\\&-2\omega\lambda_1\int_0^\tau ds\,\lambda(s)\sin\left[\omega(\tau-s)\right]-2\omega\lambda_0\int_0^\tau ds\,\lambda(s)\sin\left(\omega s\right)\Big]\end{aligned}$$

$$
\begin{aligned}
&= \int \frac{d\omega}{2\pi} \widetilde{\mathbb{G}}_c^{>}(\omega) \frac{1 - e^{i\hbar\omega(\chi_w - \chi_h)}}{\omega^2} \left| \lambda_1 e^{i\omega\tau} - \lambda_0 - i\omega \int_0^\tau ds\, \lambda(s)\, e^{i\omega s} \right|^2 \\
&= \int \frac{d\omega}{2\pi} \widetilde{\mathbb{G}}_c^{>}(\omega) \frac{1 - e^{i\hbar\omega(\chi_w - \chi_h)}}{\omega^2} \left| \int_0^\tau ds\, \dot{\lambda}(s)\, e^{i\omega s} \right|^2 \\
&= \int \frac{d\omega}{2\pi} \widetilde{\mathbb{G}}_c^{>}(\omega) \frac{1 - e^{i\hbar\omega(\chi_w - \chi_h)}}{\omega^2} A(\omega),
\end{aligned} \tag{5.3.24}
$$

Finally, summing all the terms given in equations (5.3.18) to (5.3.23), we obtain

$$
\begin{aligned}
\int \frac{d\omega}{2\pi} \widetilde{\mathbb{G}}_c^{>}(\omega) \Bigg[ \frac{1}{\omega} \Big( i\hbar\chi_w(\lambda_1^2 - \lambda_0^2) - i\hbar\chi_h\lambda_1^2 - \hbar\beta_c\lambda_0^2 \Big) + \frac{1 - e^{i\hbar\omega(\chi_w - \chi_h)}}{\omega^2} A(\omega) \Bigg] \\
+ \int \frac{d\omega}{2\pi} \mathbb{G}_c^{>}(\omega) \frac{\hbar\beta_c\lambda_0^2}{\omega}.
\end{aligned} \tag{5.3.25}
$$

Therefore, the right-hand side of Eq. (5.2.8) up to second order of driving parameter $\lambda(s)$ is given by

$$
\begin{aligned}
& i\Big(\chi_w(\lambda_1 - \lambda_0) - \chi_h\lambda_1\Big)\langle H_1\rangle_{\widetilde{\beta}_c} - \beta_c\lambda_0\Big(\langle H_1\rangle_{\widetilde{\beta}_c} - \langle H_1\rangle_{\beta_c}\Big) \\
& + \Big(i\hbar\chi_w(\lambda_1^2 - \lambda_0^2) - i\hbar\chi_h\lambda_1^2 - \hbar\beta_c\lambda_0^2\Big) \int \frac{d\omega}{2\pi} \frac{\widetilde{\mathbb{G}}_c^{>}(\omega)}{\omega} + \hbar\beta_c\lambda_0^2 \int \frac{d\omega}{2\pi} \frac{\mathbb{G}_c^{>}(\omega)}{\omega} \\
& + \int \frac{d\omega}{2\pi} \widetilde{\mathbb{G}}_c^{>}(\omega) \frac{1 - e^{i\hbar\omega(\chi_w - \chi_h)}}{\omega^2} A(\omega) + O(\lambda^3).
\end{aligned} \tag{5.3.26}
$$

Notice that the contour $C$ corresponding to the first trace in (5.1.2), contains the contributions to the statistics of total work and input heat that are solely connected to the cold reservoir inverse temperature $\beta_c$. An analogous calculation can be done for the second contour $C'$, which captures all the contributions that are connected to the hot reservoir inverse temperature $\beta_h$.

In the following, we present the formal expressions of the first and second cumulants of total work $w$ and heat exchange with the hot reservoir $q_h$. The average total work is given by

$$
\begin{aligned}
\langle w\rangle = &- (\lambda_1 - \lambda_0)\big[\langle H_1\rangle_{\beta_h} - \langle H_1\rangle_{\beta_c}\big] - \hbar(\lambda_1^2 - \lambda_0^2) \int \frac{d\omega}{2\pi} \frac{1}{\omega} \left[\mathbb{G}_h^{>}(\omega) - \mathbb{G}_c^{>}(\omega)\right] \\
&- \hbar \int \frac{d\omega}{2\pi} \frac{A(\omega)}{\omega} \left[\mathbb{G}_c^{>}(\omega) + \mathbb{G}_h^{>}(\omega)\right].
\end{aligned} \tag{5.3.27}
$$

The first two terms on the right-hand side represent the boundary terms that depend on the end values of the driving protocol. They are associated with the total change in free energy during the two unitary work strokes.

The corresponding variance (second cumulant) of total work is given by

$$\langle\langle w^2 \rangle\rangle = -\hbar^2 \int \frac{d\omega}{2\pi} A(\omega) \left[ \mathbb{G}_c^{>}(\omega) + \mathbb{G}_h^{>}(\omega) \right]. \tag{5.3.28}$$

We notice that calculating the cumulants of heat exchange $q_h$ requires more involved calculations due to the presence of shifted inverse temperatures $\widetilde{\beta}_c$ and $\widetilde{\beta}_h$. This results in connected correlators of the form $\langle\langle H_1 H_0 \rangle\rangle$, $\langle\langle H_1^I(s) H_1 H_0 \rangle\rangle$, and so on. Note that, for an arbitrary operator $X$,

$$\frac{d}{d(i\chi_h)} \langle X \rangle_{\widetilde{\beta}_\alpha} = \mp \langle\langle X H_0 \rangle\rangle_{\widetilde{\beta}_\alpha}, \tag{5.3.29}$$

$$\frac{d^2}{d(i\chi_h)^2} \langle X \rangle_{\widetilde{\beta}_\alpha} = \langle\langle X H_0^2 \rangle\rangle_{\widetilde{\beta}_\alpha}, \tag{5.3.30}$$

where $(-)$ corresponds to $\alpha = c$, and $(+)$ corresponds to $\alpha = h$, respectively. Below we list the expressions for the average heat exchange with the hot reservoir and its variance,

$$\begin{aligned}
\langle q_h \rangle =& \langle H_0 \rangle_{\beta_h} - \langle H_0 \rangle_{\beta_c} + \lambda_1 \left[ \langle H_1 \rangle_{\beta_h} - \langle H_1 \rangle_{\beta_c} \right] + \hbar\lambda_1^2 \int \frac{d\omega}{2\pi} \frac{\mathbb{G}_h^{>}(\omega) - \mathbb{G}_c^{>}(\omega)}{\omega} \\
&+ \beta_c \lambda_0 \left[ \langle\langle H_0 H_1 \rangle\rangle_{\beta_c} + \hbar\lambda_0 \int \frac{d\omega}{2\pi} \frac{\mathbb{G}_c'(\omega)}{\omega} \right] - \beta_h \lambda_1 \left[ \langle\langle H_0 H_1 \rangle\rangle_{\beta_h} + \hbar\lambda_1 \int \frac{d\omega}{2\pi} \frac{\mathbb{G}_h'(\omega)}{\omega} \right] \\
&+ \hbar \int \frac{d\omega}{2\pi} \frac{A(\omega) \mathbb{G}_c^{>}(\omega)}{\omega},
\end{aligned} \tag{5.3.31}$$

$$\begin{aligned}
\langle\langle q_h^2 \rangle\rangle =& \langle\langle H_0^2 \rangle\rangle_{\beta_c} + \langle\langle H_0^2 \rangle\rangle_{\beta_h} + 2\lambda_1 \left[ \langle\langle H_0 H_1 \rangle\rangle_{\beta_c} + \langle\langle H_0 H_1 \rangle\rangle_{\beta_h} \right] + 2\hbar\lambda_1^2 \int \frac{d\omega}{\pi} \frac{\mathbb{G}_c'(\omega) + \mathbb{G}_h'(\omega)}{\omega} \\
&- \beta_c \lambda_0 \left[ \langle\langle H_0^2 H_1 \rangle\rangle_{\beta_c} + \hbar\lambda_0 \int \frac{d\omega}{2\pi} \frac{\mathbb{G}_c''(\omega)}{\omega} \right] - \beta_h \lambda_1 \left[ \langle\langle H_0^2 H_1 \rangle\rangle_{\beta_h} + \hbar\lambda_1 \int \frac{d\omega}{2\pi} \frac{\mathbb{G}_h''(\omega)}{\omega} \right] \\
&+ 2\hbar \int \frac{d\omega}{2\pi} \frac{\mathbb{G}_c'(\omega) A(\omega)}{\omega} + \hbar^2 \int \frac{d\omega}{2\pi} A(\omega) \mathbb{G}_c^{>}(\omega),
\end{aligned} \tag{5.3.32}$$

where we have introduced a compact notation,

$$\mathbb{G}'_\alpha(\omega) = -\frac{\partial}{\partial \beta_\alpha}\, \mathbb{G}^>_\alpha(\omega), \tag{5.3.33}$$

$$\mathbb{G}''_\alpha(\omega) = \frac{\partial^2}{\partial \beta_\alpha^2}\, \mathbb{G}^>_\alpha(\omega), \tag{5.3.34}$$

with $\alpha = c, h$.

In the following section, we focus on establishing the linear response formalism for the generic quantum Otto cycle.

## 5.4 Linear response: Onsager coefficients

Let us first parameterize the driving protocol $\lambda(t)$ as

$$\lambda(t) = \lambda + \Delta\lambda\, f(t), \tag{5.4.1}$$

where, $\lambda = \lambda_0$ and $\Delta\lambda = \lambda_1 - \lambda_0$. The function $f(t)$ is defined such that $f(0) = 0$ and $f(\tau) = 1$ to ensure that $\lambda_0$ and $\lambda_1$ are the boundary values of the protocol $\lambda(t)$ at time $t = 0$ and time $t = \tau$, respectively. To identify the proper thermodynamic affinities and the corresponding conjugate fluxes, we begin with the definition of the stochastic entropy production in a single cycle:

$$\Sigma = \beta_c w + (\beta_c - \beta_h)\, q_h = (\beta_c \Delta\lambda)\, \frac{w}{\Delta\lambda} + (\beta_c - \beta_h)\, q_h. \tag{5.4.2}$$

From this expression, we identify the thermodynamic affinities as $\mathcal{A}_w = \beta_c\Delta\lambda$ and $\mathcal{A}_q = \beta_c - \beta_h$, and the corresponding integrated work and heat fluxes as $w/\Delta\lambda$ and $q_h$, respectively. One can further define the heat and work currents by dividing the integrated heat and work fluxes with total cycle time $\tau_{cyc} = 2\tau + \tau_h + \tau_c$:

$$j_w = \frac{1}{\tau_{cyc}}\frac{w}{\Delta\lambda} \quad \text{and} \quad j_q = \frac{q_h}{\tau_{cyc}}. \tag{5.4.3}$$

Consequently, the average entropy production rate in one complete cycle $\langle\sigma\rangle = \langle\Sigma\rangle/\tau_{cyc}$ can be expressed as

$$\langle\sigma\rangle = \sum_{\alpha=w,q} \langle j_\alpha\rangle \mathcal{A}_\alpha. \tag{5.4.4}$$

From this point onwards, we adopt $\beta_c = \beta$ and $\beta_c - \beta_h = \Delta\beta$, and focus on the linear response regime where $\Delta\beta \ll \beta$. In this regime, we can effectively utilize the following Taylor expansion:

$$\langle X\rangle_{\beta-\Delta\beta} = \langle X\rangle_\beta - \Delta\beta \frac{\partial}{\partial\beta}\langle X\rangle_\beta = \langle X\rangle_\beta + \Delta\beta\langle\langle X H_0\rangle\rangle_\beta. \tag{5.4.5}$$

Note that the appearance of the free Hamiltonian $H_0$ in the second term arises from the derivative with respect to $\beta$ over a canonical distribution characterized by $e^{-\beta H_0}/\operatorname{Tr}[e^{-\beta H_0}]$. To proceed with our linear response analysis for the generic Otto cycle, we calculate the average work and heat fluxes, $\langle j_w\rangle$ and $\langle j_q\rangle$, using equations (5.3.27) and (5.3.31), respectively, which are accurate up to the second order of the driving protocol $\lambda(t)$. Finally, carrying out the Taylor expansion given in (5.4.5) and keeping terms up to the linear order of the affinities, $\mathcal{A}_w$ and $\mathcal{A}_q$, we derive the following relation between the currents and affinities, connected via the Onsager matrix:

$$\begin{pmatrix} \langle j_w\rangle \\ \langle j_q\rangle \end{pmatrix} = \begin{pmatrix} L_{ww} & L_{wq} \\ L_{qw} & L_{qq} \end{pmatrix} \begin{pmatrix} \mathcal{A}_w \\ \mathcal{A}_q \end{pmatrix}, \tag{5.4.6}$$

where the Onsager transport coefficients $L_{\alpha\gamma}$, with $\alpha, \gamma = w, q$, are given by

$$L_{ww} = -\frac{1}{\tau_{cyc}}\hbar \int \frac{d\omega}{2\pi} \frac{2\,F(\omega)\,\mathbb{G}^>(\omega)}{\beta\,\omega}, \tag{5.4.7}$$

$$L_{wq} = L_{qw} = \frac{1}{\tau_{cyc}} \frac{\partial}{\partial\beta}\Big[\langle H_1\rangle_\beta + 2\hbar\lambda \int \frac{d\omega}{2\pi}\frac{\mathbb{G}^>(\omega)}{\omega}\Big], \tag{5.4.8}$$

$$L_{qq} = -\frac{1}{\tau_{cyc}} \frac{\partial}{\partial\beta}\Big[\langle H_0\rangle_\beta + \lambda\frac{\partial}{\partial\beta}\Big(\beta\langle H_1\rangle_\beta + \hbar\lambda\beta \int \frac{d\omega}{2\pi}\frac{\mathbb{G}^>(\omega)}{\omega}\Big)\Big]. \tag{5.4.9}$$

Here, note that

$$F(\omega) = \left| \int_0^\tau \dot{f}(t) e^{i\omega t} dt \right|^2 = \frac{A(\omega)}{\Delta\lambda^2} \tag{5.4.10}$$

encodes the information of driving where $\Delta\lambda$ and $f(t)$ are defined in (5.4.1). The Green's function $\mathbb{G}^>(\omega)$ is evaluated at the equilibrium temperature $\beta$.

The Onsager reciprocity relation, $L_{wq} = L_{qw}$, holds even for asymmetric drivings (i.e., when time-reversal symmetry is broken) [cf. (5.4.8)], unlike systems with asymmetric time-dependent drivings, where this relation generally breaks down [232]. The Otto cycle preserves Onsager reciprocity due to the separation of work and heat exchange strokes.

The derived expressions for the Onsager transport coefficients, characterizing the behavior of an arbitrary working medium executing the Otto cycle in the linear response regime, constitute another central result of this chapter. With these results in hand, we proceed to provide some important insights and remarks.

## 5.5 Fluctuation-Dissipation relations: violation of work–FDR

The traditional "Fluctuation-Dissipation relations" (FDRs) typically connect the diagonal elements of the Onsager matrix to equilibrium fluctuations [80].

### FDR for heat current $j_q$

In our analysis, we precisely recover the traditional FDR for the heat current $j_q$,

$$L_{qq} = \frac{\langle\langle j_q^2 \rangle\rangle}{2} \bigg|_{\{\mathcal{A}\}=0}, \tag{5.5.1}$$

where $\langle\langle j_q^2 \rangle\rangle = \langle\langle q_h^2 \rangle\rangle / \tau_{cyc}$. In order to prove the above heat-FDR, we start from (5.3.32), and take the limit of $\mathcal{A}_w = 0$ and $\mathcal{A}_q = 0$. This immediately hands over the following expression for heat-fluctuation:

$$\langle\langle j_q^2 \rangle\rangle \bigg|_{\{\mathcal{A}\}=0} = \frac{1}{\tau_{cyc}} \bigg[ \langle\langle H_0^2 \rangle\rangle_{\beta_c} + \langle\langle H_0^2 \rangle\rangle_{\beta_h} + 2\lambda_1 \big[ \langle\langle H_0 H_1 \rangle\rangle_{\beta_c} + \langle\langle H_0 H_1 \rangle\rangle_{\beta_h} \big]$$

$$
\begin{aligned}
&+ 2\hbar\lambda_1^2\int \frac{d\omega}{\pi}\frac{\mathbb{G}_c'(\omega)+\mathbb{G}_h'(\omega)}{\omega} - \beta_c\lambda_0\Big[\langle\langle H_0^2 H_1\rangle\rangle_{\beta_c} + \hbar\lambda_0\int\frac{d\omega}{2\pi}\frac{\mathbb{G}_c''(\omega)}{\omega}\Big] \\
&\quad - \beta_h\lambda_1\Big[\langle\langle H_0^2 H_1\rangle\rangle_{\beta_h} + \hbar\lambda_1\int\frac{d\omega}{2\pi}\frac{\mathbb{G}_h''(\omega)}{\omega}\Big] \\
&+ 2\hbar\int\frac{d\omega}{2\pi}\frac{\mathbb{G}_c'(\omega)A(\omega)}{\omega} + \hbar^2\int\frac{d\omega}{2\pi}A(\omega)\mathbb{G}_c^{>}(\omega)\Big]_{\{\mathcal{A}\}=0} \\
= {}& \frac{2}{\tau_{cyc}}\Big\{-\frac{\partial}{\partial\beta}\Big[\langle H_0\rangle_\beta + 2\lambda\langle H_1\rangle_\beta + 2\hbar\lambda^2\int\frac{d\omega}{2\pi}\frac{\mathbb{G}^{>}(\omega)}{\omega}\Big] \\
&\quad - \beta\lambda\frac{\partial^2}{\partial\beta^2}\Big[\langle H_1\rangle_\beta + \hbar\lambda\int\frac{d\omega}{2\pi}\frac{\mathbb{G}^{>}(\omega)}{\omega}\Big]\Big\} \\
= {}& 2\,L_{qq},
\end{aligned}
\tag{5.5.2}
$$

where we have used $\lambda = \lambda_0$ and $\beta = \beta_c$, as adopted in the previous section.

### FDR for work current $j_w$

Importantly, the same is not true for the case of work current. In fact, for the work current fluctuation, following (5.3.28), we obtain

$$
\frac{\langle\langle j_w^2\rangle\rangle}{2}\Big|_{\{\mathcal{A}\}=0} = -\frac{1}{\tau_{cyc}}\hbar^2\int\frac{d\omega}{2\pi}F(\omega)\mathbb{G}^{>}(\omega), \tag{5.5.3}
$$

which does not match the diagonal Onsager coefficient $L_{ww}$. To investigate this discrepancy further, let us rewrite the expressions for $L_{ww}$ and $\langle\langle j_w^2\rangle\rangle$ as follows:

$$
L_{ww} = -\frac{1}{\tau_{cyc}}\frac{\hbar^2}{2}\int\frac{d\omega}{2\pi}F(\omega)\frac{\tanh\left(\frac{\beta\hbar\omega}{2}\right)}{\frac{\beta\hbar\omega}{2}}\big[\mathbb{G}^{>}(\omega)+\mathbb{G}^{>}(-\omega)\big]. \tag{5.5.4}
$$

$$
\frac{\langle\langle j_w^2\rangle\rangle}{2}\Big|_{\{\mathcal{A}\}=0} = -\frac{1}{\tau_{cyc}}\frac{\hbar^2}{2}\int\frac{d\omega}{2\pi}F(\omega)\big[\mathbb{G}^{>}(\omega)+\mathbb{G}^{>}(-\omega)\big], \tag{5.5.5}
$$

Here, we have utilized an important identity involving the Green's functions,

$$
\mathbb{G}^{>}(\omega) - \mathbb{G}^{>}(-\omega) = \tanh\left(\frac{\beta\hbar\omega}{2}\right)\big[\mathbb{G}^{>}(\omega)+\mathbb{G}^{>}(-\omega)\big]. \tag{5.5.6}
$$

which arises from the KMS condition in the Fourier space, $e^{-\beta\hbar\omega}\mathbb{G}^{>}(\omega) = \mathbb{G}^{>}(-\omega)$. Now, considering the fact that $\tanh(x)/x \leq 1$, we infer from equations (5.5.5) and

(5.5.4) that

$$L_{ww} \leq \frac{\langle\langle j_w^2 \rangle\rangle}{2}\bigg|_{\{\mathcal{A}\}=0}, \tag{5.5.7}$$

highlighting a breakdown of the traditional FDR for work current. Importantly, this breakdown is purely of quantum origin. The equality is restored in the quantum-adiabatic limit, i.e., when $[H_0, H_1] = 0$. This observation aligns with the recent findings of Ref. [233, 234] where a similar breakdown was reported.

The obtained results for the Onsager coefficients and the FDR breakdown for work current have non-trivial implications in determining universal bounds on the performance of the quantum Otto cycle operating as an engine or a refrigerator.

### Thermodynamic Uncertainty Relations

Additionally, it is noteworthy that the standard thermodynamic uncertainty relation [215, 235] holds for the currents $j_w$ and $j_q$,

$$\mathrm{TUR}(j_\alpha) \coloneqq \langle \sigma \rangle \frac{\langle\langle j_\alpha^2 \rangle\rangle}{\langle j_\alpha \rangle^2} \geq 2, \tag{5.5.8}$$

for $\alpha = w, q$. These TURs remain valid independently of the mode of the Otto cycle's operation–engine, refrigerator, heater, or accelerator [75]. Bellow, we demonstrate a proof for $\mathrm{TUR}(j_w)$. Using equations (5.4.4), (5.4.6) and (5.5.7) we obtain,

$$\begin{aligned}
\mathrm{TUR}(j_w) = \langle \sigma \rangle \frac{\langle\langle j_w^2 \rangle\rangle}{\langle j_w \rangle^2} &\geq \left[\mathcal{A}_w \langle j_w \rangle + \mathcal{A}_q \langle j_q \rangle\right] \frac{2L_{ww}}{\langle j_w \rangle^2} \\
&= 2\Big[L_{ww}^2 \mathcal{A}_w^2 + 2L_{ww}L_{wq}\mathcal{A}_w\mathcal{A}_q + L_{ww}L_{qq}\mathcal{A}_q^2\Big] \frac{1}{\langle j_w \rangle^2} \\
&= 2\Big[\langle\, j_w \rangle^2 + \mathcal{A}_q^2 \big(L_{ww}L_{qq} - L_{wq}^2\big)\Big] \frac{1}{\langle j_w \rangle^2} \\
&= 2 + \frac{2\,\mathcal{A}_q^2}{\langle j_w \rangle^2} \cdot \det(L) \\
&\geq 2.
\end{aligned} \tag{5.5.9}$$

Here, we have used the positive semi-definiteness of the Onsager matrix, which implies that $\det(L) \geq 0$. The proof corresponding to TUR($j_q$) follows analogously.

## 5.6 Engine regime: Universal lower bound on the ratio of output to input fluctuations

Let us now focus on understanding bounds on nonequilibrium fluctuations when the Otto cycle works as an engine. To quantify the engine's performance, we introduce the output power as

$$\langle \mathcal{P} \rangle = -\langle w \rangle / \tau_{cyc} = -\mathcal{A}_w \langle j_w \rangle / \beta, \tag{5.6.1}$$

and the input heat current is given by $\langle j_q \rangle$. The engine operational regime of the Otto cycle is characterized by $\langle \mathcal{P} \rangle > 0$, and $\langle j_q \rangle > 0$, where, as per our sign convention, energy flowing into the working medium is considered positive. To achieve this, the necessary requirement is $\mathcal{A}_q > \mathcal{A}_w$. Following the second law of thermodynamics, $\langle \sigma \rangle \geq 0$, it is straightforward to show that the average efficiency of the Otto engine, $\langle \eta \rangle \coloneqq \langle \mathcal{P} \rangle / \langle j_q \rangle$, is universally upper bounded by the the Carnot bound $\eta_{\rm c} = \Delta\beta/\beta$ [1, 4], $\langle \eta \rangle \leq \eta_{\rm c}$. In order to derive bounds on nonequilibrium fluctuations, following Ref. [53], we construct the quantity $\eta^{(2)}$, which is the ratio of power fluctuation to the fluctuation of input heat current,

$$\eta^{(2)} = \frac{\langle\langle \mathcal{P}^2 \rangle\rangle}{\langle\langle j_q^2 \rangle\rangle}. \tag{5.6.2}$$

Recently, it was shown that in the case of a continuously coupled autonomous steady-state heat engine operating in the linear response regime, where both the work and heat FDRs are valid, the ratio of output power to input heat current fluctuations is subject to both universal lower and upper bounds [53],

$$\eta_{\rm c}^2 \geq \left[\eta^{(2)}\right]_{\rm auto} \geq \langle \eta \rangle^2, \tag{5.6.3}$$

where the subscript 'auto' stands for the autonomous steady-state heat engine. However, in our case of a generic finite-time Otto engine operating in the linear response limit, we obtain the following inequality,

$$\eta_c^2 \geq \frac{\mathcal{A}_w^2 L_{ww}}{\beta^2 L_{qq}} \geq \langle \eta \rangle^2. \tag{5.6.4}$$

***Detailed proof*:**

Let us consider the first inequality in (5.6.4). We will consider a modified version: $\eta_c^2 \beta^2 L_{qq} - L_{ww} \mathcal{A}_w^2 \geq 0$. Noticing that $\eta_c = \Delta\beta/\beta = \mathcal{A}_q/\beta$, this modified inequality can be expressed as

$$\begin{aligned}
\eta_c^2 \beta^2 L_{qq} - L_{ww} \mathcal{A}_w^2 =& L_{qq} \mathcal{A}_q^2 - L_{ww} \mathcal{A}_w^2 \\
=& \mathcal{A}_q \langle j_q \rangle - \mathcal{A}_w \langle j_w \rangle \\
=& \mathcal{A}_q \langle j_q \rangle \Big[ 1 + \frac{\langle \eta \rangle}{\eta_c} \Big] \\
\geq& 0.
\end{aligned} \tag{5.6.5}$$

In the above steps, we used the engine condition: $\langle j_w \rangle < 0$, and $\langle j_q \rangle > 0$.

Next, we focus on a modified version the second inequality in (5.6.4): $L_{ww} \langle j_w \rangle^2 - L_{qq} \langle j_q \rangle^2 \geq 0$. We observe

$$\begin{aligned}
L_{ww} \langle j_w \rangle^2 - L_{qq} \langle j_q \rangle^2 &= \big( L_{ww} L_{qq} - L_{wq}^2 \big) \Big[ L_{qq} \mathcal{A}_q^2 - L_{ww} \mathcal{A}_w^2 \Big] \\
&= \det(L) \Big[ \mathcal{A}_q \langle j_q \rangle - \mathcal{A}_w \langle j_w \rangle \Big] \\
&= \det(L)\, \mathcal{A}_q \, \langle j_q \rangle \Big[ 1 + \frac{\langle \eta \rangle}{\eta_c} \Big] \\
&\geq 0,
\end{aligned} \tag{5.6.6}$$

where, in the above steps, we have used (i) $\det(L) \geq 0$, and (ii) the engine condition: $\langle j_w \rangle < 0$ and $\langle j_q \rangle > 0$.

A key point to note here is that, contrary to the autonomous steady-state engine, we observe a violation of the traditional work-FDR in the discrete Otto cycle, as given in (5.5.7). This FDR breakdown for the work current leads to the following inequality:

$$\eta^{(2)} \geq \frac{\mathcal{A}_w^2 L_{ww}}{\beta^2 L_{qq}}. \tag{5.6.7}$$

Importantly, the equality is restored in the quantum-adiabatic driving limit, when the driving Hamiltonian commutes with the free Hamiltonian $[H_1, H_0] = 0$. As an immediate consequence of the inequality in (5.6.7), the lower bound on $\eta^{(2)}$ remains robust,

$$\eta^{(2)} \geq \langle \eta \rangle^2. \tag{5.6.8}$$

However, the upper bound on $\eta^{(2)}$ may not always hold true, $\eta^{(2)} \nleq \eta_c^2$, the reason being purely of quantum origin. This distinction is a significant departure from the autonomous case, where both the lower and upper bounds remain intact. In the discrete Otto cycle, due to the violation of the traditional work FDR, the upper bound is not guaranteed. This constitutes another central result of this work. As a direct consequence of the lower bound for $\eta^{(2)}$ in (5.6.8), a hierarchical relation between the TURs is observed. This follows from the fact that

$$\eta^{(2)} \geq \langle \eta \rangle^2 \Rightarrow \frac{\langle\langle j_w^2 \rangle\rangle}{\langle j_w \rangle^2} \geq \frac{\langle\langle j_q^2 \rangle\rangle}{\langle j_q \rangle^2}. \tag{5.6.9}$$

As a result, in the engine regime, a strict hierarchy between the TURs of work (output) and heat (input) currents is obtained:

$$\langle \sigma \rangle \frac{\langle\langle j_w^2 \rangle\rangle}{\langle j_w \rangle^2} \geq \langle \sigma \rangle \frac{\langle\langle j_q^2 \rangle\rangle}{\langle j_q \rangle^2} \geq 2. \tag{5.6.10}$$

## 5.7 Refrigerator regime: Universal upper bound on the ratio of output to input fluctuations

After our exploration of the engine regime, we now shift our focus to the refrigerator regime. In this mode of operation, the primary objective is to extract heat from the cold reservoir by utilizing external work. Following our sign convention: energy entering the working fluid is considered positive, the refrigerator regime is characterized by a positive current flowing out of the cold reservoir, $\langle j_c\rangle > 0$, and work is performed on the system, $\langle j_w\rangle > 0$. To achieve refrigeration, it is necessary that the affinities satisfy $\mathcal{A}_w > \mathcal{A}_q$. The performance of the refrigerator is quantified by its coefficient of performance (COP), also known as cooling efficiency, denoted as $\langle\varepsilon\rangle$. Notably, the COP of a refrigerator is universally upper bounded by the Carnot COP [1, 236],

$$\langle\varepsilon\rangle := \frac{\beta\langle j_c\rangle}{\mathcal{A}_w\langle j_w\rangle} \leq \varepsilon_{\rm c}, \tag{5.7.1}$$

where $\varepsilon_{\rm c} = (1-\eta_{\rm c})/\eta_{\rm c} \approx \beta/\Delta\beta$. Let us now investigate the quantity $\varepsilon^{(2)}$ defined as

$$\varepsilon^{(2)} := \frac{\beta^2\langle\langle j_c^2\rangle\rangle}{\mathcal{A}_w^2\langle\langle j_w^2\rangle\rangle}. \tag{5.7.2}$$

The CF for $q_c$ is obtained by setting $\chi_h = \chi_w = -\chi_c$ in (5.1.2). The new counting variable $\chi_c$ corresponds to the stochastic variable $(-w-q_h)$, which shares the same statistical properties as $q_c$ (see Appendix A1),

$$\mathcal{G}(\chi_c) = \iint dw\, dq_h\, P(w,q_h)\, e^{i\chi_c(-w-q_h)}. \tag{5.7.3}$$

Finally, setting $\chi_h = \chi_w = -\chi_c$ in (5.3.1), we obtain the CGF for $q_c$,

$$\begin{aligned}\ln\mathcal{G}(\chi_c) = &- i\chi_c\lambda_0\big[\langle H_1\rangle_{\widetilde{\beta}_h} - \langle H_1\rangle_{\widetilde{\beta}_c}\big] - i\chi_c\hbar\lambda_0^2\int\frac{d\omega}{2\pi}\frac{\widetilde{\mathbb{G}}_h^{>}(\omega)-\widetilde{\mathbb{G}}_c^{>}(\omega)}{\omega}\\ &- \beta_c\lambda_0\Big[\langle H_1\rangle_{\widetilde{\beta}_c} - \langle H_1\rangle_{\beta_c} + \hbar\lambda_0\int\frac{d\omega}{2\pi}\frac{\widetilde{\mathbb{G}}_c^{>}(\omega)-\mathbb{G}_c^{>}(\omega)}{\omega}\Big]\\ &- \beta_h\lambda_1\Big[\langle H_1\rangle_{\widetilde{\beta}_h} - \langle H_1\rangle_{\beta_h} + \hbar\lambda_1\int\frac{d\omega}{2\pi}\frac{\widetilde{\mathbb{G}}_h^{>}(\omega)-\mathbb{G}_h^{>}(\omega)}{\omega}\Big]\\ &+ \int\frac{d\omega}{2\pi}\frac{1-e^{-i\hbar\omega\chi_c}}{\omega^2}A(\omega)\widetilde{\mathbb{G}}_h^{>}(\omega) + \ln\langle e^{i\chi_c H_0}\rangle_{\beta_c} + \ln\langle e^{-i\chi_c H_0}\rangle_{\beta_h}.\end{aligned} \tag{5.7.4}$$

A crucial point to note here is that now the shifted inverse temperatures become $\widetilde{\beta}_c = \beta_c - i\chi_c$ and $\widetilde{\beta}_h = \beta_h + i\chi_c$, and consequently, $\widetilde{\mathbb{G}}_h^{>}(\omega)$ and $\widetilde{\mathbb{G}}_c^{>}(\omega)$ are redefined accordingly. From (5.7.4), we can obtain the expressions for the average heat extracted and its variance using (5.2.10).

For steady-state autonomous refrigerators operating in the linear response regime, the quantity $\varepsilon^{(2)}$ was reported to possess both universal upper and lower bounds [55],

$$\varepsilon_{\mathrm{c}}^2 \geq \left[\varepsilon^{(2)}\right]_{\text{auto}} \geq \langle\varepsilon\rangle^2, \tag{5.7.5}$$

where, recall that the subscript 'auto' denotes autonomous steady-state refrigerators. In our case of a discrete Otto cycle operating as a refrigerator, we derive the following inequality:

$$\varepsilon_{\mathrm{c}}^2 \geq \frac{\beta^2 L_{qq}}{\mathcal{A}_w^2 L_{ww}} \geq \langle\varepsilon\rangle^2. \tag{5.7.6}$$

***Detailed proof*:**

Here, we demonstrate the proof for the inequalities in (5.7.6). To prove the first inequality, we start with the modified version of the first inequality $L_{ww}\mathcal{A}_w^2 - \beta^2 L_{qq}/\varepsilon_{\mathrm{c}}^2 \geq 0$:

$$\begin{aligned} L_{ww}\mathcal{A}_w^2 - \beta^2 L_{qq}/\varepsilon_{\mathrm{c}}^2 =& L_{ww}\mathcal{A}_w^2 - L_{qq}\mathcal{A}_q^2 \\ =& \mathcal{A}_w\langle j_w\rangle - \mathcal{A}_q\langle j_q\rangle \\ \approx& \mathcal{A}_w\langle j_w\rangle + \mathcal{F}_q\langle j_c\rangle \\ =& \mathcal{A}_w\langle\mathcal{A}_w\rangle\left[1 + \frac{\langle\varepsilon\rangle}{\varepsilon_{\mathrm{c}}}\right] \\ \geq& 0. \end{aligned} \tag{5.7.7}$$

Here, we have used the refrigerator condition: $\langle j_c\rangle > 0$, and $\langle j_w\rangle > 0$. For the second inequality,

$$\begin{aligned} L_{qq}\langle j_c\rangle^2 - L_{ww}\langle j_w\rangle^2 &= \left(L_{ww}L_{qq} - L_{wq}^2\right)\left[L_{ww}\mathcal{A}_w^2 - L_{qq}\mathcal{A}_q^2\right] \\ &= \det(L)\left[\mathcal{A}_w\langle j_w\rangle + \mathcal{A}_q\langle j_c\rangle\right] \\ &= \det(L)\,\mathcal{A}_w\langle j_w\rangle\left[1 + \frac{\langle\varepsilon\rangle}{\varepsilon_{\mathrm{c}}}\right] \\ &\geq 0. \end{aligned} \tag{5.7.8}$$

The two ingredients required for this proof are–

1. The positive semi-definiteness of the Onsager matrix, $\det(L) \geq 0$, and
2. Refrigerator operational regime condition: $\langle j_c \rangle > 0$ and $\langle j_w \rangle > 0$.

Importantly, the breakdown of the traditional work-FDR leads to the following inequality for the quantity $\varepsilon^{(2)}$:

$$\varepsilon^{(2)} \leq \frac{\beta^2 L_{qq}}{\mathcal{A}_w^2 L_{ww}}, \tag{5.7.9}$$

where it is worth noting that the opposite inequality arises due to the presence of $\langle\langle j_w^2 \rangle\rangle$ in the denominator of the definition of $\varepsilon^{(2)}$. As a consequence, we observe a contrasting trend compared to what was observed the engine regime. Specifically, in the refrigeration regime, the lower bound may not always be valid,

$$\varepsilon^{(2)} \ngeq \langle \varepsilon \rangle^2 \Rightarrow \frac{\langle\langle j_c^2 \rangle\rangle}{\langle j_c \rangle^2} \ngeq \frac{\langle\langle j_w^2 \rangle\rangle}{\langle j_w \rangle^2}, \tag{5.7.10}$$

whereas the upper bound remains intact,

$$\varepsilon^{(2)} \leq \varepsilon_c^2. \tag{5.7.11}$$

Furthermore, the potential violation of the lower bound for $\varepsilon^{(2)}$, as can be seen in (5.7.10), leads to the loss of the hierarchy in the TURs within the refrigerator regime. A similar observation was recently reported for a specific model-dependent periodically driven system [63].

## 5.8 Example

To illustrate our findings, we now examine a specific model example. Our working medium consists of $N$ non-interacting bosons confined in a one-dimensional parabolic trap with frequency $\omega_0$. During the unitary strokes, the potential is perturbed with time. The unperturbed and the perturbing Hamiltonians of the working medium are given by

$$H_0 = \sum_{i=1}^{N} \frac{p_i^2}{2m} + \frac{1}{2} m\omega_0^2 x_i^2, \tag{5.8.1}$$

$$H_1 = \sum_{i=1}^{N} m\omega_0^2 x_i^2, \tag{5.8.2}$$

respectively, such that $H(t) = H_0 + \lambda(t) H_1$, where, $\lambda(0) = \lambda$ and $\lambda(\tau) = \lambda + \Delta\lambda$. In the second-quantized formulation, we have

$$H_0 = \sum\nolimits_m \epsilon_m a_m^\dagger a_m, \tag{5.8.3}$$

$$\begin{aligned} H_1 = \frac{\hbar\omega_0}{2} \sum\nolimits_m & \sqrt{(m+1)(m+2)} \left( a_m^\dagger a_{m+2} + a_{m+2}^\dagger a_m \right) \\ & + (1+2m) a_m^\dagger a_m, \end{aligned} \tag{5.8.4}$$

where $m \in \mathbb{N}$. Here $\epsilon_m = \hbar\omega_0(m + \frac{1}{2})$ represents the single-particle energy-spectrum of $H_0$ and $a_m$ ($a_m^\dagger$) is the bosonic annihilation (creation) operator for the $m$-th energy level. Due to the number conservation, $\sum_m a_m^\dagger a_m = N$, we are restricted to work with the canonical ensemble description. The central repercussion of this constraint is that it induces correlations between the occupation numbers of different single-particle occupation states. However, one can still compute the canonical partition function $Z_N$ for $N$ bosonic particles via a set of recursion relations starting from $N = 1$ [237–243],

$$Z_N = \frac{1}{N} \sum_{k=1}^{N} Z_1(k\beta)\, Z_{N-k}. \tag{5.8.5}$$

Here, $Z_1(k\beta) = \sum_m e^{-k\beta\epsilon_m}$ represents the partition function for a single-particle state. For our model example, the Green's function $\mathbb{G}^{>}(\omega)$ depends on the two-point correlation involving the occupation number operator. Let $n_m = a_m^\dagger a_m$ be the occupation number operator corresponding to the $m$-th energy level, and $\overline{\cdot\cdot}^{(N)}$ represents thermal averaging with respect to the canonical $N$-particle density matrix

$$\rho_N = \frac{1}{Z_N} e^{-\beta \sum_m \epsilon_m n_m} \delta_{\sum_m n_m, N}. \tag{5.8.6}$$

The average occupation of $m$-th level can be computed using the following recursion relations [237]

$$\overline{n}_m^{(N)} = \frac{1}{Z_N}\sum_{k=1}^{N} e^{-\beta\epsilon_m k} Z_{N-k}, \tag{5.8.7}$$

$$\overline{n}_m^{(N+1)} = \frac{Z_N}{Z_{N+1}} e^{-\beta\epsilon_m}\big(1+\overline{n}_m^{(N)}\big). \tag{5.8.8}$$

starting from $Z_0 = 1$ and $\overline{n}_m^{(0)} = 0$.

In order to calculate the Onsager transport coefficients, the key non-trivial quantity required is the greater Green's function, given by

$$\begin{aligned}\mathbb{G}_N^{>}(\omega) = -2\pi\frac{\omega_0^2}{4}\sum\nolimits_m (m+1)(m+2)\Big[\delta(\omega-2\omega_0)\big(\overline{n}_m^{(N)} + \overline{n_m n}_{m+2}^{(N)}\big) \\ + \delta(\omega+2\omega_0)\big(\overline{n}_{m+2}^{(N)} + \overline{n_{m+2}n}_m^{(N)}\big)\Big] \\ - 2\pi\frac{1}{\hbar^2}\sum\nolimits_{m,m'}\epsilon_m\epsilon_{m'}\big(\overline{n_m n}_{m'}^{(N)} - \overline{n}_m^{(N)}\overline{n}_{m'}^{(N)}\big)\delta(\omega).\end{aligned} \tag{5.8.9}$$

The challenge of calculating the two-level occupation correlation can be circumvented by using the relation [237–243]

$$\overline{n_m n}_{m'}^{(N)} = -\frac{e^{\beta\epsilon_m}\overline{n}_m^{(N)} - e^{\beta\epsilon_m'}\overline{n}_{m'}^{(N)}}{e^{\beta\epsilon_m} - e^{\beta\epsilon_m'}}, \tag{5.8.10}$$

which simplifies the expression for the Green's function in (5.8.9),

$$\begin{aligned}\mathbb{G}_N^{>}(\omega) &= -2\pi\frac{\omega_0^2}{4}\sum\nolimits_m (m+1)(m+2)\big(\overline{n}_m^{(N)} - \overline{n}_{m+2}^{(N)}\big) \\ &\quad \big[\{1+n_B(2\omega_0)\}\delta(\omega-2\omega_0) + n_B(2\omega_0)\delta(\omega+2\omega_0)\big] \\ &\quad - 2\pi\frac{1}{\hbar^2}\sum\nolimits_{m,m'}\epsilon_m\epsilon_{m'}\big(\overline{n_m n}_{m'}^{(N)} - \overline{n}_m^{(N)}\overline{n}_{m'}^{(N)}\big)\delta(\omega) \\ &= -2\pi\frac{\omega_0}{\hbar}\sum\nolimits_m \epsilon_m\overline{n}_m^{(N)}\big[\{1+n_B(2\omega_0)\}\delta(\omega-2\omega_0) \\ &\quad + n_B(2\omega_0)\delta(\omega+2\omega_0)\big] \\ &\quad - 2\pi\frac{1}{\hbar^2}\sum\nolimits_{m,m'}\epsilon_m\epsilon_{m'}\big(\overline{n_m n}_{m'}^{(N)} - \overline{n}_m^{(N)}\overline{n}_{m'}^{(N)}\big)\delta(\omega),\end{aligned} \tag{5.8.11}$$

where $n_B(\omega) = [e^{\beta\hbar\omega} - 1]^{-1}$ is the Bose-Einstein distribution function. The two summations in the above expression correspond to the average energy and the variance of energy of the unperturbed Hamiltonian $H_0$.

Finally, we derive the formal expressions for the Onsager transport coefficients as follows,

$$\begin{aligned} L_{ww} =& \frac{1}{\tau_{cyc}}\Big[\langle\langle E^2\rangle\rangle + \frac{\langle E\rangle}{\beta}F(2\omega_0)\Big], && (5.8.12)\\ L_{wq} =& L_{qw} = -\frac{1}{\tau_{cyc}}\Big[\langle\langle E^2\rangle\rangle - \lambda\beta\langle\langle E^3\rangle\rangle\Big], && (5.8.13)\\ L_{qq} =& \frac{1}{\tau_{cyc}}\Big[(1+2\lambda)\langle\langle E^2\rangle\rangle - \lambda\beta\Big\{\langle\langle E^3\rangle\rangle + \frac{\lambda}{2}\big(\beta\langle\langle E^4\rangle\rangle - 3\langle\langle E^3\rangle\rangle\big)\Big\}\Big], && (5.8.14) \end{aligned}$$

where the $n$-th cumulant of energy $\langle\langle E^n\rangle\rangle$ corresponding to $H_0$ is given by

$$\langle\langle E^n\rangle\rangle = (-1)^n\frac{\partial^n}{\partial\beta^n}\ln Z_N. \tag{5.8.15}$$

Additionally, the variance of the total work current can be computed following (5.5.3):

$$\frac{\langle\langle j_w^2\rangle\rangle}{2} = \frac{1}{\tau_{cyc}}\Big[\langle\langle E^2\rangle\rangle + \frac{\langle E\rangle}{\beta}(\beta\hbar\omega_0)\coth\big(\beta\hbar\omega_0\big)F(2\omega_0)\Big]. \tag{5.8.16}$$

Notice that the breakdown of the traditional work-FDR in this model is evident from the fact that $\coth(x) > \frac{1}{x}$ for $x > 0$, as reported in (5.5.7). The appearance of the higher order cumulant of energy $\langle\langle E^n\rangle\rangle$ is a consequence of the presence of the interaction term $\lambda H_1$ in the initial total Hamiltonian $H(0)$.

In the following, we present numerical results for $N = 5$ bosons confined in a harmonic trap. Starting from the single particle partition function $Z_1 = \text{csch}\big(\beta\hbar\omega_0/2\big)/2$, we use the recursion relation given in (5.8.5) to calculate $Z_5$. The various Onsager coefficients are computed numerically using equations (5.8.12) to (5.8.14). We investigate bounds on the quantities $\eta^{(2)}$ [defined in (5.6.7)] in the engine operational regime, and $\varepsilon^{(2)}$ [defined in (5.7.2)] in the refrigerator operational regime. In Fig. 5.3 (a) we display the ratio $\eta^{(2)}/\langle\eta\rangle^2$, which validates the existence of the lower bound, and in contrast to the autonomous continuous engine, the violation of the upper bound on $\eta^{(2)}$ is observed in Fig. 5.3 (b). Furthermore, we observe the

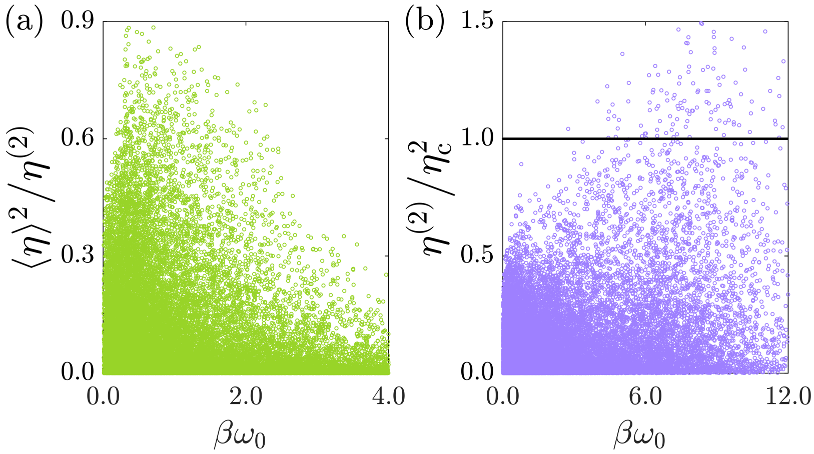


Figure 5.3: Engine regime: $\langle j_w \rangle < 0$, $\langle j_q \rangle > 0$ (necessary requirement: $\mathcal{A}_q > \mathcal{A}_w$). Parameters chosen from uniform distributions: $\beta \in [0, 4]$, $\omega_0 \in [0, 3]$, $\Delta\beta \in [0, 0.3\,\beta]$, $\lambda \in [0, 0.3]$, and $\Delta\lambda \in [0, 0.1]$. Simulations were performed over one million points. (a) Validity of the lower bound, $\eta^{(2)} \geq \langle\eta\rangle^2$ and (b) Violation of the upper bound, $\eta^{(2)} \nleq \eta_c^2$, can be observed.

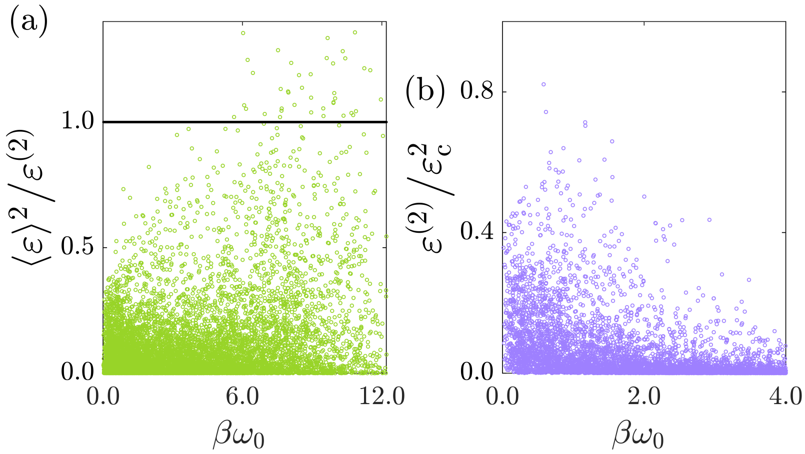


Figure 5.4: Refrigerator regime: $\langle j_c \rangle > 0$, $\langle j_w \rangle > 0$ (necessary requirement: $\mathcal{A}_w > \mathcal{A}_q$). Parameters chosen from uniform distributions: $\beta \in [0, 4]$, $\omega_0 \in [0, 3]$, $\Delta\beta \in [0, 0.3\,\beta]$, $\lambda \in [0, 0.3]$, and $\Delta\lambda \in [0, 0.1]$. Simulations were performed over one million points. (a) Violation of the lower bound, $\varepsilon^{(2)} \ngeq \langle\varepsilon\rangle^2$, and (b) validity of the upper bound, $\varepsilon^{(2)} \leq \varepsilon_c^2$, can be observed.

opposite trend in the refrigerator regime: the violation of the lower bound, and the existence of the upper bound, as shown in Fig. 5.4 (a) and (b), respectively. These observations precisely match our analytical predictions.

## 5.9 Summary

In this work, we utilized the Schwinger-Keldysh nonequilibrium Green's function formalism to derive an analytical expression for the joint CGF for total work and heat from the hot reservoir in the quantum Otto cycle with an arbitrary many-body working medium. The derived CGF is valid up to the second order of the driving protocol $\lambda(t)$ and satisfies the heat engine fluctuation relation. This CGF is applicable to arbitrary perturbative protocols and interaction Hamiltonians. Furthermore, we developed a consistent linear response framework by focusing on the first and second cumulants of total work and heat in the limit of small driving amplitude and small temperature difference. Our analysis revealed the violation of the traditional FDR for the work current as a consequence of quantum non-adiabatic driving during the work strokes. However, for the heat current, the traditional FDR remains valid since the heat exchange stroke in the Otto cycle does not directly experience external driving. These findings have significant implications as they establish different universal bounds on fluctuations for the engine and refrigerator regimes. Specifically, in the engine regime, we observed that the ratio of output to input fluctuations is bounded from below, whereas in the refrigerator regime, the opposite trend is observed–the ratio of fluctuations is bounded from above.

These results stand in stark contrast to the behavior observed for autonomous steady-state engines in earlier studies. Moreover, we found that the bounds on the ratio of fluctuations become similar for the two different families of machines only when the Otto cycle is driven in a quantum-adiabatic manner. This highlights the role of quantum effects in determining the bounds on fluctuations for thermal machines.

# 6

# Closing Remarks and Outlook

In this chapter, we conclude the thesis by summarizing key findings and discussing future research directions.

## 6.1 Results

In Chapter 2, we investigated three-terminal quantum absorption refrigerators operating in the linear response regime. By analyzing the current fluctuations among the cold, hot, and work terminals, we uncovered an emergent hierarchy among these fluctuations. This allowed us to derive novel bounds on cooling power and efficiency, going beyond traditional thermodynamic uncertainty relations (TURs). We demonstrated that the tightest bound on cooling power is determined by the fluctuation of the work current, which can lead to stricter bounds than those predicted by standard TURs, particularly in systems with tight coupling between currents.

In Chapter 3, we extended our focus to continuous machines with broken time-reversal symmetry. By symmetrizing the operational regime, we derived universal bounds on current fluctuations even in the absence of Onsager reciprocity. Our analysis was applied to a classical example of a non-autonomous continuous machine, the overdamped Brownian heat engine. We found that the output current fluctuations are constrained by those of the input current, offering new perspectives on nonequilibrium fluctuation relations for systems that lack time-reversal symmetry.

In Chapter 4, we turned our attention to discrete thermodynamic machines, particularly the quantum Otto cycle. We examined specific working fluids—a single qubit and a harmonic oscillator—due to the absence of a general linear response formalism for Otto cycles. In this far-from-equilibrium regime, we established bounds on work and heat fluctuations in both engine and refrigerator modes, revealing that these fluctuation bounds behave differently from those of continuous machines. Additionally, we derived generalized thermodynamic uncertainty relations (GTURs) for the qubit-Otto cycle, which remain valid even under far-from-equilibrium driving.

In Chapter 5, we developed a linear response framework for Otto cycles using the Schwinger-Keldysh nonequilibrium Green's function (NEGF) technique. Our analysis revealed the presence of robust Onsager reciprocity, despite asymmetric driving, due to the separation of work and heat exchange strokes in the Otto cycle. Moreover, we observed a violation of the fluctuation-dissipation relation (FDR) for work, while the heat FDR remained intact. This discrepancy explained the differences in fluctuation bounds between discrete and continuous machines.

## 6.2 Future Research Directions

**Problem 1:** **Multi-terminal Quantum Devices**– Our study in Chapter 2 was confined to three-terminal setups. Extending this analysis to multi-terminal configurations offers a compelling direction for future work. Specifically, investigating the bounds on the relative fluctuations of individual currents in multi-terminal systems could uncover new performance limits in in hybrid operational regimes [244].

**Problem 2:** **Far-from-equilibrium Continuous Machines**– In Chapters 2 and 3, our analysis was restricted to the linear response regime. A natural extension of this work involves exploring continuous machines far from equilibrium using driven-dissipative dynamics. Incorporating the Floquet formalism for periodically driven systems could provide new insights into their long-term stability and performance under time-periodic driving, especially in the presence of time-dependent fluctuations.

**Problem 3:** **Finite-time Quantum Otto Cycles**– In Chapter 4 (and 5), our results assumed complete thermalization during the heat exchange strokes of the quantum Otto cycle. A future direction would be to relax this assumption and explore finite-time effects on work and heat fluctuations. By incorporating non-adiabatic corrections, it would be possible to analyze how these effects manifest across different working fluids, providing a more comprehensive understanding of discrete machines.

**Problem 4:** **Exploring Other Trap Potentials in Quantum Otto Cycles**– In Chapter 5, we used a model of $N$ bosons trapped in a harmonic potential to demonstrate our findings. A future research direction could involve studying other types of trap potentials, such as square or triangular traps, or considering particles that obey different symmetries (e.g., bosons versus fermions) [69, 245]. These investigations would offer further insights into nonequilibrium fluctuations in diverse quantum setups operating under Otto cycles.

**Problem 5:** **Universality of Fluctuation Bounds across Different Cycles**– While our study focused on the quantum Otto cycle, it would be valuable to investigate whether the fluctuation bounds we derived are universal across other thermodynamic cycles, such as the Carnot or Stirling cycles. This could lead to a broader understanding of the performance constraints of both quantum and classical machines.

# Appendix

## A1 Statistics of heat from the cold bath $q_c$ from $P(w, q_h)$

****Appendix for Chapters 4 and 5****

In this appendix, we provide a concise demonstration of how to calculate the cumulants of $q_c$ using the joint probability distribution $P(w, q_h)$. In cases of perfect thermalization, we show that the stochastic variable $q_c$ and its counterpart $\tilde{q}_c = -w - q_h$ share identical statistical properties. To capture the statistics of the stochastic variables $w_1$, $q_h$, $w_3$, and $q_c$, we introduce quantum projective measurements after each stroke and at the beginning of each cycle [246].

Let the successive energy measurement results be denoted as $E_0$, $E_1$, $E_2$, $E_3$, and $E_{0'}$, which take values from the sets of energy eigenvalues $\epsilon_k[\lambda_i]$ and $\epsilon_j[\lambda_f]$, corresponding to the initial Hamiltonian $H[\lambda_i] = \sum_k \epsilon_k[\lambda_i]\Pi_k^{\lambda_i}$ (for $E_0$, $E_3$, and $E0'$) and the final Hamiltonian $H[\lambda_f] = \sum_j \epsilon_j[\lambda_f]\Pi_j^{\lambda_f}$ (for $E_1$ and $E_2$). Here, $\Pi_{k(j)}^{\lambda_{i(f)}} = |k(j); \lambda_{i(f)}\rangle\langle k(j); \lambda_{i(f)}|$ represents the eigen-projectors.

The heat exchanged with the cold bath is determined by

$$q_c = E_{0'} - E_3, \tag{A1}$$

where $E_{0'}$ refers to the energy measured after the final thermalization with the cold bath. We now aim to understand the relationship between $q_c$ and the variable

$$\tilde{q}_c = -(w_1 + w_3 + q_h) = E_0 - E_3. \tag{A2}$$

For perfect thermalization (or even in a limit cycle with imperfect thermalization), energy conservation—through the First Law of Thermodynamics—implies that $\langle \tilde{q}_c \rangle = \langle q_c \rangle$. We extend this reasoning by asking whether the stronger condition $\langle \tilde{q}_c^r \rangle = \langle q_c^r \rangle$ holds for any positive integer $r$. If so, we conclude that $q_c$ and $\tilde{q}_c$ share identical statistics.

The conditional probability for the forward process, giving the outcomes $E_0 = \epsilon_n[\lambda_i]$, $E_1 = \epsilon_m[\lambda_f]$, $E_2 = \epsilon_k[\lambda_f]$, $E_3 = \epsilon_l[\lambda_i]$, and $E_{0'} = \epsilon_{n'}[\lambda_i]$, is given by

$$p_f(n', l, k, m, n) = \mathcal{T}^{\beta_c}_{l\to n'} \mathcal{T}^{II}_{k\to l} \mathcal{T}^{\beta_h}_{m\to k} \mathcal{T}^{I}_{n\to m} p_{\beta_c}(n), \tag{A3}$$

where $p_{\beta_c}(n) = \exp(-\beta_c \epsilon_n[\lambda_i])/\mathcal{Z}_c[\lambda_i]$ is the Gibbs distribution. The transition probabilities for the two work strokes were introduced in (4.2.2) in Chapter 4. For the heat strokes, the general transition matrix for the hot bath stroke is:

$$\mathcal{T}^{\beta_h}_{m\to k} = \mathrm{Tr}\left\{ \Pi^{\lambda_f}_k \Phi_{\beta_h}\left[\Pi^{\lambda_f}_m\right] \right\}, \tag{A4}$$

where $\Phi_{\beta_h}[\bullet]$ represents the completely positive trace-preserving (CPTP) map associated with the thermalization process governed by the Lindblad equation. In the case of perfect thermalization, this map yields a thermal density matrix independent of the initial state, leading to:

$$\mathcal{T}^{\beta_h}_{m\to k} = p_{\beta_h}(k), \tag{A5}$$

where $p_{\beta_h}(k) = \exp(-\beta_h \epsilon_k[\lambda_f])/\mathcal{Z}_h[\lambda_f]$. Similarly, the cold bath heat stroke transition matrix is:

$$\mathcal{T}^{\beta_c}_{l\to n'} = \mathrm{Tr}\left\{ \Pi^{\lambda_i}_{n'} \Phi_{\beta_c}\left[\Pi^{\lambda_i}_l\right] \right\}, \tag{A6}$$

and under perfect thermalization, it simplifies to:

$$\mathcal{T}^{\beta_c}_{l\to n'} = p_{\beta_c}(n'). \tag{A7}$$

With this, the marginal probability distributions for $q_c$ and $\tilde{q}c$ are:

$$P_f(q_c) = \sum_{n',l,k,m,n} \delta\left(q_c - \epsilon_{n'}[\lambda_i] + \epsilon_l[\lambda_i]\right) p_f(n', l, k, m, n), \tag{A8}$$

$$P_f(\tilde{q}_c) = \sum_{n',l,k,m,n} \delta\left(\tilde{q}_c - \epsilon_{n}[\lambda_i] + \epsilon_l[\lambda_i]\right) p_f(n', l, k, m, n). \tag{A9}$$

Using these distributions and the joint probability from (A3), we compute the $r$-th raw moments as:

$$\langle q_c^r \rangle_f = \sum_{n',l,k,m,n} \left(\epsilon_{n'}[\lambda_i] - \epsilon_l[\lambda_i]\right)^r \mathcal{T}^{\beta_c}_{l\to n'} \mathcal{T}^{II}_{k\to l} \mathcal{T}^{\beta_h}_{m\to k} \mathcal{T}^{I}_{n\to m} p_{\beta_c}(n), \tag{A10}$$

$$\langle \tilde{q}_c^r \rangle_f = \sum_{n',l,k,m,n} \left(\epsilon_{n}[\lambda_i] - \epsilon_l[\lambda_i]\right)^r \mathcal{T}^{\beta_c}_{l\to n'} \mathcal{T}^{II}_{k\to l} \mathcal{T}^{\beta_h}_{m\to k} \mathcal{T}^{I}_{n\to m} p_{\beta_c}(n). \tag{A11}$$

For imperfect thermalization, where the transition probabilities depend on the initial state as in (A4) and (A6), we generally find:

$$\langle q_c^r \rangle_f \neq \langle \tilde{q}_c^r \rangle_f. \tag{A12}$$

However, in the case of perfect thermalization, we use (A5) and (A7), leading to simplified expressions:

$$\langle q_c^r \rangle_f = \sum_{n',l,k,m,n} \Big(\epsilon_{n'}[\lambda_i] - \epsilon_l[\lambda_i]\Big)^r p_{\beta_c}(n') \mathcal{T}^{II}_{k\to l} p_{\beta_h}(k) \mathcal{T}^{I}_{n\to m} p_{\beta_c}(n), \tag{A13}$$

$$\langle \tilde{q}_c^r \rangle_f = \sum_{n',l,k,m,n} \Big(\epsilon_{n}[\lambda_i] - \epsilon_l[\lambda_i]\Big)^r p_{\beta_c}(n') \mathcal{T}^{II}_{k\to l} p_{\beta_h}(k) \mathcal{T}^{I}_{n\to m} p_{\beta_c}(n). \tag{A14}$$

Finally, applying the normalization condition $\sum_n p_{\beta_c}(n) = \sum_{n'} p_{\beta_c}(n') = 1$ and the property:

$$\begin{aligned}
\sum_m \mathcal{T}^{I}_{n\to m} &= \sum_m \left|\langle m; \lambda_f | U_{\mathcal{E}} | n; \lambda_i\rangle\right|^2 \\
&= \sum_m \langle n; \lambda_i | U_{\mathcal{E}}^\dagger | m; \lambda_f\rangle \langle m; \lambda_f | U_{\mathcal{E}} | n; \lambda_i\rangle \\
&= \langle n; \lambda_i | U_{\mathcal{E}}^\dagger(\tau_1) U_{\mathcal{E}}(\tau_1) | n; \lambda_i\rangle \\
&= 1,
\end{aligned} \tag{A15}$$

of the transition probabilities, we find that under perfect thermalization:

$$\langle q_c^r \rangle_f = \sum_{n',l,k} \left(\epsilon_{n'}[\lambda_i] - \epsilon_l[\lambda_i]\right)^r \mathcal{T}^{II}_{k\to l} p_{\beta_h}(k) p_{\beta_c}(n'), \tag{A16}$$

$$\langle \tilde{q}_c^r \rangle_f = \sum_{l,k,n} \left(\epsilon_{n}[\lambda_i] - \epsilon_l[\lambda_i]\right)^r \mathcal{T}^{II}_{k\to l} p_{\beta_h}(k) p_{\beta_c}(n), \tag{A17}$$

giving the clear result

$$\langle q_c^r \rangle_f = \langle \tilde{q}_c^r \rangle_f. \tag{A18}$$

For the reverse process, using similar analogy for the perfect thermalization in the two heat exchange strokes, it can be shown that

$$\langle q_c^r \rangle_r = \langle \tilde{q}_c^r \rangle_r. \tag{A19}$$

This is indeed the formal justification for the result that four consecutive measurements during the quantum Otto are enough to get the statistics of all three energy exchanges, as mentioned in the main text.

# Bibliography


[1]H. Callen, *Thermodynamics and an Introduction to Thermostatistics*, 2nd ed. (Wiley, New York, 1985).

[2]M. Zemansky, *Heat and Thermodynamics: An Intermediate Textbook* (McGraw-Hill, New York, 1968).

[3]Y. A. Çengel and M. A. Boles, *Thermodynamics : an engineering approach*, McGraw-Hill series in mechanical engineering (McGraw-Hill, Boston, 2002).

[4]E. H. Lieb and J. Yngvason, "The physics and mathematics of the second law of thermodynamics", Phys. Rep. **310**, 1–96 (1999).

[5]J. P. S. Peterson, T. B. Batalhão, M. Herrera, A. M. Souza, R. S. Sarthour, I. S. Oliveira, and R. M. Serra, "Experimental characterization of a spin quantum heat engine", Phys. Rev. Lett. **123**, 240601 (2019).

[6]N. M. Myers, O. Abah, and S. Deffner, "Quantum thermodynamic devices: from theoretical proposals to experimental reality", AVS Quantum Science **4**, 027101 (2022).

[7]V. Blickle and C. Bechinger, "Realization of a micrometre-sized stochastic heat engine", Nat. Phys. **8**, 143–146 (2012).

[8]I. A. Martínez, É. Roldán, L. Dinis, D. Petrov, J. M. Parrondo, and R. A. Rica, "Brownian Carnot engine", Nat. Phys. **12**, 67–70 (2016).

[9]I. A. Martínez, É. Roldán, L. Dinis, and R. A. Rica, "Colloidal heat engines: a review", Soft Matter **13**, 22–36 (2017).

[10]Q. Bouton, J. Nettersheim, S. Burgardt, D. Adam, E. Lutz, and A. Widera, "A quantum heat engine driven by atomic collisions", Nat. Commun. **12**, 1–7 (2021).

[11]G. Maslennikov, S. Ding, R. Hablützel, J. Gan, A. Roulet, S. Nimmrichter, J. Dai, V. Scarani, and D. Matsukevich, "Quantum absorption refrigerator with trapped ions", Nat. Commun. **10**, 202 (2019).

[12]O. Abah, J. Roßnagel, G. Jacob, S. Deffner, F. Schmidt-Kaler, K. Singer, and E. Lutz, "Single-ion heat engine at maximum power", Phys. Rev. Lett. **109**, 203006 (2012).

[13]J. Roßnagel, S. T. Dawkins, K. N. Tolazzi, O. Abah, E. Lutz, F. Schmidt-Kaler, and K. Singer, "A single-atom heat engine", Science **352**, 325–329 (2016).

[14]J.-W. Zhang, J.-Q. Zhang, G.-Y. Ding, J.-C. Li, J.-T. Bu, B. Wang, L.-L. Yan, S.-L. Su, L. Chen, F. Nori, Ş. K. Özdemir, F. Zhou, H. Jing, and M. Feng, "Dynamical control of quantum heat engines using exceptional points", Nat. Commun. **13**, 6225 (2022).

[15]S. Bhattacharjee and A. Dutta, "Quantum thermal machines and batteries", Eur. Phys. J. B **94**, 239 (2021).

[16]F. Carollo, F. M. Gambetta, K. Brandner, J. P. Garrahan, and I. Lesanovsky, "Nonequilibrium quantum many-body Rydberg atom engine", Phys. Rev. Lett. **124**, 170602 (2020).

[17]Y.-Y. Chen, G. Watanabe, Y.-C. Yu, X.-W. Guan, and A. del Campo, "An interaction-driven many-particle quantum heat engine and its universal behavior", npj Quantum Inf. **5**, 88 (2019).

[18]K.-W. Sun, R. Li, and G.-F. Zhang, "A quantum heat engine based on Tavis-Cummings model", Eur. Phys. J. D **71**, 230 (2017).

[19]F. Altintas, A. U. C. Hardal, "Quantum correlated heat engine with spin squeezing", Phys. Rev. E **90**, 032102 (2014).

[20]G. Thomas and R. S. Johal, "Coupled quantum otto cycle", Phys. Rev. E **83**, 031135 (2011).

[21]X. L. Huang, H. Xu, X. Y. Niu, and Y. D. Fu, "A special entangled quantum heat engine based on the two-qubit Heisenberg XX model", Phys. Scr. **88**, 065008 (2013).

[22]N. M. Myers, F. J. Peña, O. Negrete, P. Vargas, G. D. Chiara, and S. Deffner, "Boosting engine performance with bose–einstein condensation", New J. Phys. **24**, 025001 (2022).

[23]M. J. Henrich, G. Mahler, and M. Michel, "Driven spin systems as quantum thermodynamic machines: Fundamental limits", Phys. Rev. E **75**, 051118 (2007).

[24]X. L. Huang, L. C. Wang, and X. X. Yi, "Quantum Brayton cycle with coupled systems as working substance", Phys. Rev. E **87**, 012144 (2013).

[25]S. Singh and S. Rebari, "Multi-level quantum diesel engine of non-interacting fermions in a one-dimensional box", Eur. Phys. J. B **93**, 150 (2020).

[26]J Jaramillo, M Beau, and A del Campo, "Quantum supremacy of many-particle thermal machines", New J. Phys. **18**, 075019 (2016).

[27]T. Denzler, J. F. G. Santos, E. Lutz, and R. M. Serra, "Nonequilibrium fluctuations of a quantum heat engine", Quantum Sci. Technol. **9**, 045017 (2024).

[28]K. Sekimoto, *Stochastic energetics* (Springer Berlin, Heidelberg, 2010).

[29]L. Peliti and S. Pigolotti, *Stochastic thermodynamics: An introduction* (Princeton University Press, 2021).

[30]N. Shiraishi, *An introduction to stochastic thermodynamics: from basic to advanced* (Springer, Singapore, 2023).

[31]C. V. den Broeck, "Stochastic thermodynamics: A brief introduction", in *Physics of complex colloids*, edited by C. Bechinger, F. Sciortino, and P. Ziherl (IOS Press, Amsterdam, 2013), pp. 155–194.

[32]U. Seifert, "From stochastic thermodynamics to thermodynamic inference", Annu. Rev. Condens. Matter Phys. **10**, 171–192 (2019).

[33]S. Vinjanampathy and J. Anders, "Quantum thermodynamics", Contemp. Phys. **57**, 545–579 (2016).

[34]R. Kosloff, "Quantum thermodynamics: a dynamical viewpoint", Entropy **15**, 2100–2128 (2013).

[35]M. Esposito, U. Harbola, and S. Mukamel, "Nonequilibrium fluctuations, fluctuation theorems, and counting statistics in quantum systems", Rev. Mod. Phys. **81**, 1665–1702 (2009).

[36]M. Campisi, P. Hänggi, and P. Talkner, “Colloquium: quantum fluctuation relations: foundations and applications”, Rev. Mod. Phys. **83**, 771–791 (2011).

[37]C. Jarzynski, “Equalities and inequalities: irreversibility and the second law of thermodynamics at the nanoscale”, Annu. Rev. Condens. Matter Phys. **2**, 329–351 (2011).

[38]G. Benenti, G. Casati, K. Saito, and R. S. Whitney, “Fundamental aspects of steady-state conversion of heat to work at the nanoscale”, Phys. Rep. **694**, 1–124 (2017).

[39]J. Anders and M. Esposito, “Focus on quantum thermodynamics”, New J. Phys. **19**, 010201 (2017).

[40]J. Goold, M. Huber, A. Riera, L. del Rio, and P. Skrzypczyk, “The role of quantum information in thermodynamics—a topical review”, J. Phys. A: Math. Theor. **49**, 143001 (2016).

[41]N. Shiraishi, K. Saito, and H. Tasaki, “Universal trade-off relation between power and efficiency for heat engines”, Phys. Rev. Lett. **117**, 190601 (2016).

[42]P. Pietzonka and U. Seifert, “Universal trade-off between power, efficiency, and constancy in steady-state heat engines”, Phys. Rev. Lett. **120**, 190602 (2018).

[43]G. Benenti, G. Casati, and J. Wang, “Power, efficiency, and fluctuations in steady-state heat engines”, Phys. Rev. E **102**, 040103 (2020).

[44]K. Sekimoto, “Langevin Equation and Thermodynamics”, Prog. Theor. Phys. Suppl. **130**, 17–27 (1998).

[45]V. Holubec and A. Ryabov, “Fluctuations in heat engines”, J. Phys. A: Math. Theor. **55**, 013001 (2021).

[46]M. Campisi, J. Pekola, and R. Fazio, “Nonequilibrium fluctuations in quantum heat engines: theory, example, and possible solid state experiments”, New J. Phys. **17**, 035012 (2015).

[47]T. Denzler and E. Lutz, “Efficiency fluctuations of a quantum heat engine”, Phys. Rev. Res. **2**, 032062 (2020).

[48]G. Watanabe and Y. Minami, “Finite-time thermodynamics of fluctuations in microscopic heat engines”, Phys. Rev. Res. **4**, L012008 (2022).

[49]K. Ito, C. Jiang, and G. Watanabe, *Universal bounds for fluctuations in small heat engines*, 2019, arXiv:1910.08096 [cond-mat.stat-mech].

[50]T. Denzler and E. Lutz, "Efficiency fluctuations of a quantum heat engine", Phys. Rev. Res. **2**, 032062 (2020).

[51]G. Jiao, S. Zhu, J. He, Y. Ma, and J. Wang, "Fluctuations in irreversible quantum Otto engines", Phys. Rev. E **103**, 032130 (2021).

[52]T. Kamijima, S. Otsubo, Y. Ashida, and T. Sagawa, "Higher-order efficiency bound and its application to nonlinear nanothermoelectrics", Phys. Rev. E **104**, 044115 (2021).

[53]S. Saryal, M. Gerry, I. Khait, D. Segal, and B. K. Agarwalla, "Universal bounds on fluctuations in continuous thermal machines", Phys. Rev. Lett. **127**, 190603 (2021).

[54]S. Saryal and B. K. Agarwalla, "Bounds on fluctuations for finite-time quantum Otto cycle", Phys. Rev. E **103**, L060103 (2021).

[55]S. Mohanta, S. Saryal, and B. K. Agarwalla, "Universal bounds on cooling power and cooling efficiency for autonomous absorption refrigerators", Phys. Rev. E **105**, 034127 (2022).

[56]O. Abah and E. Lutz, "Optimal performance of a quantum Otto refrigerator", EPL **113**, 60002 (2016).

[57]R. Kosloff and Y. Rezek, "The quantum harmonic Otto cycle", Entropy **19**, 032102 (2017).

[58]S. Lee, M. Ha, J.-M. Park, and H. Jeong, "Finite-time quantum Otto engine: Surpassing the quasistatic efficiency due to friction", Phys. Rev. E **101**, 022127 (2020).

[59]B. Lin and J. Chen, "Performance analysis of an irreversible quantum heat engine working with harmonic oscillators", Phys. Rev. E **67**, 046105 (2003).

[60]J. Wang, J. He, and Y. Xin, "Performance analysis of a spin quantum heat engine cycle with internal friction", Phys. Scr. **75**, 227–234 (2007).

[61]S. Chand, S. Dasgupta, and A. Biswas, "Finite-time performance of a single-ion quantum Otto engine", Phys. Rev. E **103**, 032144 (2021).

[62]M. Kloc, P. Cejnar, and G. Schaller, "Collective performance of a finite-time quantum Otto cycle", Phys. Rev. E **100**, 042126 (2019).

[63]A. Das, S. Mahunta, B. K. Agarwalla, and V. Mukherjee, "Precision bound and optimal control in periodically modulated continuous quantum thermal machines", Phys. Rev. E **108**, 014137 (2023).

[64]M. Beau, J. Jaramillo, and A. del Campo, "Scaling-up quantum heat engines efficiently via shortcuts to adiabaticity", Entropy **18**, 168 (2016).

[65]H. Vroylandt, M. Esposito, and G. Verley, "Collective effects enhancing power and efficiency", EPL **120**, 30009 (2018).

[66]W. Niedenzu and G. Kurizki, "Cooperative many-body enhancement of quantum thermal machine power", New J. Phys. **20**, 113038 (2018).

[67]V. Mukherjee and U. Divakaran, "Many-body quantum thermal machines", J. Phys.: Condens. Matter **33**, 454001 (2021).

[68]G. Watanabe, B. P. Venkatesh, P. Talkner, M.-J. Hwang, and A. del Campo, "Quantum statistical enhancement of the collective performance of multiple bosonic engines", Phys. Rev. Lett. **124**, 210603 (2020).

[69]N. M. Myers and S. Deffner, "Bosons outperform Fermions: The thermodynamic advantage of symmetry", Phys. Rev. E **101**, 012110 (2020).

[70]D. Gelbwaser-Klimovsky, A. Bylinskii, D. Gangloff, R. Islam, A. Aspuru-Guzik, and V. Vuletic, "Single-atom heat machines enabled by energy quantization", Phys. Rev. Lett. **120**, 170601 (2018).

[71]M. Boubakour, T. Fogarty, and T. Busch, "Interaction-enhanced quantum heat engine", Phys. Rev. Res. **5**, 013088 (2023).

[72]A. Levy and D. Gelbwaser-Klimovsky, "Quantum features and signatures of quantum thermal machines", in *Thermodynamics in the quantum regime: fundamental aspects and new directions*, edited by F. Binder, L. A. Correa, C. Gogolin, J. Anders, and G. Adesso (Springer International Publishing, Cham, 2018), pp. 87–126.

[73]R. Kosloff and A. Levy, "Quantum heat engines and refrigerators: continuous devices", Annu. Rev. Phys. Chem. **65**, 365–393 (2014).

[74] L. Buffoni, A. Solfanelli, P. Verrucchi, A. Cuccoli, and M. Campisi, "Quantum measurement cooling", Phys. Rev. Lett. **122**, 070603 (2019).

[75] A. Solfanelli, M. Falsetti, and M. Campisi, "Nonadiabatic single-qubit quantum Otto engine", Phys. Rev. B **101**, 054513 (2020).

[76] H. B. Callen and T. A. Welton, "Irreversibility and generalized noise", Phys. Rev. **83**, 34–40 (1951).

[77] M. S. Green, "Markoff Random Processes and the Statistical Mechanics of Time-Dependent Phenomena", J. Chem. Phys. **20**, 1281–1295 (1952).

[78] M. S. Green, "Markoff Random Processes and the Statistical Mechanics of Time-Dependent Phenomena. II. Irreversible Processes in Fluids", The Journal of Chemical Physics **22**, 398–413 (1954).

[79] R. Kubo, "Statistical-mechanical theory of irreversible processes. i. general theory and simple applications to magnetic and conduction problems", J. Phys. Soc. Jpn. **12**, 570–586 (1957).

[80] R Kubo, "The fluctuation-dissipation theorem", Rep. Prog. Phys. **29**, 255 (1966).

[81] R. Kubo, M. Toda, and N. Hashitsume, *Statistical physics ii: nonequilibrium statistical mechanics*, Springer Series in Solid-State Sciences (Springer Berlin Heidelberg, 2012).

[82] S. de Groot and P. Mazur, *Non-equilibrium thermodynamics*, Dover Books on Physics (Dover Publications, 1984).

[83] R. Zwanzig, *Nonequilibrium statistical mechanics* (Oxford University Press, 2001).

[84] U. M. B. Marconi, A. Puglisi, L. Rondoni, and A. Vulpiani, "Fluctuation–dissipation: response theory in statistical physics", Physics Reports **461**, 111–195 (2008).

[85] H. Nyquist, "Thermal agitation of electric charge in conductors", Phys. Rev. **32**, 110–113 (1928).

[86] U. M. B. Marconi, A. Puglisi, L. Rondoni, and A. Vulpiani, "Fluctuation–dissipation: response theory in statistical physics", Phys. Rep. **461**, 111–195 (2008).

[87] M. Baiesi, C. Maes, and B. Wynants, "Fluctuations and response of nonequilibrium states", Phys. Rev. Lett. **103**, 010602 (2009).

[88]G. S. Agarwal, "Fluctuation-dissipation theorems for systems in non-thermal equilibrium and applications", Z. Phys. **252**, 25–38 (1972).

[89]U. Seifert and T. Speck, "Fluctuation-dissipation theorem in nonequilibrium steady states", EPL **89**, 10007 (2010).

[90]J. Mehl, V. Blickle, U. Seifert, and C. Bechinger, "Experimental accessibility of generalized fluctuation-dissipation relations for nonequilibrium steady states", Phys. Rev. E **82**, 032401 (2010).

[91]J.-T. Hsiang and B.-L. Hu, "Fluctuation-dissipation relation for open quantum systems in a nonequilibrium steady state", Phys. Rev. D **102**, 105006 (2020).

[92]W. Sutherland, "Xviii. ionization, ionic velocities, and atomic sizes", The London, Edinburgh, and Dublin Philosophical Magazine and Journal of Science **3**, 161–177 (1902).

[93]W. Sutherland, "Lxxv. a dynamical theory of diffusion for non-electrolytes and the molecular mass of albumin", The London, Edinburgh, and Dublin Philosophical Magazine and Journal of Science **9**, 781–785 (1905).

[94]A. Einstein, "Über die von der molekularkinetischen theorie der wärme geforderte bewegung von in ruhenden flüssigkeiten suspendierten teilchen", Ann. Phys. **322**, 549–560 (1905).

[95]M. von Smoluchowski, "Zur kinetischen theorie der brownschen molekularbewegung und der suspensionen", Ann. Phys. **326**, 756–780 (1906).

[96]J. B. Johnson, "Thermal agitation of electricity in conductors", Phys. Rev. **32**, 97–109 (1928).

[97]H. Nyquist, "Thermal agitation of electric charge in conductors", Phys. Rev. **32**, 110–113 (1928).

[98]L. Onsager, "Reciprocal relations in irreversible processes. i.", Phys. Rev. **37**, 405–426 (1931).

[99]L. Onsager, "Reciprocal relations in irreversible processes. ii.", Phys. Rev. **38**, 2265–2279 (1931).

[100]L. Onsager and S. Machlup, "Fluctuations and irreversible processes", Phys. Rev. **91**, 1505–1512 (1953).

[101]S. Machlup and L. Onsager, "Fluctuations and irreversible process. ii. systems with kinetic energy", Phys. Rev. **91**, 1512–1515 (1953).

[102]S. Berber, Y.-K. Kwon, and D. Tománek, "Unusually high thermal conductivity of carbon nanotubes", Phys. Rev. Lett. **84**, 4613–4616 (2000).

[103]H. U. Baranger and A. D. Stone, "Electrical linear-response theory in an arbitrary magnetic field: a new fermi-surface formation", Phys. Rev. B **40**, 8169–8193 (1989).

[104]C. Jarzynski, "Nonequilibrium equality for free energy differences", Phys. Rev. Lett. **78**, 2690–2693 (1997).

[105]C. Jarzynski, "Equilibrium free-energy differences from nonequilibrium measurements: a master-equation approach", Phys. Rev. E **56**, 5018–5035 (1997).

[106]G. E. Crooks, "Entropy production fluctuation theorem and the nonequilibrium work relation for free energy differences", Phys. Rev. E **60**, 2721–2726 (1999).

[107]G. E. Crooks, "Path-ensemble averages in systems driven far from equilibrium", Phys. Rev. E **61**, 2361–2366 (2000).

[108]D. J. Evans, E. G. D. Cohen, and G. P. Morriss, "Probability of second law violations in shearing steady states", Phys. Rev. Lett. **71**, 2401–2404 (1993).

[109]G. Gallavotti and E. G. D. Cohen, "Dynamical ensembles in nonequilibrium statistical mechanics", Phys. Rev. Lett. **74**, 2694–2697 (1995).

[110]T. Hatano and S.-i. Sasa, "Steady-state thermodynamics of langevin systems", Phys. Rev. Lett. **86**, 3463–3466 (2001).

[111]J. Kurchan, "Fluctuation theorem for stochastic dynamics", J. Phys. A: Math. Gen. **31**, 3719 (1998).

[112]J. L. Lebowitz and H. Spohn, "A gallavotti–cohen-type symmetry in the large deviation functional for stochastic dynamics", J. Stat. Phys. **95**, 333–365 (1999).

[113]K. Kim, C. Kwon, and H. Park, "Heat fluctuations and initial ensembles", Phys. Rev. E **90**, 032117 (2014).

[114]C. Jarzynski and D. K. Wójcik, "Classical and quantum fluctuation theorems for heat exchange", Phys. Rev. Lett. **92**, 230602 (2004).

[115]U. Seifert, "Entropy production along a stochastic trajectory and an integral fluctuation theorem", Phys. Rev. Lett. **95**, 040602 (2005).

[116]U. Seifert, "Stochastic thermodynamics, fluctuation theorems and molecular machines", Rep. Prog. Phys. **75**, 126001 (2012).

[117]U. Seifert, "Stochastic thermodynamics: principles and perspectives", Eur. Phys. J. B **64**, 423–431 (2008).

[118]C. Maes and K. Netočný, "Time-reversal and entropy", J. Stat. Phys. **110**, 269–310 (2003).

[119]M. Esposito and C. Van den Broeck, "Three detailed fluctuation theorems", Phys. Rev. Lett. **104**, 090601 (2010).

[120]M. Esposito and C. Van den Broeck, "Three faces of the second law. i. master equation formulation", Phys. Rev. E **82**, 011143 (2010).

[121]T. Sagawa and M. Ueda, "Generalized jarzynski equality under nonequilibrium feedback control", Phys. Rev. Lett. **104**, 090602 (2010).

[122]T. Sagawa and M. Ueda, "Fluctuation theorem with information exchange: role of correlations in stochastic thermodynamics", Phys. Rev. Lett. **109**, 180602 (2012).

[123]Z. Gong and H. T. Quan, "Jarzynski equality, crooks fluctuation theorem, and the fluctuation theorems of heat for arbitrary initial states", Phys. Rev. E **92**, 012131 (2015).

[124]M Sahoo, S Lahiri, and A. M. Jayannavar, "Fluctuation theorems and atypical trajectories", J. Phys. A: Math. Theor. **44**, 205001 (2011).

[125]H. Tasaki, *Jarzynski relations for quantum systems and some applications*, 2000, arXiv:`cond-mat/0009244 [cond-mat.stat-mech]`.

[126]P. Talkner and P. Hänggi, "The tasaki–crooks quantum fluctuation theorem", J. Phys. A: Math. Theor. **40**, F569 (2007).

[127]P. Talkner, M. Campisi, and P. Hänggi, "Fluctuation theorems in driven open quantum systems", J. Stat. Mech. **2009**, P02025 (2009).

[128]P. Talkner, E. Lutz, and P. Hänggi, "Fluctuation theorems: Work is not an observable", Phys. Rev. E **75**, 050102 (2007).

[129] A. C. Barato and U. Seifert, "Thermodynamic uncertainty relation for biomolecular processes", Phys. Rev. Lett. **114**, 158101 (2015).

[130] T. R. Gingrich, J. M. Horowitz, N. Perunov, and J. L. England, "Dissipation bounds all steady-state current fluctuations", Phys. Rev. Lett. **116**, 120601 (2016).

[131] J. M. Horowitz and T. R. Gingrich, "Thermodynamic uncertainty relations constrain non-equilibrium fluctuations", Nat. Phys. **16**, 15–20 (2020).

[132] K. Macieszczak, K. Brandner, and J. P. Garrahan, "Unified thermodynamic uncertainty relations in linear response", Phys. Rev. Lett. **121**, 130601 (2018).

[133] Y. Hasegawa and T. Van Vu, "Fluctuation theorem uncertainty relation", Phys. Rev. Lett. **123**, 110602 (2019).

[134] G. Falasco, M. Esposito, and J.-C. Delvenne, "Unifying thermodynamic uncertainty relations", New J. Phys. **22**, 053046 (2020).

[135] A. M. Timpanaro, G. Guarnieri, J. Goold, and G. T. Landi, "Thermodynamic uncertainty relations from exchange fluctuation theorems", Phys. Rev. Lett. **123**, 090604 (2019).

[136] G. Guarnieri, G. T. Landi, S. R. Clark, and J. Goold, "Thermodynamics of precision in quantum nonequilibrium steady states", Phys. Rev. Res **1**, 033021 (2019).

[137] K. Brandner, T. Hanazato, and K. Saito, "Thermodynamic bounds on precision in ballistic multiterminal transport", Phys. Rev. Lett. **120**, 090601 (2018).

[138] J. Liu and D. Segal, "Thermodynamic uncertainty relation in quantum thermoelectric junctions", Phys. Rev. E **99**, 062141 (2019).

[139] S. K. Manikandan, D. Gupta, and S. Krishnamurthy, "Inferring entropy production from short experiments", Phys. Rev. Lett. **124**, 120603 (2020).

[140] H. J. D. Miller, M. H. Mohammady, M. Perarnau-Llobet, and G. Guarnieri, "Thermodynamic uncertainty relation in slowly driven quantum heat engines", Phys. Rev. Lett. **126**, 210603 (2021).

[141] M. F. Sacchi, "Thermodynamic uncertainty relations for bosonic Otto engines", Phys. Rev. E **103**, 012111 (2021).

[142]S. Saryal, O. Sadekar, and B. K. Agarwalla, “Thermodynamic uncertainty relation for energy transport in a transient regime: a model study”, Phys. Rev. E **103**, 022141 (2021).

[143]Y. Hasegawa, “Thermodynamic uncertainty relation for general open quantum systems”, Phys. Rev. Lett. **126**, 010602 (2021).

[144]B. K. Agarwalla and D. Segal, “Assessing the validity of the thermodynamic uncertainty relation in quantum systems”, Phys. Rev. B **98**, 155438 (2018).

[145]J. M. Horowitz and T. R. Gingrich, “Proof of the finite-time thermodynamic uncertainty relation for steady-state currents”, Phys. Rev. E **96**, 020103 (2017).

[146]P. Pietzonka, F. Ritort, and U. Seifert, “Finite-time generalization of the thermodynamic uncertainty relation”, Phys. Rev. E **96**, 012101 (2017).

[147]K. Proesmans and C. V. den Broeck, “Discrete-time thermodynamic uncertainty relation”, EPL **119**, 20001 (2017).

[148]D. Chiuchiù and S. Pigolotti, “Mapping of uncertainty relations between continuous and discrete time”, Phys. Rev. E **97**, 032109 (2018).

[149]D. H. Wolpert, “Uncertainty relations and fluctuation theorems for bayes nets”, Phys. Rev. Lett. **125**, 200602 (2020).

[150]K. Yoshimura and S. Ito, “Thermodynamic uncertainty relation and thermodynamic speed limit in deterministic chemical reaction networks”, Phys. Rev. Lett. **127**, 160601 (2021).

[151]T. R. Gingrich and J. M. Horowitz, “Fundamental bounds on first passage time fluctuations for currents”, Phys. Rev. Lett. **119**, 170601 (2017).

[152]J. P. Garrahan, “Simple bounds on fluctuations and uncertainty relations for first-passage times of counting observables”, Phys. Rev. E **95**, 032134 (2017).

[153]K. Liu, Z. Gong, and M. Ueda, “Thermodynamic uncertainty relation for arbitrary initial states”, Phys. Rev. Lett. **125**, 140602 (2020).

[154]S. Pigolotti, I. Neri, E. Roldán, and F. Jülicher, “Generic properties of stochastic entropy production”, Phys. Rev. Lett. **119**, 140604 (2017).

[155]A. C. Barato, R. Chetrite, A. Faggionato, and D. Gabrielli, “Bounds on current fluctuations in periodically driven systems”, New J. Phys. **20**, 103023 (2018).

[156]T. Koyuk, U. Seifert, and P. Pietzonka, “A generalization of the thermodynamic uncertainty relation to periodically driven systems”, J. Phys. A: Math. Theor. **52**, 02LT02 (2018).

[157]P. P. Potts and P. Samuelsson, “Thermodynamic uncertainty relations including measurement and feedback”, Phys. Rev. E **100**, 052137 (2019).

[158]T. V. Vu and Y. Hasegawa, “Uncertainty relation under information measurement and feedback control”, J. Physics A: Math. Theor. **53**, 075001 (2020).

[159]G. Paneru, S. Dutta, T. Tlusty, and H. K. Pak, “Reaching and violating thermodynamic uncertainty bounds in information engines”, Phys. Rev. E **102**, 032126 (2020).

[160]K. Proesmans and J. M. Horowitz, “Hysteretic thermodynamic uncertainty relation for systems with broken time-reversal symmetry”, J. Stat. Mech. **2019**, 054005 (2019).

[161]Z. Cao, J. Su, H. Jiang, and Z. Hou, “Effective entropy production and thermodynamic uncertainty relation of active Brownian particles”, Physics of Fluids **34**, 053310 (2022).

[162]M. Shreshtha and R. J. Harris, “Thermodynamic uncertainty for run-and-tumble–type processes”, Europhys. Lett. **126**, 40007 (2019).

[163]F. Carollo, R. L. Jack, and J. P. Garrahan, “Unraveling the large deviation statistics of markovian open quantum systems”, Phys. Rev. Lett. **122**, 130605 (2019).

[164]D Andrieux, P Gaspard, T Monnai, and S Tasaki, “The fluctuation theorem for currents in open quantum systems”, New J. Phys. **11**, 043014 (2009).

[165]M. T. Mitchison and P. P. Potts, *Physical implementations of quantum absorption refrigerators*, edited by F. Binder, L. A. Correa, C. Gogolin, J. Anders, and G. Adesso (Springer International Publishing, Cham, 2018).

[166]N. Linden, S. Popescu, and P. Skrzypczyk, “How small can thermal machines be? The smallest possible refrigerator”, Phys. Rev. Lett. **105**, 130401 (2010).

[167]J. P. Palao, R. Kosloff, and J. M. Gordon, “Quantum thermodynamic cooling cycle”, Phys. Rev. E **64**, 056130 (2001).

[168]A. Levy and R. Kosloff, "Quantum absorption refrigerator", Phys. Rev. Lett. **108**, 070604 (2012).

[169]L. A. Correa, J. P. Palao, D. Alonso, and G. Adesso, "Quantum-enhanced absorption refrigerators", Sci. Rep. **4**, 3949 (2014).

[170]L. A. Correa, J. P. Palao, G. Adesso, and D. Alonso, "Performance bound for quantum absorption refrigerators", Phys. Rev. E **87**, 042131 (2013).

[171]L. A. Correa, "Multistage quantum absorption heat pumps", Phys. Rev. E **89**, 042128 (2014).

[172]A. Mu, B. K. Agarwalla, G. Schaller, and D. Segal, "Qubit absorption refrigerator at strong coupling", New J. Phys. **19**, 123034 (2017).

[173]M. Kilgour and D. Segal, "Coherence and decoherence in quantum absorption refrigerators", Phys. Rev. E **98**, 012117 (2018).

[174]D. Segal, "Current fluctuations in quantum absorption refrigerators", Phys. Rev. E **97**, 052145 (2018).

[175]H. M. Friedman and D. Segal, "Cooling condition for multilevel quantum absorption refrigerators", Phys. Rev. E **100**, 062112 (2019).

[176]J. Liu and D. Segal, "Coherences and the thermodynamic uncertainty relation: insights from quantum absorption refrigerators", Phys. Rev. E **103**, 032138 (2021).

[177]S. K. Manikandan, E. Jussiau, and A. N. Jordan, "Autonomous quantum absorption refrigerators", Phys. Rev. B **102**, 235427 (2020).

[178]J. B. Brask and N. Brunner, "Small quantum absorption refrigerator in the transient regime: time scales, enhanced cooling, and entanglement", Phys. Rev. E **92**, 062101 (2015).

[179]Y.-X. Chen and S.-W. Li, "Quantum refrigerator driven by current noise", EPL **97**, 40003 (2012).

[180]S. Nimmrichter, J. Dai, A. Roulet, and V. Scarani, "Quantum and classical dynamics of a three-mode absorption refrigerator", Quantum **1**, 37 (2017).

[181]P. Skrzypczyk, N. Brunner, N. Linden, and S. Popescu, "The smallest refrigerators can reach maximal efficiency", J. Phys. A: Math. Theor. **44**, 492002 (2011).

[182] J. O. González, J. P. Palao, and D. Alonso, "Relation between topology and heat currents in multilevel absorption machines", New J. Phys. **19**, 113037 (2017).

[183] J. M. Gordon and K. C. Ng, *Cool thermodynamics* (Cambridge International Science, Cambridge, 2000).

[184] F. P. E. Carré, "Improvement in apparatus for freezing liquids", pat. U.S. Patent No. 30,201 (Oct. 1860).

[185] P. P. Hofer, M. Perarnau-Llobet, J. B. Brask, R. Silva, M. Huber, and N. Brunner, "Autonomous quantum refrigerator in a circuit qed architecture based on a josephson junction", Phys. Rev. B **94**, 235420 (2016).

[186] M. T. Mitchison, M. Huber, J. Prior, M. P. Woods, and M. B. Plenio, "Realising a quantum absorption refrigerator with an atom-cavity system", Quantum Sci. Technol. **1**, 015001 (2016).

[187] P. A. Erdman, B. Bhandari, R. Fazio, J. P. Pekola, and F. Taddei, "Absorption refrigerators based on coulomb-coupled single-electron systems", Phys. Rev. B **98**, 045433 (2018).

[188] D. Venturelli, R. Fazio, and V. Giovannetti, "Minimal self-contained quantum refrigeration machine based on four quantum dots", Phys. Rev. Lett. **110**, 256801 (2013).

[189] D. M. Busiello and S. Pigolotti, "Hyperaccurate currents in stochastic thermodynamics", Phys. Rev. E **100**, 060102 (2019).

[190] André, M. Timpanaro, G. Guarnieri, and G. T. Landi, *Hyperaccurate thermoelectric currents*, 2021, arXiv:`2108.05325 [quant-ph]`.

[191] K. Brandner, K. Saito, and U. Seifert, "Strong bounds on onsager coefficients and efficiency for three-terminal thermoelectric transport in a magnetic field", Phys. Rev. Lett. **110**, 070603 (2013).

[192] K. Brandner and U. Seifert, "Multi-terminal thermoelectric transport in a magnetic field: bounds on Onsager coefficients and efficiency", New J. Phys. **15**, 105003 (2013).

[193]G. Benenti, K. Saito, and G. Casati, "Thermodynamic bounds on efficiency for systems with broken time-reversal symmetry", Phys. Rev. Lett. **106**, 230602 (2011).

[194]K. Saito, G. Benenti, G. Casati, and T. c. v. Prosen, "Thermopower with broken time-reversal symmetry", Phys. Rev. B **84**, 201306 (2011).

[195]B. Sothmann, R. Sánchez, and A. N. Jordan, "Thermoelectric energy harvesting with quantum dots", Nanotechnology **26**, 032001 (2014).

[196]K. Brandner, K. Saito, and U. Seifert, "Thermodynamics of micro- and nano-systems driven by periodic temperature variations", Phys. Rev. X **5**, 031019 (2015).

[197]V. Holubec and A. Ryabov, "Cycling tames power fluctuations near optimum efficiency", Phys. Rev. Lett. **121**, 120601 (2018).

[198]H. B. G. Casimir, "On Onsager's principle of microscopic reversibility", Rev. Mod. Phys. **17**, 343–350 (1945).

[199]J.-H. Jiang, B. K. Agarwalla, and D. Segal, "Efficiency statistics and bounds for systems with broken time-reversal symmetry", Phys. Rev. Lett. **115**, 040601 (2015).

[200]R. Kosloff, "Quantum thermodynamics and open-systems modeling", J. Chem. Phys. **150**, 204105 (2019).

[201]E. Geva and R. Kosloff, "A quantum-mechanical heat engine operating in finite time. A model consisting of spin-1/2 systems as the working fluid", J. Chem. Phys. **96**, 3054–3067 (1992).

[202]T. Feldmann and R. Kosloff, "Performance of discrete heat engines and heat pumps in finite time", Phys. Rev. E **61**, 4774–4790 (2000).

[203]T. D. Kieu, "The second law, Maxwell's demon, and work derivable from quantum heat engines", Phys. Rev. Lett. **93**, 140403 (2004).

[204]M. J. Henrich, F. Rempp, and G. Mahler, "Quantum thermodynamic Otto machines: A spin-system approach", Eur. Phys. J.: Spec. Top. **151**, 032102 (2007).

[205]M. O. Scully, "Quantum afterburner: improving the efficiency of an ideal heat engine", Phys. Rev. Lett. **88**, 050602 (2002).

[206]G. Watanabe, B. P. Venkatesh, P. Talkner, and A. del Campo, "Quantum performance of thermal machines over many cycles", Phys. Rev. Lett. **118**, 050601 (2017).

[207]Y. Rezek and R. Kosloff, "Irreversible performance of a quantum harmonic heat engine", New J. Phys. **8**, 83–83 (2006).

[208]O. Abah, J. Roßnagel, G. Jacob, S. Deffner, F. Schmidt-Kaler, K. Singer, and E. Lutz, "Single-ion heat engine at maximum power", Phys. Rev. Lett. **109**, 203006 (2012).

[209]Y. Zheng, P. Hänggi, and D. Poletti, "Occurrence of discontinuities in the performance of finite-time quantum Otto cycles", Phys. Rev. E **94**, 012137 (2016).

[210]J Jaramillo, M Beau, and A del Campo, "Quantum supremacy of many-particle thermal machines", New J. Phys. **18**, 075019 (2016).

[211]S. Chand and A. Biswas, "Single-ion quantum Otto engine with always-on bath interaction", EPL **118**, 60003 (2017).

[212]R. Shastri and B. P. Venkatesh, "Optimization of asymmetric quantum Otto engine cycles", Phys. Rev. E **106**, 024123 (2022).

[213]V. Singh, "Performance bounds of nonadiabatic quantum harmonic Otto engine and refrigerator under a squeezed thermal reservoir", Phys. Rev. E **102**, 062123 (2020).

[214]M. Campisi, "Fluctuation relation for quantum heat engines and refrigerators", J. Phys. A: Math. Theor. **47**, 245001 (2014).

[215]M. F. Sacchi, "Multilevel quantum thermodynamic swap engines", Phys. Rev. A **104**, 012217 (2021).

[216]S. Deffner and E. Lutz, "Nonequilibrium work distribution of a quantum harmonic oscillator", Phys. Rev. E **77**, 021128 (2008).

[217]K. Husimi, "Miscellanea in Elementary Quantum Mechanics, II", Prog. Theor. Phys. **9**, 381–402 (1953).

[218]R. Kosloff and Y. Rezek, "The quantum harmonic Otto cycle", Entropy **19**, 062123 (2017).

[219]R. Uzdin, A. Levy, and R. Kosloff, "Equivalence of quantum heat machines, and quantum-thermodynamic signatures", Phys. Rev. X **5**, 031044 (2015).

[220]Z. Fei and H. T. Quan, "Nonequilibrium Green's Function's approach to the calculation of work statistics", Phys. Rev. Lett. **124**, 240603 (2020).

[221]V. Cavina, S. S. Kadijani, M. Esposito, and T. L. Schmidt, "A convenient Keldysh contour for thermodynamically consistent perturbative and semiclassical expansions", SciPost Phys. **15**, 209 (2023).

[222]J. Rammer and H. Smith, "Quantum field-theoretical methods in transport theory of metals", Rev. Mod. Phys. **58**, 323–359 (1986).

[223]J. Schwinger, "Brownian motion of a quantum oscillator", J. Math. Phys. **2**, 407–432 (1961).

[224]J. Weber, "Fluctuation dissipation theorem", Phys. Rev. **101**, 1620–1626 (1956).

[225]B. U. Felderhof, "On the derivation of the fluctuation-dissipation theorem", J. Phys. A: Math. Gen. **11**, 921 (1978).

[226]R. Pathria and P. Beale, *Statistical mechanics*, 3rd ed. (Elsevier, New York, 2011).

[227]S. Mohanta, M. Saha, B. P. Venkatesh, and B. K. Agarwalla, "Bounds on nonequilibrium fluctuations for asymmetrically driven quantum Otto engines", Phys. Rev. E **108**, 014118 (2023).

[228]M. Campisi, J. Pekola, and R. Fazio, "Nonequilibrium fluctuations in quantum heat engines: theory, example, and possible solid state experiments", New J. Phys. **17**, 035012 (2015).

[229]H.-P. Breuer and F. Petruccione, *The Theory of Open Quantum Systems* (Oxford University Press, 2007).

[230]H. Carmichael, *An open systems approach to quantum optics, Lectures presented at the université libre de bruxelles, october 28 to november 4, 1991*, 1st ed., Lecture Notes in Physics Monographs (Springer Berlin, Heidelberg, 1993).

[231]P. C. Martin and J. Schwinger, "Theory of many-particle systems. I", Phys. Rev. **115**, 1342–1373 (1959).

[232] S. Saryal, S. Mohanta, and B. K. Agarwalla, “Bounds on fluctuations for machines with broken time-reversal symmetry: A linear response study”, Phys. Rev. E **105**, 024129 (2022).

[233] H. J. D. Miller, M. Scandi, J. Anders, and M. Perarnau-Llobet, “Work fluctuations in slow processes: Quantum signatures and optimal control”, Phys. Rev. Lett. **123**, 230603 (2019).

[234] M. Scandi, H. J. D. Miller, J. Anders, and M. Perarnau-Llobet, “Quantum work statistics close to equilibrium”, Phys. Rev. Research **2**, 023377 (2020).

[235] M. F. Sacchi, “Thermodynamic uncertainty relations for bosonic Otto engines”, Phys. Rev. E **103**, 012111 (2021).

[236] O. Abah and E. Lutz, “Optimal performance of a quantum Otto refrigerator”, EPL **113**, 60002 (2016).

[237] H. Barghathi, J. Yu, and A. Del Maestro, “Theory of noninteracting fermions and bosons in the canonical ensemble”, Phys. Rev. Res. **2**, 043206 (2020).

[238] W. Magnus, L. Lemmens, and F. Brosens, “Quantum canonical ensemble: a projection operator approach”, Physica A **482**, 1–13 (2017).

[239] W. J. Mullin and J. P. Fernández, “Bose–Einstein condensation, fluctuations, and recurrence relations in statistical mechanics”, Am. J. Phys. **71**, 661–669 (2003).

[240] O. Giraud, A. Grabsch, and C. Texier, “Correlations of occupation numbers in the canonical ensemble and application to a bose-einstein condensate in a one-dimensional harmonic trap”, Phys. Rev. A **97**, 053615 (2018).

[241] P. Borrmann, J. Harting, O. Mülken, and E. R. Hilf, “Calculation of thermodynamic properties of finite bose-einstein systems”, Phys. Rev. A **60**, 1519–1522 (1999).

[242] K. Schönhammer, “Deviations from wick’s theorem in the canonical ensemble”, Phys. Rev. A **96**, 012102 (2017).

[243] A. Grabsch, S. N. Majumdar, G. Schehr, and C. Texier, “Fluctuations of observables for free fermions in a harmonic trap at finite temperature”, SciPost Phys. **4**, 014 (2018).

[244] K. Hammam, G. Manzano, and G. De Chiara, "Quantum coherence enables hybrid multitask and multisource regimes in autonomous thermal machines", Phys. Rev. Res. **6**, 013310 (2024).

[245] Y. Zheng and D. Poletti, "Quantum statistics and the performance of engine cycles", Phys. Rev. E **92**, 012110 (2015).

[246] X. Ding, J. Yi, Y. W. Kim, and P. Talkner, "Measurement-driven single temperature engine", Phys. Rev. E **98**, 042122 (2018).